AN ADAPTIVE OPTIMUM SMES CONTROLLER FOR

PERFORMANCE EHANCEMENT OF PMSG WIND SYSTEM

BY

MUHAMMAD HARIS KHAN

A Thesis Presented to the

DEANSHIP OF GRADUATE STUDIES

KING FAHD UNIVERSITY OF PETROLEUM & MINERALS

DHAHRAN, SAUDI ARABIA

In Partial Fulfillment of the
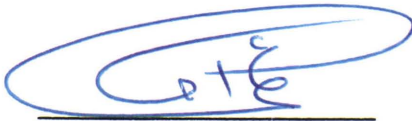Requirements for the Degree of

MASTER OF SCIENCE

In

ELECTRICAL ENGINEERING

DECEMBER 2012

KING FAHD UNIVERSITY OF PETROLEUM & MINERALS

DHAHRAN- 31261, SAUDI ARABIA

DEANSHIP OF GRADUATE STUDIES

This thesis, written by **MUHAMMAD HARIS KHAN** under the direction of his thesis advisor and approved by his thesis committee, has been presented and accepted by the Dean of Graduate Studies, in partial fulfillment of the requirements for the degree of **MASTER OF SCIENCE IN ELECTRICAL ENGINEERING.**

Thesis Committee
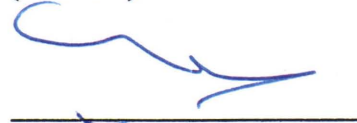
Dr. Ali A. Al-Shaikhi
Department Chairman

Dr. A. H. Abdur-Rahim
(Advisor)

Dr. Salam A. Zummo
Dean of Graduate Studies

Dr. Ibrahim M. El Amin
(Member)

5|1|13
Date

Dr. Samir Al Baiyat
(Member)

Dedicated to

My Parents

And

My Wife

ACKNOWLEDGMENTS

TABLE OF CONTENTS

LIST OF FIGURES

LIST OF TABLES

ABSTRACT (ENGLISH)

Full Name   : Muhammad Haris Khan

Thesis Title   : An Adaptive Optimum SMES Controller For Performance
                 Enhancement Of PMSG Wind System

Major Field   : Electrical Engineering

Date of Degree : Dec, 2012

Permanent magnet synchronous generator (PMSG) wind generators gained popularity over other variable speed devices because of their advantages in terms of simple rotor design, lack of slip rings, no necessity for external excitation, higher efficiency, etc. Though it performs satisfactorily under normal conditions, it is sensitive to sudden wind gusts and also extremely low grid voltage conditions. This research considers superconducting magnetic energy storage (SMES) control to improve the dynamic performance of the PMSG system.

A dynamic model of the PMSG system with an SMES controller connected at the inverter terminal is presented. The SMES controller strategy with variations of real power and terminal voltage as the input has been derived. The performance of the controller depends on the values of the controller gains and time constants when large excursions are experienced by the system. An online adaptive strategy employing radial basis function neural network (RBFNN) for updating the parameters of the SMES controller has been presented. The nominal weights of the RBFNN have been created by presenting the neural network from a large input-output data set. The training data was created through an improved particle swarm (IPSO) optimization technique.

The proposed adaptive RBFNN SMES control strategy was tested on the PMSG wind system for various disturbances like large torque pulses, wind gust and severe low voltage conditions on the grid. It is observed that the SMES controller can damp the power system oscillations effectively and restore normal operating conditions in reasonable time. A proper selection of the weighting matrix obtained through IPSO and radial basis function neural network helped adaptive algorithm to find the parameters very fast.

KING FAHD UNIVERSITY OF PETROLEUM AND MINERALS,

DHAHRAN

DEC, 2012

ABSTRACT (ARABIC)

خلاصة الرسالة

الاسم	محمد حارث خان
عنوان الرسالة	التكيف الأمثل لأنظمة التحكم (SMES) لتعزيز مراقب أداء أنظمة مولدات الرياح (PMSG)
الدرجة	الماجستير في العلوم
التخصص	الهندسة الكهربائية
تاريخ التخرج	ديسمبر 2012م

المولد المتزامن دائم المغنطة (PMSG) المستخدم في مولدات الرياح تكتسب شعبية فائقة مقارنةً بغيرها من المولدات ذات السرعة المتغيرة و ذلك نتيجة لبساطة تصميم الدوار المتحرك، ولعدم وجود حلقات الإنزلاق، وكذلك لا يحتاج لإثارة خارجية، ولإرتفاع كفائته. على الرغم من أنه يعمل بصورة مرضية في ظل الظروف العادية ، ألا أنه حساس لهبوب الرياح المفاجئة و العمل في مستوى جهد منخفض جداً. يتطرق هذا البحث إلى التحكم بالموصلات الفائقة لخزانات الطاقة المغناطيسية (SMES) للمساهمة في تطوير الآداء الديناميكي لأنظمة (PMSG).

سيرد في هذا البحث عملية التوصيل بين محطة التحويل و النموذج الديناميكي المستخدم في أنظمة (PMSG) مع وحدة التحكم (SMES). تمت عملية الإشتقاق للإستراتيجية المتبعة لدى نظام التحكم المستمد إشاراته من قيمة فرق الجهد و كذلك قيمة الطاقة. يعتمد قياس آداء نظام التحكم على قيم

المعاملات و المتغيرات المكونة لهذا النظام المختبرة تحت الرحلات الطويلة لعمل هذا الجهاز. عملية التكييف المباشر لمعاملات نظم التحكم و تحديثها تتم بالأستعانة بإستراتيجية توظيف الأساس الإشعاعي للشبكة العصبية (RBFNN) وقد تم إنشاء الأوزان الاسمية لـ(RBFNN) من خلال تقديم الشبكة العصبية مجموعة كبيرة من البيانات المدخلات والمخرجات. تم إنشاء بيانات التدريب من خلال تقنية سرب الجسيمات الـمحسن (IPSO).

تم اختبار نظام التحكم المقترح في المولد المتزامن دائم المغنطة (PMSG) المستخدم في مولدات الرياح تحت ظروف إظطرابات مختلفة مثل الزيادة الكبيرة في عزم الدوران و عاصفة الرياح الشديدة والظروف الجهد المنخفض على الشبكة. لوحظ أن وحدة التحكم المقترح يمكنه أن يخمد ذبذبات نظام الطاقة على نحو فعال واستعادة ظروف التشغيل العادية في فترة زمنية معقولة. ساعد حسن الاختيار معاملات المصفوفة التي يتم الحصول عليها من خلال (IPSO) و(RBFNN) لإيجاد المعلمات بسرعة فائقة.

درجة الماجستير في العلوم
جامعة الملك فهد للبترول والمعادن
الظهران، المملكة العربية السعودية

CHAPTER 1

INTRODUCTION

Due to the increasing concern about the environment and the depletion of natural resources such as fossil fuels, much research is now focused on obtaining new environmental friendly sources of power. To preserve our planet for future generations, natural renewable sources like solar, wind and nuclear energy are being closely studied and harvested for our energy needs. Recent technological advancements in wind turbine aerodynamics and power electronic interfaces, wind energy is considered to be an excellent supplementary energy source. Because it is environmentally friendly, inexhaustible, safe, and capable of supplying substantial amounts of power. However, due to wind's erratic nature, intelligent control strategies must be implemented to harvest wind energy as much as possible while it is available [1].

The largest power producer from wind energy is China. By the end of 2011, China had generating capacity of 62 GW [2], followed by the United States of America producing 49,802 MW [3]. Germany is the third largest power producer in the world from the wind energy which produces 29,000 MW [4]. The largest onshore wind farms are located in the United States of America. The Roscoe wind farm is producing 781.5 MW and it is the largest onshore wind farm in the world. The Horse Hollow wind energy center generates 735.5 MW.

It has 291 GE wind turbines of each 1.5 MW, and 130 Siemens 2.3 MW installed in Taylor and Nolan County Texas respectively. The list of the installed offshore wind turbine is given in Table.1 [5].

The interest in producing electricity puts certain requirements on the electrical machines and drives. Mechanical energy from renewables injected to electrical machines is not controllable. This challenge has led to much technological advancement in induction machines and permanent magnet synchronous generator (PMSG) controllers used in wind generation [6].

Wind farm	Capacity (MW)	Country	Commissioned
Greater Gabbard	504	United Kingdom	2012
Walney	367	United Kingdom	2012
Thanet	300	United Kingdom	2010
Horns Rev II	209	Denmark	2009
Rødsand II	207	Denmark	2010
Lynn and Inner Dowsing	194	United Kingdom	2008
Robin Rigg (Solway Firth)	180	United Kingdom	2010
Gunfleet Sands	172	United Kingdom	2010
Nysted (Rødsand I)	166	Denmark	2003

Table 1World's largest offshore wind farms

1.1 Types of Wind Turbine According to Speed

The earlier generators were fixed speed systems using squirrel cage induction machines. In fixed speed wind systems, the rotor speed is determined by the grid frequency and its variation is limited to around ±1% of the nominal speed.

Usually, the fixed speed wind systems are designed in such a way that it has its optimum wind speed equal to site mean wind speed. No means for power control is applied and the advantage is simplicity of system operation. Disadvantages are low efficiency of wind energy system in other wind conditions aside from the mean wind speed and poor dynamic performance. Since no control method is implemented, any fluctuations of power are passed through the system without any damping. This effects the quality of the delivered power to the grid and also causes mechanical stress on the wind turbine rotor [7].

The variable speed wind machine is quite popular for both kW and MW sizes. Compared with fixed speed wind machines, variable speed wind turbines generate 10-15% more power. Variable speed wind turbines have lower stress on the mechanical components especially the blades and shafts, and cause less power fluctuations. A typical wind energy system is mainly comprised of blades, generator, power control system and a back to back convertor. The blades transform the wind energy into rotational mechanical energy so as to drive the generator. The electricity generated is variable frequency and variable voltage which cannot fed into the grid directly. An AC/DC and DC/AC converter is necessary to change the electricity into constant frequency and constant voltage so that grid connection would be possible. The generator side converter converts AC to DC which accomplishes the power control and maintains DC link voltage. The grid side converter is a general PWM voltage rectifier, which converts DC to AC. The power quality of these wind energy

systems is much better compared to their fixed speed counterparts. Furthermore, they have lower noise in low wind conditions [8].

1.2 Variable Speed Wind Generators

The generator and drive system plays an important role in the variable speed wind turbine. Both induction and synchronous generators can be equipped in the variable speed wind turbine and interfaced with grid through power converters. Most modern large-scale variable speed wind turbines are based on the doubly-fed induction generator (DFIG) and permanent magnet synchronous generator (PMSG). In the DFIG configuration, the stator of a DFIG is directly connected to the grid and the rotor winding is connected to a back-to-back voltage source converter (VSC) which provides variable-frequency rotor voltage. The main advantage of this configuration is that the power converter has to handle just a fraction of the rated wind turbine power, typically around 25-30% of the rated power. However, in the PMSG configuration, the stator is directly connected to the grid. The use of permanent magnet on rotor eliminates the rotor winding and its copper losses. PMSG is a self-excited generator. Self-excitation allows the PMSG to operate at high power factor and high efficiency [9,10]. The generator is connected to the grid via a full scale back-to-back converter through a DC link capacitor. Some of the advantages of a PMSG system are,

1. Higher efficiency and energy yield.
2. No external power supply needed for magnet field excitation.

3. Improvement in thermal properties due to the absence of field losses.

4. Higher reliability due to absence of mechanical parts such as slip rings and brushes.

5. Lighter and therefore higher power to weight ratio.

This research considers some control aspects of a PMSG system.

1.3 Control of Permanent Magnet Synchronous Generator

Integration of wind generators in the power grid brings many challenges. The power generation fluctuation in a wind energy conversion system may cause some problems for the grid, especially in a weak grid [11,12]. An energy storage system could be employed to solve this problem. The energy storage devices can provide active power when the PMSG output is lower, or store the excessive power generated by the PMSG when its output is higher than usual because of increased wind speed.

Active damping techniques on the generator side or on the grid side of the convertors of PMSG has been investigated in [13]. The voltage-frequency of the standalone PMSG control using a voltage source converter (VSC) integrated with battery energy storage system (BESS) is reported by Sheeja [14]. Ki-Hong proposed a robust control strategy of controlling the generator side converter instead of the grid side converter for the grid voltage sag [15]. The DC-link voltage control strategy by the generator-side converter has also been proposed in [16,17]. An optimal power control model which includes maximum power extraction control model under low wind speed and pitch angle control model under the high wind speed is established in [18]. Min designed the fuzzy controller

for PMSG for maximum energy captured through compensated pitch angle [19]. The unified power control of PMSG under different grid conditions is reported in [20]. In [21] unity power factor control strategy of the PMSG using stator flux orientation has been proposed.

As mentioned earlier that energy storage device can play a vital role in performance enhancement of PMSG. Storage devices which may be used are: STATCOM, battery energy storage system (BESS), supercapacitor and superconducting magnetic energy storage (SMES) system. Each of them has their own advantages and disadvantages. BESS has some disadvantages like limited life cycles, current limitations and environmental limitations. Supercapacitor has low specific energy, high self-discharge, higher than most batteries, low cell voltage requiring serial connection with voltage balancing, and high cost per watt. A STATCOM, controller design using a pole-assignment approach is discussed in [22]. Stability enhancement of a power system with PMSG and DFIG based wind farm using static var compensator (SVC) is presented in [23]. Braking resistor may be inserted into the dc circuit of the frequency converter, in parallel with the capacitor. It is used to dissipate the excessive energy during grid faults [24]. One reason for the power oscillations in PMSG is because of the wind speed fluctuations. Abedini addressed this problem by using the supercapacitor with PMSG in [25]. Dong proposed an low-voltage ride through (LVRT) of PMSG under the grid fault condition for varying wind speed using the energy storage system ESS [26]. The STATCOM, SVC and supercapacitor can provide or absorb reactive power from the system for voltage support but there is a need for a device which can provide real and reactive power simultaneously.

SMES is a device which can deliver both real and reactive power and hence provide good damping to the PMSG system. An SMES unit utilized to carry out power-flow control and damping improvement of a grid connected wind farm with permanent magnet generators is reported in [27]. Hasan proposed a strategy to minimize frequency fluctuations of wind generator using SMES in [28]. Zhou used large capacity SMES to improve the power quality and stability of wind farms in [29]. The STATCOM/SMES system with a voltage-source IGBT converter is proposed as a controllable energy storage system in [30]. Shi used SMES for improvement of voltage stability of DFIG in [31].

From the above it is observed that SMES has found wide spread applications in power system. However, studies on application of this powerful energy storage device in PMSG wind generator system is virtually missing. Because of the erratic nature of wind speed variations, this storage device which can compensate for both real and reactive power, is expected to be a useful control tool.

1.4 Motivation for the Proposed Work

Wind turbulences and grid faults are the main concerns in PMSG wind turbine system because of them system are not able to meet the active and reactive power demand during these faults. The energy storage devices may improve the wind system performance by providing the active power to the system at the time of contingencies. Variable speed wind generators integrated with an energy storage system is getting attention at recent times. In this work, a variable speed PMSG wind generation system will be investigated with superconducting magnetic energy storage (SMES) system. The main motivation for

choosing SMES system in this work is its ability to provide real and reactive power to the system simultaneously. SMES system has the ability of fast response. It can switch charge to discharge state or vice versa within seconds. SMES has some other advantages like absence of moving parts, infinite cycling capability, and energy recovery rate close to 100%. Design of an SMES controller for performance improvement of a PMSG system has been addressed here.

1.5 Thesis Objectives and Contributions

The proposed research on the dynamic performance of a permanent magnet synchronous generator (PMSG) wind system with SMES control is broken up into following tasks:

1. Develop a model of permanent magnet synchronous generator (PMSG) including a superconducting magnetic energy storage system (SMES).

2. Design a control strategy for real and reactive power control.

3. Determine the controller parameters which will provide satisfactory transient response. This phase involves the following:

   - Design an online adaptive algorithm to tune the controller parameters using radial basis function neural network (RBFNN).

- The training data for generating the nominal weights of the RBFNN to be determined by using an improved particle swarm optimization (IPSO).

4. Test the controller for various contingencies on the wind system.

5. Evaluate the performance of the PMSG system with the proposed adaptive SMES control.

1.6 Thesis Organization

The organization of the thesis is as follows. Chapter 2 presents the literature survey of wind generators including the energy storage systems and various control schemes. Chapter 3 describes the dynamic model of the permanent magnet synchronous generator with superconducting magnetic energy storage system. Generation of training data of the system from improved particle swarm optimization (IPSO) and the adaptive radial basis function neural network (RBFNN) is presented in chapter 4. Chapter 5 gives the simulation results followed by conclusions and future research in chapter 6.

CHAPTER 2

LITERATURE REVIEW

Wind energy is the world's fastest growing renewable energy resource. The average annual growth rate of wind turbine installation is around 30% around the world during last 10 years. In 2005, the global wind electricity generating capacity increased from 59,091 MW to 74,223 MW. It is expected that by the end of 2020 this figure will increase to well over 1,260,000 MW, which will be 12% of the world's electricity consumption. The countries with the highest total installed capacity are Germany (20,622 MW), Spain (11,615 MW), the USA (11,603 MW), India (6270 MW) and Denmark (3136 MW) [32]. The development of modern wind power conversion technology has been starting since 1970s, and the rapid development has started since 1990s [33]. Various wind turbine concepts have been developed and different wind generators have been built. Three types of typical generator systems for large wind turbines exist. The first type is a fixed-speed wind turbine system. The second one is a variable speed wind turbine system with a multi-stage gearbox and a doubly fed induction generator (DFIG), where the power electronic converter feeding the rotor winding has a power rating of 30% of the generating capacity. The stator winding of the DFIG is directly connected to the grid. The third type is also a variable speed wind turbine, but it is a gearless wind turbine system with a direct-drive generator, and full-scale power electronic converters are used [34].

2.1 Wind Turbine Concepts

There are different kinds of generators that could be used in wind turbines but variable wind speed generators are quite popular nowadays. The power quality of variable speed wind turbine is much better as compared to fixed speed wind turbines because of the power electronics involvement. Modern large-scale variable speed wind turbines are based on the doubly-fed induction generator (DFIG) and permanent magnet synchronous generator (PMSG). Some of the generators are discussed below,

1. DC Generator

2. Asynchronous (induction) generator

    - Squirrel cage induction generator (SCIG)

    - Wound rotor induction generator (WRIG)

3. Doubly Fed Induction Generator

4. Synchronous generator (With external field excitation)

5. Permanent magnet generator (PMSG)

2.1.1 DC Generator

The application of DC generator in wind energy systems is not widely used, because of the high maintenance requirement of brushes, commutator and a need of a full scale inverter in order to get connected to alternative current (AC) grid.

Usually, DC generators are restricted to non-grid-connected wind energy systems with small DC loads, i.e. battery chargers [35].

2.1.2 Asynchronous (Induction) Generators

Three phase Induction generator can be used as off-grid configuration. In [36] voltage-frequency control of induction generator is suggested. An isolated three-phase induction generator (IG) with fixed frequency and controllable output voltage using a three-phase Static Synchronous Compensator (STATCOM) is presented in [37]. Ferreira reported the analysis of voltage regulation at the point of common connection (PCC) using squirrel cage induction wind generator [38]. Induction generator consumes reactive power which leads to a poor power factor of the machine. The power factor of smaller induction machines is lower as compared to the larger ones. The consumption of reactive power is penalized by many grid operators, since it causes losses in the grid. Some solutions are offered for active or passive compensation of reactive power. They include capacitor banks or condensers Hence these solutions are costly [39]. Fixed speed wind energy systems including conventional squirrel Cage / Short-circuit Induction Generator (SCIG) and a gearbox have been in use for decades. The big advantage is simplicity in operation and control of the system. However, there are also some disadvantages. In general, the wind is gusty and turbulent particularly in urban areas, which very often varies the speed of the rotor and as a result a lower average efficiency is gained.

2.1.3 Doubly-Fed Induction Generators (DFIG)

Voltage stability is a key issue to achieve the uninterrupted operation of wind farms equipped with doubly fed induction generators (DFIGs) during grid faults.

Ganesh investigated the application of a static synchronous compensator (STATCOM) to assist with the uninterrupted operation of a wind turbine driving a DFIG, which is connected to a power network, during the grid faults [40]. Yang presented the Dynamic performance improvement of DFIG using STATCOM is also investigated in [41]. PI controllers were used in the control loop for controlling the rotor speed and reactive power in [42]. The active and reactive power control of DFIG using STATCOM is presented in [43]. The impact of DFIG wind turbines on power system oscillations has been presented in [44]. The modeling of DFIG equipped with battery energy storage system is used in [45]. The controlling of the DFIG wind turbine under voltage sags is presented in [38]. Comparison between fixed speed and doubly fed induction wind turbines was studied in [46].

In Doubly Fed Induction Generator (DFIG) is a variable speed wind system including induction machine where also the rotor is connected to the grid. Part of the power is either provided from the grid or delivered to the grid through the rotor. This power is called the slip power. The frequency of the slip power is varied in such a way that the rotor field frequency is maintained constant. Variation of the frequency of the slip power is established by means of back to back converters. Bidirectional flow of the power in the back to back converters gives the opportunity to work in sub synchronous mode as well as over synchronous mode [47]. Back to back converter in DFIG consists of one machine-side-converter, a DC link capacitor and a grid-side-converter. The Role of the machine-side-converter is to control the speed or the torque of DFIG and

the machine power factor, while the role of the grid-side-converter is to minimize DC link capacitor's voltage ripple [48].

The benefit with the back-to-back converters is the possibility of utilization of conventional induction generators in a wider speed range and still obtains high efficiency. Because the converter is connected to the rotor, it only has to carry part of the power instead of entire rated power. Thus, the converter in DFIG is dimensioned in accordance to the required speed range. Usually the operating speed range does not exceed ±40 % of the synchronous speed. In most of the wind systems on the market today, this is ±30% [49].It has been shown that the converter rated at 30% of generator rated power is adequate for control of wind turbine rotor within a reasonable speed range. In other applications which will be introduced later on, the converter is dimensioned for the full power. Thus the cost and the losses of the converters in DFIG are lower in comparison to the full power converters. This might be an issue for large wind systems. Other advantage is that the reactive power can be controlled independently from the active power. It means that DFIG can operate close to the unity power factor. The drawbacks with conventional DFIGs with gearbox are:

- High maintenance due to the slip rings.

- Limited capability of supplying reactive power.

- High torques in the machine during faulty conditions.

- Additional measures are required to limit the start-up current.

DFIG-based wind turbines are very sensitive to voltage dips because its stator winding is directly connected to the grid. This over current, which can be seven to ten times the nominal value of current, can easily damage the motor windings and the power semiconductors of the rotor-side converter [50]. Moreover, the most complex control, especially regarding converters in wind systems are related to DFIG, which makes them essentially more economical for large wind systems rather than small systems.

2.1.4 Synchronous Generator

The synchronous machines have many advantages over induction machines. One of them is a higher efficiency. It is because the magnetizing current is not a part of the stator current. In induction machines reactive power for rotor excitation is carried by stator winding as well as the active power for conversion. Accordingly, synchronous generators will have better efficiency and better power factor. In variable speed wind systems, usually, the synchronous generators are connected to the grid via a power electronic converter. The amount of deliverable active power from synchronous generator (SG) depends on the rating of a converter in Volt-Amperes and the power factor of SG. Thus, for the same rating of the converter, the closer the power factor gets to unity, the more active power can be delivered [51]. Additionally the rotor speed does not depend on the electrical load conditions. In wind systems it is more convenient to control the rotor speed merely based on the wind speed. The other advantage is that they can have longer air gaps compared to induction machines. In induction machines, the air gap length is kept small to limit the magnetization current and to improve the power factor [52]. In

synchronous machines, it is desirable to have a longer air gap as it helps to reduce armature reaction and the synchronous reactance which in turn improves the stability.

Two classical types of synchronous generators have often been used in the wind turbine industry: the wound rotor synchronous generator (WRSG) and the permanent magnet synchronous generator (PMSG).

2.1.5 Permanent magnet synchronous generator (PMSG)

The PMSG output voltage and power is improved through STATCOM is presented in [53]. The off grid configuration of PMSG with BESS is used in [54]. Application of the SMES combination with PMSG for improvement of the power quality is presented in [55]. Xia reported the speed controlling of PMSG through input-output feedback linearization with the boost chopper converter in [56]. The power flow control of PMSG through pitch controlling is suggested in [57]. A new way of modeling of PMSG wind turbines and back propagation neural network for power flow controlling is presented in [58]. To control the wind generator power two modes were applied: an operating at maximum power point tracking to extract the maximum wind power, and the other one is to operating at constant power which is used to limit the turbine speed at its nominal value in the case of high wind (Pitch angle control) [59].

PMSG is self-excited device brings about various benefits. One is the elimination of the rotor copper losses. Hence PMSGs are more efficient compared to WRSGs. Unlike WRSG no external power supply is needed. The maintenance is eliminated since brushes and slip rings as well as the rotor

16

windings are removed. The common issue with WRSG is the relation between the frequency induced and the mechanical speed of the rotor. With the advancement of power electronics technology, direct-driven permanent magnet synchronous generators (PMSG) have increasingly drawn more interests to wind turbine manufactures due to its advantages over other WTGs [60]. In modern PMSG WTGs designs, the power conditioning system (PCS) is typically built using a full-scale power converter made up of a two-stage power conversion hardware topology. These converters meet all the constraints of high quality electric power, flexibility and reliability imposed for applications of modern distributed energy resources [61]. This PCS design is composed of a back-to-back converter that enables to control simultaneously and independently the active and reactive power flows exchanged with the electric grid. Lower maintenance requirements and thus lower cost are the main reasons that's why PMSGs are proposed with variable speed wind systems [62]. Yet another issue is that needs to be considered is the risk of demagnetization of magnets due to the temperature rise; the magnets can be partially or fully demagnetized. In partial demagnetization the magnetic properties are weakened. In full demagnetization magnetic properties are completely lost and they require re-magnetization which is a tedious task and in some cases impossible and a new rotor is required. Thus a thermal study is suggested to guarantee that the magnet working temperature is, in any conditions, preserved low. Additionally, the partial demagnetization is usually a case during a short circuit where some parts of the magnets are exposed to high opposing magnetic fields [49,63,64].

However, the advancement in magnetic material science may reduce the cost of permanent magnet and improve its characteristics in the near future. Recently, the PMSG based WECS are changing their profile from prototype to main stream WECS, being installed on large scale. In PMSG based directly driven WECS the full rating AC/DC/AC conversion system is used to convert variable frequency into a compatible grid frequency.

In [65] it is shown that PMSGs are more suitable for gearless applications compared to wound rotor synchronous generators (WRSGs). In comparison of PMSG and WRSG and varying the number of poles, it can be shown that once the number of poles reaches high values, the rotor yoke height of WRSG becomes thicker. Consequently, weight and size of WRSG surpasses that of PMSG.

2.1.5.1 PMSG Configuration

The PMSG is connected through full scale voltage source converters, generator converter is used to control the torque and the speed of the generator and grid side converter used to control the power flow in order to keep the DC-link voltage constant. The two converters are connected by a DC link capacitor in order to have a separate control for each converter [66]. Fig. 2.1 shows the PMSG configuration.
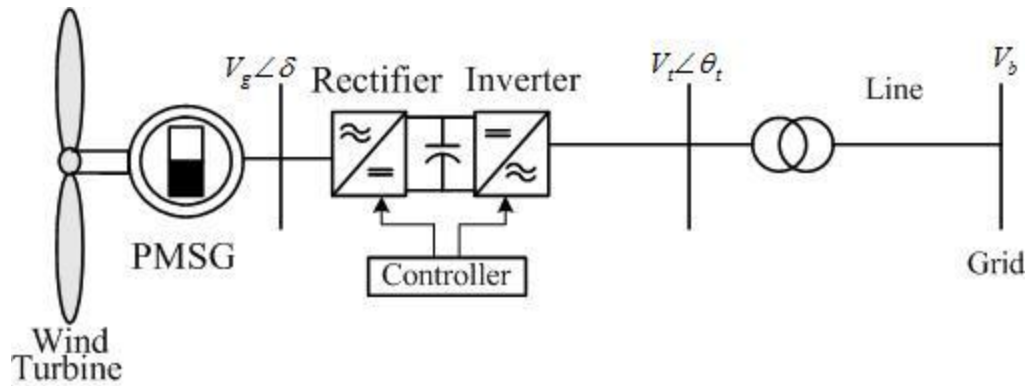
Figure 2.1 PMSG wind generation system

2.1.5.2 Power Electronics Concepts

Nowadays, the scarcity of cheap energy sources requires a particular effort in optimizing the performance of all conversions. The electric power vector is particularly expected to grow in importance, in conjunction with the development of renewable energy sources. Research in the field of power electronics considers several aspects, including conversion topologies, command strategy as well as the structure and performance of power switches and converters. The price to power ratio is going less as compared to the old days, and power converters are becoming more and more attractive and efficient [67].

2.1.5.3 Rectifiers and inverters

A traditional frequency converter, also called an adjustable speed drive, consists of:

- The generator side converter controls its speed to extract maximum power at different wind speeds.

- Energy storage (capacitors).

- Grid-side-converter regulates the output voltage and the power factor is determined by the grid.

2.1.5.4 Power Conditioning System (PCS)

The function of PCS is to connect the individual wind turbine generator to the distribution grid requires the flexible, efficient and reliable generation of high quality electric power [60,61]. The PCS is composed of a back-to-back AC-DC-AC converter. Since the variable speed rotor of the WTG is directly coupled to the permanent magnet synchronous generator, it produces an output voltage with variable amplitude and frequency. This situation demands the use of another inverter to meet the amplitude and frequency requirements of the utility grid, resulting in a back-to-back converter topology [68]. Two voltage source inverters (VSIs) compose the core of the back-to-back converter, i.e. a machine-side inverter and a grid-side inverter.

2.2 Energy Storage Device

Energy storage devices provide valuable benefits to improve stability, power quality and reliability of supply. Storage technologies have been developed significantly in order to meet the challenges of wind energy systems applications. There are many storage technologies are available in the market. The most known are pumped storage hydroelectric systems, battery energy storage systems (BESS), flywheels, compressed air and superconducting magnetic energy storage (SMES) systems.

2.2.1 Batteries

Batteries store energy in electrochemical form creating electrically charged ions. When the battery charges, a direct current is converted into chemical energy, when discharges, the chemical energy is converted back into a flow of electrons in the direct current form. The use of power electronic converters in the batteries for rectifies the alternate current into the direct current. But they have some disadvantages like current limit, limited life-cycles and environmental hazards[69].

2.2.2. Compressed Air

In compressed air energy storage, off-peak hours power is taken from the grid and used to pump and compress air into a sealed underground cavern to a high pressure. The pressurized air is then kept underground for peak periods use. When needed, this high pressure air can drive turbines as the air in the cavern is released and slowly heated [70]. The major disadvantage of compressed air energy storage facilities is their dependence on geographical location. It is difficult to identify underground reservoirs where a wind generator turbine can be constructed, is close to the electric grid, is able to retain compressed air and is large enough for the specific application [71].

2.2.3 Supercapacitors

Supercapacitors are the latest innovational devices in the field of electrical energy storage. In comparison with a battery or a traditional capacitor, the supercapacitor allows a much powerful power and energy density [72]. Supercapacitor energy storage system has a very low energy storage density leading to very high capital costs for large scale applications. Also, they are heavier and bulkier than conventional batteries.

2.2.4 Superconducting Magnetic Storage System (SMES)

Superconducting magnetic energy storage (SMES) system is a superconducting coil, can inject or absorb both real and reactive power into or from the power system to provide stability to the system. The superconducting coil stores energy in it by passing the DC current through it. Its fast response and unlimited charging/discharging phenomenon has edge over other energy storage systems[73].

Although superconductivity was discovered in 1911, SMES has been under study for electric utility energy storage application since the early 1970s [74]. Because of the fast response, SMES can provide load following, system stability, automatic generation control, used as a spinning reserve, bulk energy management, dynamic voltage stability, tie line control, power quality improvement, backup power supply and minimization of power and voltage fluctuations of wind generator. The other major advantage of SMES is that it can deliver large amount of energy in a very small duration of time [73,75–80].The structure of SMES device is shown in Fig. 2.2.
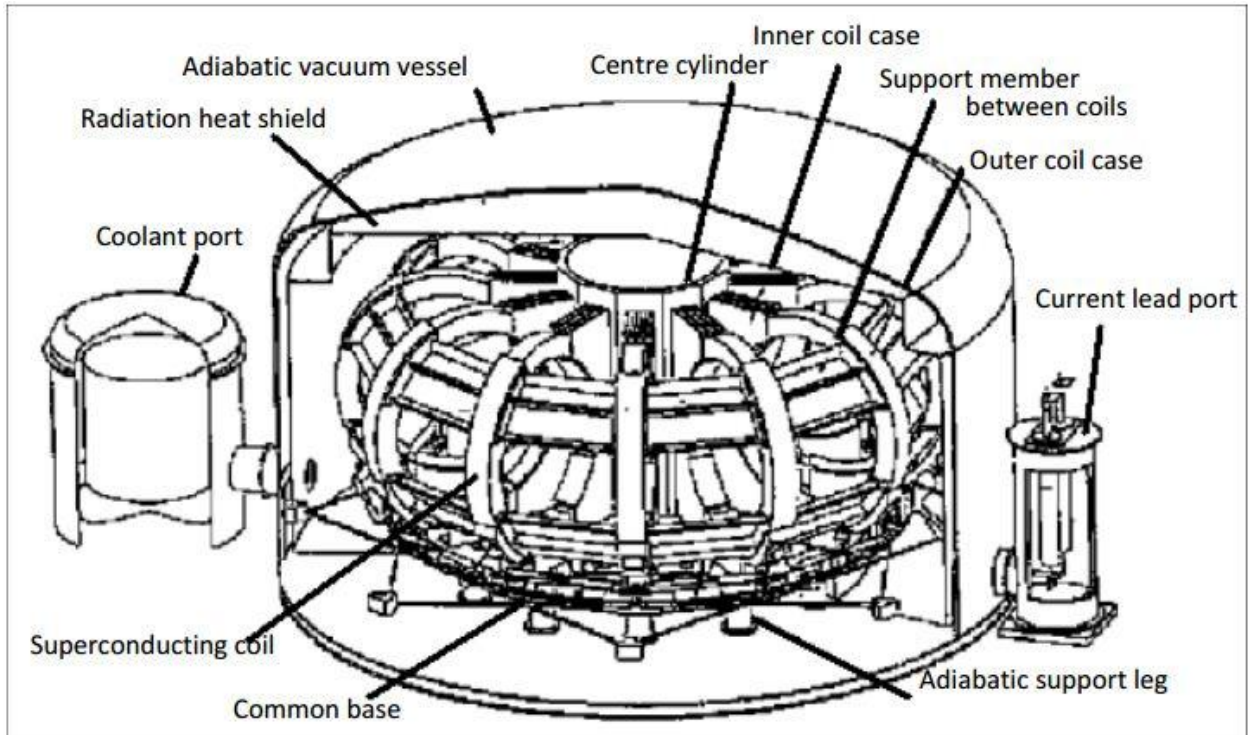
Figure 2.2 Structure of SMES device

2.2.4.1 Overview of SMES Technology

An SMES device is stores energy in the form of magnetic field which is generate by the flow of DC current in a coil. This coil is cryogenically cooled. This technology has been used to improve the power quality of the industries. SMES technology use superconducting coil which is resistance less, If SMES use conventional wire like copper, the magnetic energy would be dissipated as heat due to the wire's resistance to the flow of current [81].

2.2.4.2 Some Applications of SMES

It has the fast response that makes SMES able to provide benefit to many potential utility applications. The applications of SMES are described in the following.

2.2.4.2.1 Energy storage

Superconducting magnetic energy storage system unit can deliver the energy storage up to 5000 MWh with a high return efficiency (up to 97% for a large unit) and a fast response time for dynamic change of energy flow (milliseconds) [82,83]. This makes it ideal for large variations in energy requirements in peak times as a result of major unit's trips [84,85]. SMES can fulfill the spinning reserve requirements. This may provide for the potential reduction of spinning reserve requirements [86,87].

2.2.4.2.2 Improving Voltage Stability

Dynamic voltage instability can occur when there is a major loss of generation unit or insufficient dynamic reactive power to support voltages. Voltages will go down slowly over the time and can result in a voltage collapse. SMES is capable to provide voltage stability by supplying real and reactive powers simultaneously[85,88].

2.2.4.2.3 Load Following

SMES continuous track the system load changes because of the wind generator provide constant power to the load, when it feels the system load has to be changed or wind generator produced fluctuation in power because of change in

wind speed so it provides power to the load as a backup power supply to compensate the mitigation of the power [89].

2.2.4.2.4 Wind generator stabilization

Wind generators have transient stability problems during network disturbances or wind disturbance. An SMES unit based on a self-commutated inverter using IGBT or gate-turn OFF (GTO) thyristor is capable of controlling both the active and reactive powers simultaneously. Therefore, it can act as a good tool to stabilize the wind generator system considerably [90].

2.4. Control Schemes for Wind Generator Systems

2.4.1 PI Controller

A control strategy for a rectifier with variable speed PMSG to achieve maximum power point tracking (MPPT), the rotating speed of wind turbines should be adjusted in the real time according to wind speeds. The anti-windup PI controller of inner current loop is used instead of the traditional PI controller to improve the performances of PMSG is presented in [91]. Ghani suggested an adaptive Fuzzy-PI speed controller for PMSG, he also made a comparison between fuzzy-PI controller and traditional PI controller [92]. The implementation of Fuzzy-PID controller on PMSG has been proposed in [93], whose PID parameters can be adjusted online, controller takes into account various disturbances and suppresses them. Hui proposed a small wind generation system with neural network principles applied for wind speed estimation and PI control for maximum wind power extraction. The mechanical power of the wind turbine can be well tracked for both

dynamic and steady state, but the power deviation and speed tracking errors are large with transient response for almost 20 sec [94].

2.4.2 Artificial Neural Network Based SMES Controllers

Artificial neural network (ANN) based SMES controller has been proposed in [95]. ANN is used for improvement of transient stability of power system. The proposed controller is tested on single machine infinite bus system with different fault conditions. For the effectiveness of the ANN, author generates the training pattern, where generator voltage and speed deviation used as input signals and P_d and Q_d used as output signals. The learning of the network is performed by back- propagation method. In [96], PI controller parameters determine by Eigen value criteria then ANN is applied on PI controllers to find the optimum controller parameters.

2.4.3 Robust and Non Linear Controllers

In [97] robust damping controller for a power system with SMES has been proposed. The author starts by the selection of nominal plant function satisfying the performance criterion and robust stability. The loop-shaping procedure has been employed to design a robust damping controller for a power system with SMES. The changes in the operating conditions reflect in A, B and C matrices. These perturbations are modeled as multiplicative uncertainties in this work. The robust transient stabilizer for power system with SMES is observed in [98]. The author designs the quadratic stabilizer by using the descriptor type H_∞ control theory.

2.4.4 Fuzzy Logic Controllers

Fuzzy logic controllers are also used in controlling the SMES. In [99,100] comparison of fuzzy logic controlled SMES with static nonlinear controlled SMES has been proposed. The parameters of the proposed fuzzy logic controller are optimally tuned by the genetic algorithm (GA) method. The author tested the fuzzy logic controlled SMES on multi-machine system after applying balanced and unbalanced fault. In [101] author present a new concept of implementing fuzzy logic controllers on power systems. They design two independent fuzzy logic controllers, one for the voltage control and other for the frequency control. An additional control signal is added to the output of the fuzzy frequency control. The importance of this additional control, when the power system is affected by a large disturbance.

2.4.5 Converter Control

Nguyen proposed a robust control scheme for the grid-connected single-phase converter of permanent magnet synchronous generator (PMSG) wind turbines under distorted grid voltages [102]. Jeung reported a robust control strategy of the PMSG wind power system for the grid voltage sag. The DC-link voltage control is achieved by the generator side converter instead of the grid-side converter. He considers the nonlinear relationship between generator speed and DC-link capacitor voltage, a DC-link voltage controller is designed using feedback linearization technique [15].

2.4.6 Radial Basis Function Network

Radial Basis Function (RBF) Networks have been widely used in many applications of engineering and sciences. It has three layers artificial neural network (ANN). This uses Radial Basis Functions that uses nonlinearity in the neurons of the hidden layer. The output layer has linear mapping. Each hidden units computes a nonlinear function of a measure distance between the network input and unit's weight vector [103]. e.g. Gaussian functions. A hybrid learning process for training RBFNN, which updates the radial basis function centers together with the output weights is suggested in [104]. The training of radial basis function neural networks offers a solution to the tradeoff between performance and training speed and can make RBFNN serious competitors to feed forward neural networks (FFNNs). Lin proposed the design of a fuzzy sliding mode loss-minimization control for the speed of a PMSG and a high-performance on-line training (RBFNN) for the turbine pitch angle control [105]. Ming proposed the design of a high performance on-line training of RBFNN using back-propagation learning algorithm regulating controller for the sensor less control of a PMSG [106].

CHAPTER 3

PMSG WIND GENERATOR SYSTEM MODEL

A PMSG connected to a power grid is shown in Fig. 3.1. The wind turbine shaft is directly coupled to the generator rotor. The generator is connected to the full scale back-to-back converters. The generator side and grid side back-to-back converters are connected to each other through a DC link capacitor. The superconducting magnetic energy storage device is connected at the inverter terminal along with a local load. The inverter terminal is connected to the transmission line through a step-up transformer. The system dynamic model consist PMSG, wind turbine, the converters, model SMES, load and the transmission line.
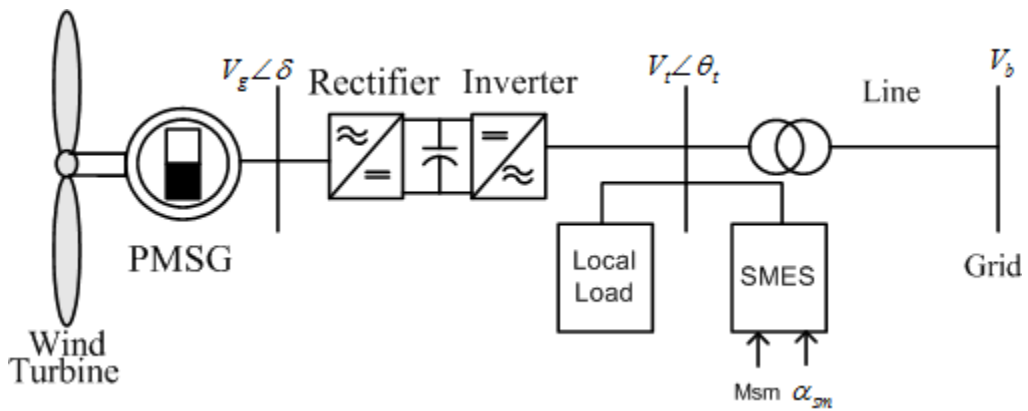
Figure 3.1 PMSG wind generation system with local load and SMES

3.1 Nonlinear Model

3.1.1 Permanent Magnet Synchronous Generator Model

The dynamic model of PMSG is derived from two-phase synchronous reference frame in which the q-axis is ahead of $90°$ by d-axis with respect to the direction of rotation, following assumptions considered in the modeling are

1. Negligible iron losses.
2. Electric and magnetic symmetry.
3. Sinusoidal distribution of stator winding.
4. Unsaturated magnetic circuit.

The relationship of voltage-current-flux for PMSG are written as,

$$\psi_d = -x_d i_{gd} + x_{afd} i_{fd} \tag{3.1}$$

$$\psi_q = -x_q i_{gq} \tag{3.2}$$

$$\psi_{fd} = -x_{afd} i_{gd} + x_{ffd} i_{fd} \tag{3.3}$$

$$v_{gd} = -R_a i_{gd} - \omega\psi_q + \frac{\dot{\psi}_d}{\omega_\circ}$$
$$\tag{3.4}$$
$$v_{gq} = -R_a i_{gq} + \omega\psi_d + \frac{\dot{\psi}_q}{\omega_\circ}$$

$$x_{afd} i_{fd} = \psi_\circ \tag{3.5}$$

where, $\psi_\circ$ is the flux that is constant due to permanent magnets, ψ_d and ψ_q are d-q

fluxes.

Using eq (3.5), eq (3.1) and (3.4) becomes,

$$\psi_d = -x_d i_{gd} + \psi_\circ \tag{3.6}$$

$$v_{gd} = -R_a i_{gd} - x_q i_{gq} + \frac{X_d}{\omega_\circ} \dot{i}_{gd}$$

$$v_{gq} = -R_a i_{gq} - \omega x_d i_{gd} + \omega \psi_\circ - \frac{X_q}{\omega_\circ} \dot{i}_{gq} \tag{3.7}$$

where, ω is stator frequency, R_a is the stator winding resistance, v_{gd} and v_{gq} are

d-q axis generator bus voltages

The stator d-q axis voltages of PMSG is shown in Fig. 3.2,
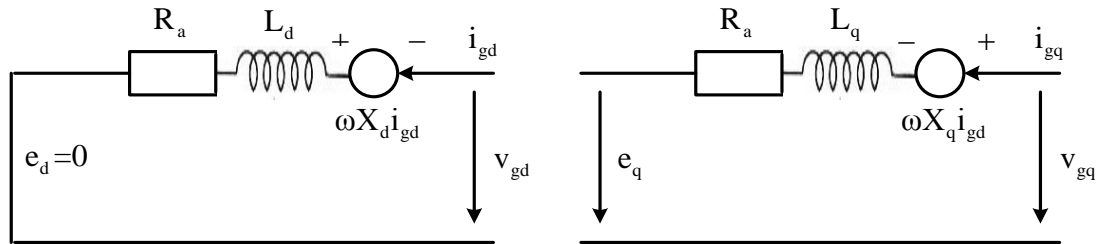
Figure 3.2 Equivalent circuit of PMSG in the synchronous frame

The d-q axis generator currents equations can be written from eq (3.7) as,

$$\dot{i}_{gd} = \frac{\omega_o}{x_d}(R_a i_{gd} + x_q i_{gq}\omega - v_{gd})$$

$$\dot{i}_{gq} = \frac{\omega_o}{x_q}(-x_d i_{gd}\omega - R_a i_{gq} + \psi_o\omega - v_{gq})$$

(3.8)

where, $\dot{i}_{gd}$ and $\dot{i}_{gq}$ are d-q axis generator currents.

The rotor angle of the PMSG is given by,

$$\dot{\delta} = \omega_o(\omega - 1)$$

(3.9)

3.1.2 Wind Turbine Model and Drive Train Model

The mechanical power captured by a wind turbine can be written as,

$$P_m = \frac{1}{2}\xi.A_r.V_w^3.C_p(\psi,b)$$

(3.10)

where, ξ is the air density , A_r is the blade swept area, V_w is the wind speed, and C_p is the dimensionless power coefficient and is a nonlinear function of ψ and b, ψ is the tip speed ratio, b is the blade pitch angle.

The expression for C_p is [107],

$$C_p(\psi_k,b) = 0.5176(\frac{116}{\psi_k} - 0.4b - 5).e^{\frac{-21}{\psi_k}} + 0.0068\psi$$

(3.11)

where,

$$\frac{1}{\psi_k} = \frac{1}{\psi + 0.08b} - \frac{0.035}{b^3 + 1}$$

$$\psi = \frac{R_{blade}.\omega_{blade}}{V_W}$$

(3.12)

where, ω_{blade} is the blade angular speed , R_{blade} is the blade radius.

The variation of mechanical power with respect to the turbine speed for a particular wind speed at blade pitch angle b=0°, is shown in Fig. 3.3
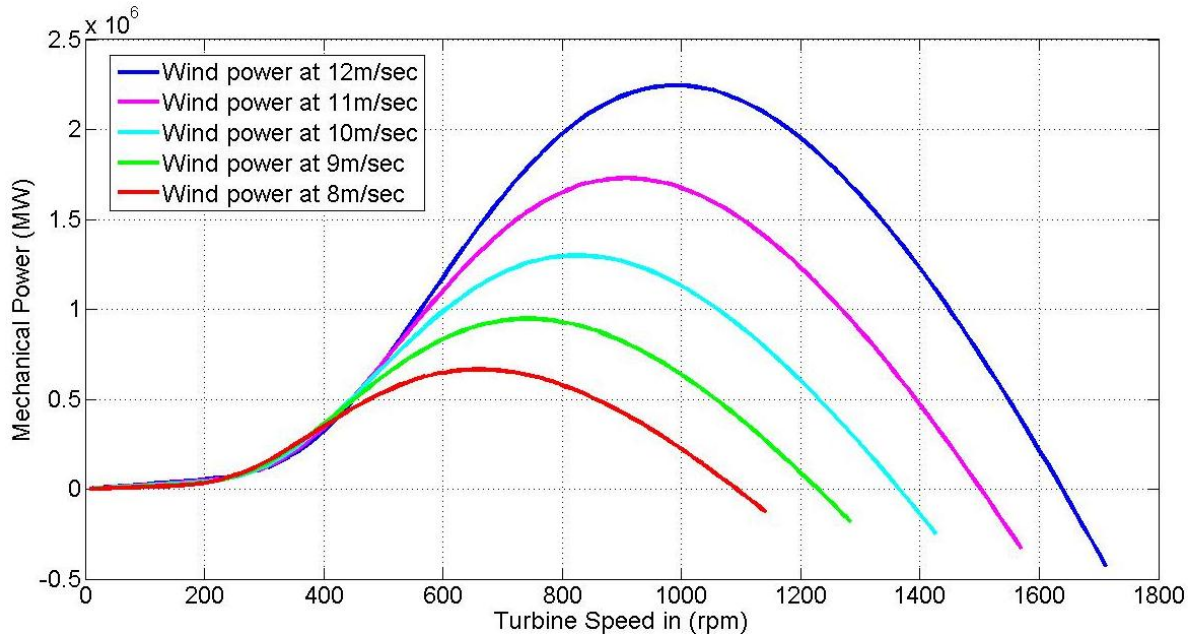
Figure 3.3 Mechanical power for various wind speed at blade pitch angle b=0°

PMSG wind systems are adapted for gearless operation. This solution has become more reliable, more efficient and less noisy. The two-mass drive train model shown in Fig. 3.4 is used in this study. The equivalent shaft stiffness of the two-mass system is K_S. The H_t and H_g represent the inertia constant (sec) of wind turbine and generator respectively.
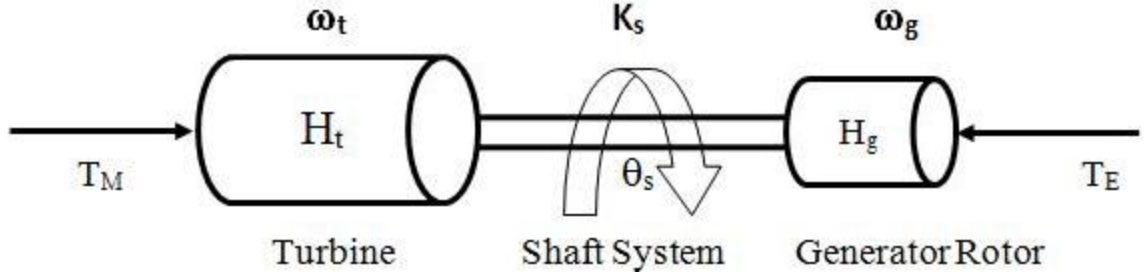
Figure 3.4 The two-mass shaft model

The generator speed, shaft twist angle and turbine speed for two-mass system are expressed as,

$$\dot{\omega} = \frac{1}{2H_g}(K_s\theta_s - P_e - D_g(\omega - 1)) \tag{3.13}$$

$$\dot{\theta}_s = \omega_o(\omega_t - \omega) \tag{3.14}$$

$$\dot{\omega}_t = \frac{1}{2H_t}(P_m - K_s\theta_s - D_t(\omega_t - 1)) \tag{3.15}$$

where, D_g and D_t are damping coefficients of the turbine and generator respectively, P_m is the mechanical power of the rotor.

3.1.3 Power Electronic Converters

In permanent magnet synchronous generator, the generated power is variable both in frequency and voltage. The power electronic interface is required to convert the variable voltage and frequency into a constant grid voltage and frequency. A back-to-back PWM-VSI based bi-directional power converters is

used as shown in Fig. 3.5. The generator side converter acts as a rectifier and the grid side converter as inverter. Both of them are considered to be lossless in this study.
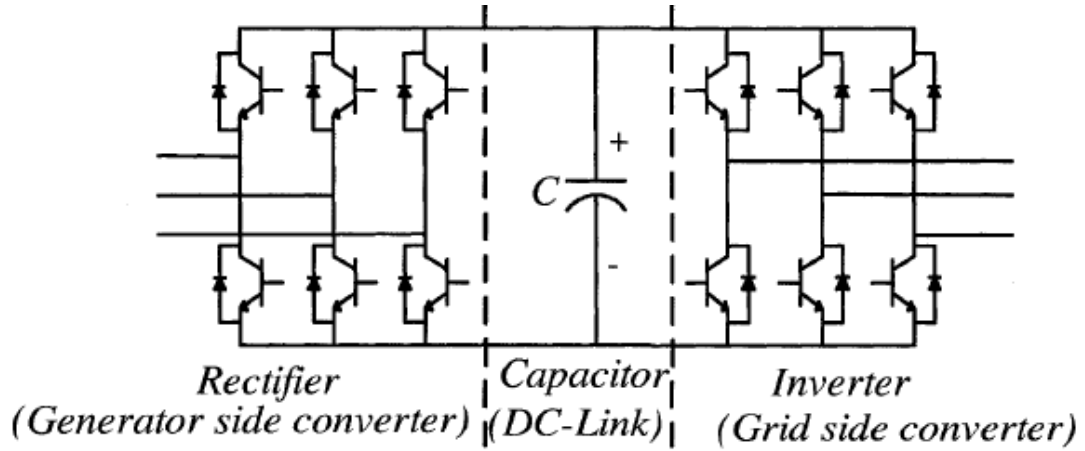
Figure 3.5 Schematic of Back-to-Back Converter

Rectifier output is connected to the DC link capacitor with voltage V_c, rectifier d-q axis voltage V_{gd} and V_{gq} can be written as,

$$v_{gd} = m_{gc} V_c \cos \alpha_{gc} \tag{3.16}$$

$$v_{gq} = m_{gc} V_c \sin \alpha_{gc} \tag{3.17}$$

where, m_{gc} and α_{gc} are the modulation index and firing angle of the rectifier (generator side converter), similar to the rectifier converter, the inverter equations can be written as

$$v_{id} = m_{ic} V_c \cos \alpha_{ic} \tag{3.18}$$

$$v_{iq} = m_{ic} V_c \sin\alpha_{ic} \tag{3.19}$$

where, V_{id} and V_{iq} are d-q axis voltage of the inverter, m_{ic} and α_{ic} are the modulation index and firing angle of the grid side converter.

3.1.4 DC-Link Capacitor

From power balance at the DC capacitor we get,

$$CV_c \frac{dV_c}{dt} = P_{in} - P_o \tag{3.20}$$

where, C is the capacitance of DC-Link capacitor.

The electrical power to the rectifier is

$$P_{in} = v_{gd} i_{gd} + v_{gq} i_{gq} \tag{3.21}$$

The power output from the inverter is

$$P_o = v_{id} i_{id} + v_{iq} i_{iq} \tag{3.22}$$

Here, i_{id} and i_{iq} are d-q axis currents of the inverter.

By using set of equations (3.16) to (3.19) and (3.21-22), equation (3.20) becomes

$$\dot{V}_c = \frac{1}{C}(m_{gc} i_{gd} \cos\alpha_{gc} + m_{gc} i_{gq} \sin\alpha_{gc} - m_{ic} i_{id} \cos\alpha_{ic} - m_{ic} i_{iq} \cos\alpha_{ic}) \tag{3.23}$$

3.1.5 The Inverter Model
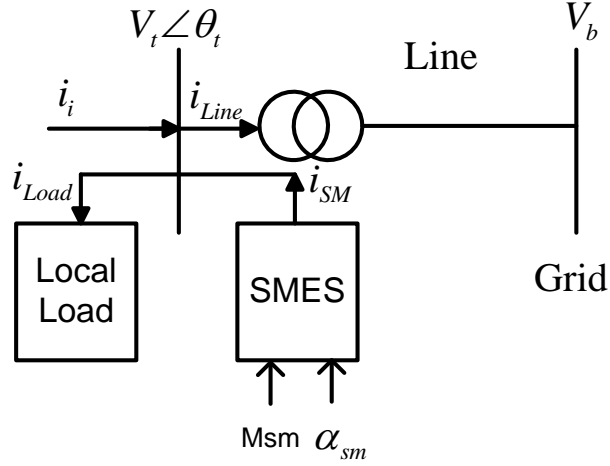
Figure 3.6 Grid side section of the system

Referring Fig 3.6, the KCL at the inverter bus gives

$$i_i + i_{SM} = i_{Load} + i_{Line} \tag{3.24}$$

where, i_i is the inverter current, i_{SM} is the SMES current, i_{Load} is the load current and i_{Line} is transmission line current.

$$(i_{id} + ji_{iq}) + (i_{smd} + ji_{smq}) = V_t Y_{Load} + (V_t - V_b) Y_{Line} \tag{3.25}$$

Assuming that the grid bus voltage is along d-axis and breaking (3.25) along d-q axes give,

$$v_{td} = k_1(i_{id} + i_{smd}) + k_2(i_{iq} + i_{smq}) + (k_1 g_{Line} + k_2 b_{Line}) V_b \tag{3.26}$$

$$v_{tq} = k_3(i_{id} + i_{smd}) + k_4(i_{iq} + i_{smq}) + (k_3 g_{Line} + k_4 b_{Line}) V_b \tag{3.27}$$

where,

$$\begin{pmatrix} k_1 & k_2 \\ k_3 & k_4 \end{pmatrix} = \begin{pmatrix} (g_{Load}+g_{Line}) & -(b_{Load}+b_{Line}) \\ (b_{Load}+b_{Line}) & (g_{Load}+g_{Line}) \end{pmatrix}^{-1}$$

(3.28)

Referring to Fig. 3.6, the KVL at the inverter bus the inverter voltage equations as,

$$V_i = V_t + R_i i_i + \frac{x_i}{\omega_o}\dot{i}_i$$

(3.29)

where, $V_i = v_{id} + jv_{iq}$, $V_t = v_{td} + jv_{tq}$

(3.30)

Putting the d-q axis components of V_i, V_t and i_i into (3.29), the d-q axis currents of the inverter is written as,

$$\dot{i}_{id} = (\frac{\omega_o}{x_i})(v_{id} - v_{td} - R_i i_{id} + \omega x_i i_{iq})$$

(3.31)

$$\dot{i}_{iq} = (\frac{\omega_o}{x_i})(v_{iq} - v_{tq} - R_i i_{iq} - \omega x_i i_{id})$$

(3.32)

Here, Y_{Line} and Y_{Load} are the admittance of the line and the local load respectively, v_{td} and v_{tq} are the d-q axis voltage of the AC bus, i_{smd} and i_{smq} are the bi-directional d-q axis currents of the SMES, i_{id} and i_{iq} are the d-q axis currents of the inverter (grid side converter), V_b is the grid voltage, g and b represent conductance and susceptance of the subscripts and $Z_i = R_i + jX_i$ is the impedance between the inverter and the AC bus.

3.1.6 Superconducting Magnetic Energy Storage (SMES) System

SMES is capable of supplying both real and reactive power by adjusting the firing angle and the modulation index of its converter. The assumptions made in modeling are: (1) The superconducting coil resistance is zero because of heat dissipation, (2) it has a large inductance because of the high amount of energy storage, (3) the voltage drop in the converter is small, (4) harmonic power generated in the converter is also negligible [108,109]. The basic circuit diagram of the SMES with its controller unit is shown in Fig. 3.7. The SMES unit consists of a superconductive coil (SC) and an AC-to-DC power converter. The latter interfaces the DC current of the SC to an external AC bus. The power supplied can be properly controlled by tuning both modulation index (M_{SM}) and phase angle (α_{sm}) of the VSC. The values of modulation index and phase angle are computed from the demanded real and reactive powers.
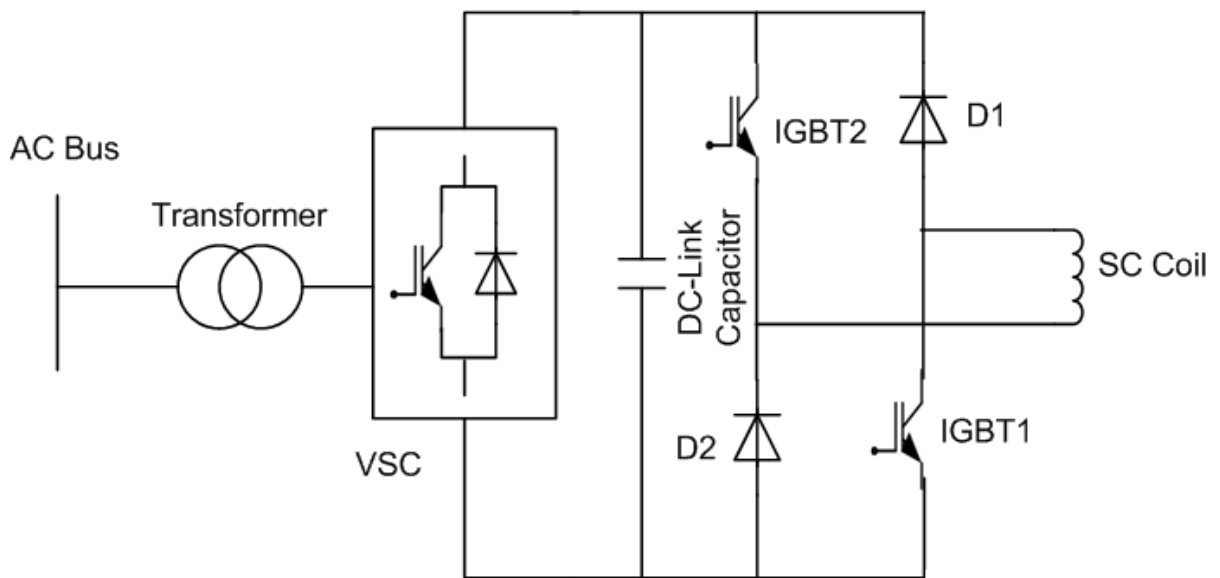
Figure 3.7 The SMES with its controller

The differential equation relating the change of DC current I_{smdc} of the SMES can be written as,

$$L_{sc}\dot{I}_{smdc}=-I_{smdc}R_{sc}+\sqrt{v_{td}^2+v_{tq}^2}\cos\alpha_{sm}-(\pi/12)I_{smdc}X_{cm}$$

(3.33)

The total DC current is,

$$I_{dc}=I_{smdc}+I_{smdco}$$ (3.33a)

The equations of the d-q axis currents of SMES,

$$i_{smd}=M_{SM}I_{dc}\cos(\theta_t-\alpha_{SM})$$ (3.34)

$$i_{smq}=M_{SM}I_{dc}\sin(\theta_t-\alpha_{SM})$$ (3.35)

The expressions for P_{SM}, Q_{SM} can be written as

$$P_{SM}=v_{td}i_{smd}+v_{tq}i_{smq}$$ (3.36)

$$Q_{SM}=v_{td}i_{smq}-v_{tq}i_{smd}$$ (3.37)

Referring to Figs. 3.8-9, at steady state the generator power error ΔP_g and generator bus voltage error ΔV_g will be zero but when the system is perturbed, the generator power P_g and generator bus voltage V_g will change from the steady state value. For the activation of the controller, reference power P_{gref} and reference voltage V_{gref} will be compared with power P_g and V_g. The dynamic process of compensating the power from SMES is depending on thyristor (or

40

IGBT) excitation angles α_{sm} and modulation index M_{SM} of VSC. Figs. 3.8-9 show that real power (P_{SM}) and reactive power (Q_{SM}) of SMES can be affected through variation of real power (ΔP_g) and terminal voltage (ΔV_g) of the wind generator.
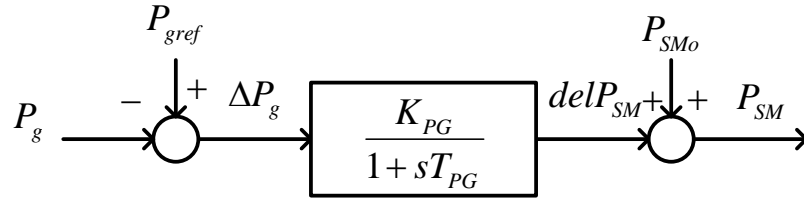
Figure 3.8 Block diagram of active power of SMES
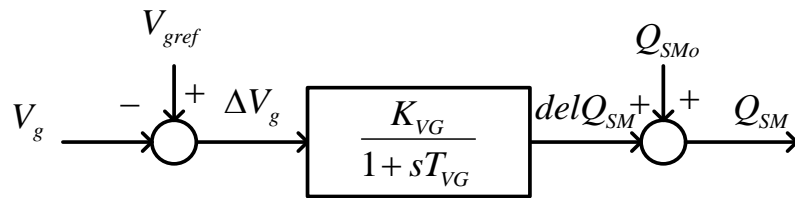
Figure 3.9 Block diagram of reactive power of SMES

The differential equations for the Figs. 3.8-9 can be written as

$$\text{del}\dot{P}_{SM} = \frac{1}{T_{PG}}(K_{PG}\Delta P_g\text{-delP}_{SM}) \tag{3.38}$$

$$\text{del}\dot{Q}_{SM} = \frac{1}{T_{VG}}(K_{VG}\Delta V_g\text{-delQ}_{SM}) \tag{3.39}$$

Using P_{SM} and Q_{SM} from Figs.3.8-9, signals M_{SM} and α_{SM} are generated as,

$$M_{SM} = \frac{\sqrt{P_{SM}{}^2 + Q_{SM}{}^2}}{V_t I_{dc}} \tag{3.40}$$

$$\alpha_{SM} = \tan^{-1}\left(\frac{Q_{SM}}{P_{SM}}\right) \tag{3.41}$$

Combining equation (3.8-19), (3.13-15), (3.23), (3.31-32), (3.33) and (3.38-39) the complete system model is written as,

$$\dot{X} = f\,[x, u] \tag{3.42}$$

Where $x = [i_{gd}, i_{gq}, \delta, \omega, \theta_s, \omega_t, V_c, i_{id}, i_{iq}, I_{smdc}, P_{sm}, Q_{sm}]$
$u = [K_{pg}, K_{vg}, T_{pg}, T_{vg}]$

u shows the SMES controller parameters. For proper function of the SMES controller these parameters need to be adaptively tuned.

3.2 Linear Model

The PMSG-SMES based WECS model described in the previous section is nonlinear. For optimization purposes, it is more convenient to work with linear model of Eq (3.42).

3.2.1 Permanent Magnet Synchronous Generator Model

Linearizing the equation (3.9-3.12), the PMSG stator d-q axis currents and rotor angle equations becomes,

$$
\begin{aligned}
\Delta \dot{i}_{gd} = &-\left(\frac{\omega_o R_a}{x_d}\right)\Delta i_{gd} + \left(\frac{\omega_o x_q}{x_d}\right)\Delta i_{gq} - \left(\frac{\omega_o}{x_d} m_{gco} V_{co}\cos\delta_o\right)\Delta\delta + \\
&\left(\frac{\omega_o x_q i_{gqo}}{x_d}\right)\Delta\omega - \left(\frac{\omega_o}{x_d} m_{gco}\sin\delta_o\right)\Delta V_c - \left(\frac{\omega_o}{x_d} V_{co}\sin\delta_o\right)\Delta m_{gc}
\end{aligned}
\tag{3.43}
$$

$$\Delta \dot{i}_{gq} = -(\frac{\omega_o x_d}{x_q})\Delta i_{gd} - (\frac{\omega_o R_a}{x_q})\Delta i_{gq} + (\frac{\omega_o}{x_q}m_{gco}V_{co}\sin\delta_o)\Delta\delta +$$

$$\frac{\omega_o}{x_q}(E_{FDo} - x_d \dot{i}_{gdo})\Delta\omega - (\frac{\omega_o}{x_q}m_{gco}\cos\delta_o)\Delta V_c - (\frac{\omega_o}{x_q}V_{co}\cos\delta_o)\Delta m_{gc} \qquad (3.44)$$

$$\Delta \dot{\delta} = \omega_o \Delta\omega \qquad (3.45)$$

3.2.2 Drive Train Model

For generator speed linearization, power P_e needs to be linearize which is appear in appendix B, so the linearized form of (3.13) is

$$\Delta \dot{\omega} = -\frac{(m_{gco}V_{co}\sin\delta_o + 2i_{gdo}R_a)}{2H_g}\Delta i_{gd} - \frac{(m_{gco}V_{co}\cos\delta_o + 2i_{gqo}R_a)}{2H_g}\Delta i_{gq} -$$

$$\frac{(m_{gco}V_{co}i_{gdo}\cos\delta_o - m_{gco}V_{co}i_{gqo}\sin\delta_o)}{2H_g}\Delta\delta - \frac{D_g}{2H_g}\Delta\omega + \frac{K_s}{2H_g}\Delta\theta_s - \qquad (3.46)$$

$$\frac{(m_{gco}i_{gdo}\sin\delta_o + m_{gco}i_{gqo}\cos\delta_o)}{2H_g}\Delta V_c - \frac{(V_{co}i_{gdo}\sin\delta_o + V_{co}i_{gqo}\cos\delta_o)}{2H_g}\Delta m_{gc}$$

Linearized version of (3.14) can be written as

$$\Delta \dot{\theta}_s = \omega_o(\Delta\omega_t - \Delta\omega) \qquad (3.47)$$

Finally, the linearized form of turbine speed is

$$\Delta \dot{\omega}_t = -\frac{K_s}{2H_t}\Delta\theta_s - \frac{D_t}{2H_t}\Delta\omega_t \qquad (3.48)$$

43

3.2.3 DC-Link Capacitor

For the linearization of DC-Link capacitor voltage equation (3.23), first we need to linearize P_{in}, P_{out}, v_{id} and v_{iq} which is appear in appendix B, so the linearized form of DC-Link capacitor voltage is

$$
\begin{aligned}
\Delta \dot{V}_c = {} & \frac{(m_{gco}\sin\delta_o)}{C}\Delta i_{gd} + \frac{(m_{gco}\cos\delta_o)}{C}\Delta i_{gq} + \frac{(m_{gco}i_{gdo}\cos\delta_o - m_{gco}i_{gqo}\sin\delta_o)}{C}\Delta\delta + \\
& \frac{(m_{gco}i_{gdo}\sin\delta_o + m_{gco}i_{gqo}\cos\delta_o - m_{ico}i_{ido}\cos\alpha_{ico} - m_{ico}i_{iqo}\sin\alpha_{ico})}{CV_{co}}\Delta V_c + \\
& \frac{(i_{gdo}\sin\delta_o + i_{gqo}\cos\delta_o)}{C}\Delta m_{gc} - \frac{(i_{ido}\cos\alpha_{ico} + i_{iqo}\sin\alpha_{ico})}{C}\Delta m_{ic} + \\
& \frac{(m_{ico}i_{ido}\sin\alpha_{ico} - m_{ico}i_{iqo}\cos\alpha_{ico})}{C}\Delta\alpha_{ic}
\end{aligned}
$$

$$(3.49)$$

3.2.4 Grid Side Converter Currents

First linearize $i_{smd}, i_{smq}, v_{td}, v_{tq}, v_{id}$ and v_{iq}, (3.31-32) can be linearized to

$$
\begin{aligned}
\Delta \dot{i}_{id} = {} & T_{38}\Delta\omega + T_{39}\Delta V_c + T_{53}\Delta i_{id} + T_{54}\Delta i_{iq} + T_{55}\Delta I_{SMDC} + T_{56}\Delta delP_{SM} \\
& + T_{57}\Delta delQ_{SM} + T_{48}\Delta m_{ic} - T_{49}\Delta\alpha_{ic}
\end{aligned}
$$

$$(3.50)$$

T_{XX} are the linearized constants, appear in appendix D.

The q-axis inverter current is

$$
\begin{aligned}
\Delta \dot{i}_{iq} = {} & T_{40}\Delta\omega + T_{41}\Delta V_c + T_{58}\Delta i_{id} + T_{59}\Delta i_{iq} + T_{60}\Delta I_{SMDC} + T_{61}\Delta delP_{SM} \\
& + T_{62}\Delta delQ_{SM} + T_{48}\Delta m_{ic} + T_{49}\Delta\alpha_{ic}
\end{aligned}
$$

$$(3.51)$$

3.2.5 Superconducting magnetic energy storage system

After the linearization of the PMSG model, The SMES current as well as the SMES compensated real and reactive power equations found in the nonlinear model are linearized at this stage. The detail of the linearization of SMES model is appearing in appendix B.

Linearized form of (3.33) can be written as

$$\Delta \dot{I}_{SMDC} = T_{63} \Delta i_{id} + T_{64} \Delta i_{iq} + T_{65} \Delta I_{SMDC} + T_{66} \Delta delP_{SM} + T_{67} \Delta delQ_{SM} \tag{3.52}$$

After linearizing the (3.38), the deviation of SMES real power is,

$$
\begin{aligned}
\Delta \dot{delP}_{SM} = & -\frac{K_{PG}}{T_{PG}}(m_{gco}V_{co}\sin\delta_o + 2i_{gdo}R_a)\Delta i_{gdo} - \frac{K_{PG}}{T_{PG}}(m_{gco}V_{co}\cos\delta_o + 2i_{gqo}R_a)\Delta i_{gqo} - \\
& \frac{K_{PG}}{T_{PG}}(m_{gco}V_{co}i_{gdo}\cos\delta_o - m_{gco}V_{co}i_{gqo}\sin\delta_o)\Delta\delta - \\
& \frac{K_{PG}}{T_{PG}}(m_{gco}i_{gdo}\sin\delta_o + m_{gco}i_{gqo}\cos\delta_o)\Delta V_c - \frac{1}{T_{PG}}\Delta delP_{SM} - \\
& \frac{K_{PG}}{T_{PG}}(V_{co}i_{gdo}\sin\delta_o + V_{co}i_{gqo}\cos\delta_o)\Delta m_{gc}
\end{aligned}
\tag{3.53}
$$

And linearized form of (3.39) gives,

$$\Delta del\dot{Q}_{SM} = -\frac{K_{VG}}{T_{VG}V_{go}}(m_{gco}V_{gdo}V_{co}\cos\delta_o + m_{gco}V_{gqo}V_{co}\sin\delta_o)\Delta\delta -$$

$$\frac{K_{VG}}{T_{VG}V_{go}}(m_{gco}V_{gdo}\sin\delta_o + m_{gco}V_{gqo}\cos\delta_o)\Delta V_c - \frac{1}{T_{VG}}\Delta del Q_{SM} -$$

$$\frac{K_{VG}}{T_{VG}V_{go}}(V_{gdo}V_{co}\sin\delta_o + V_{gqo}V_{co}\cos\delta_o)\Delta m_{gc}$$

(3.54)

Combining the above state equations from (3.43-54) in a state form gives

$$\Delta\dot{x} = A\,\Delta x + B\,\Delta u$$

(3.55)

where, Δx is the change in original state. Appendix C gives the detail of the matrix A components. The Matrix A is given below.

$$
\begin{pmatrix}
\Delta \dot{i}_{gd} \\
\Delta \dot{i}_{gq} \\
\Delta \dot{\delta} \\
\Delta \dot{\omega} \\
\Delta \dot{\theta}_{s} \\
\Delta \dot{\omega}_{t} \\
\Delta \dot{V}_{c} \\
\Delta \dot{i}_{id} \\
\Delta \dot{i}_{iq} \\
\Delta \dot{I}_{dc} \\
\Delta \dot{P}_{SM} \\
\Delta \dot{Q}_{SM}
\end{pmatrix}
=
\begin{pmatrix}
a(1,1) & a(1,2) & a(1,3) & a(1,4) & 0 & 0 & a(1,7) & 0 & 0 & 0 & 0 & 0 \\
a(2,1) & a(2,2) & a(2,3) & a(2,4) & 0 & 0 & a(2,7) & 0 & 0 & 0 & 0 & 0 \\
0 & 0 & 0 & a(3,4) & 0 & 0 & 0 & 0 & 0 & 0 & 0 & 0 \\
a(4,1) & a(4,2) & a(4,3) & a(4,4) & a(4,5) & 0 & a(4,7) & 0 & 0 & 0 & 0 & 0 \\
0 & 0 & 0 & a(5,4) & 0 & a(5,6) & 0 & 0 & 0 & 0 & 0 & 0 \\
0 & 0 & 0 & 0 & a(6,5) & a(6,6) & 0 & 0 & 0 & 0 & 0 & 0 \\
a(7,1) & a(7,2) & a(7,3) & 0 & 0 & 0 & a(7,7) & a(7,8) & a(7,9) & 0 & 0 & 0 \\
0 & 0 & 0 & a(8,4) & 0 & 0 & a(8,7) & a(8,8) & a(8,9) & a(8,10) & a(8,11) & a(8,12) \\
0 & 0 & 0 & a(9,4) & 0 & 0 & a(9,7) & a(9,8) & a(9,9) & a(9,10) & a(9,11) & a(9,12) \\
0 & 0 & 0 & 0 & 0 & 0 & 0 & a(10,8) & a(10,9) & a(10,10) & a(10,11) & a(10,12) \\
a(11,1) & a(11,2) & a(11,3) & 0 & 0 & 0 & a(11,7) & 0 & 0 & 0 & a(11,11) & 0 \\
0 & 0 & a(12,3) & 0 & 0 & 0 & a(12,7) & 0 & 0 & 0 & 0 & a(12,12)
\end{pmatrix}
\begin{pmatrix}
\Delta i_{gd} \\
\Delta i_{gq} \\
\Delta \delta \\
\Delta \omega \\
\Delta \theta_{s} \\
\Delta \omega_{t} \\
\Delta V_{c} \\
\Delta i_{id} \\
\Delta i_{iq} \\
\Delta I_{dc} \\
\Delta P_{SM} \\
\Delta Q_{SM}
\end{pmatrix}
\qquad (3.56)
$$

CHAPTER 4

THE SMES CONTROL STRATEGY

The SMES controller model presented in section 3.1.6 shows that the modulation index (M_{SM}) and phase angle (α_{SM}) are controlled depending on the variation of real power and terminal voltage of the generator bus. Controller parameters (K_{PG}, K_{VG}, T_{PG}, and T_{VG}) are considered constants for normal operation of the system. Since the system transients can vary significantly in a wind system, adjustment of the parameters is needed for satisfactory response over a wide range of operation. This chapter presents an adaptive strategy for tuning these parameters using radial basis function neural network (RBFNN). The control determination involves the following steps:

1. An improved particle swarm optimization which generates the optimum parameters of SMES controller for maximum system damping.

2. Training of the RBFNN is employed to select the SMES controller parameters at different operating conditions and different contingencies.

3. Finally, adapt the RBFNN weights to tune the controller parameters online depending on the transient variations.

The following section gives a brief review of the IPSO, RBFNN and an adaptive RBFNN methods employed in this work.

4.1 Improved Particle Swarm Optimization (IPSO) Algorithm

In improved particle swarm optimization (IPSO), each particle shows a candidate solution to the optimization problem. Each particle has its own direction and velocity in the search space. These movements of the particles are controlled by the best position in a search area and position a particle has visited. In this proposed improved particle swarm optimization, each particle updates its velocity and position by updating the inertia weight (w). Each particle modifies its velocity and position using the best solution among the particles achieved and gbest of neighborhood particles. It is same happen in the social society that the better decisions could make by the group of leaders. However, in standard PSO, only a gbest of neighborhood particles is employed. This process using some neighborhood particles that can be called 'intensifying' and 'enhancing' the social influence. Based on this technique, we should intensify these particles which could lead individuals to better fitness.

For the evaluation of each particle, eigenvalue based objective function will be used. Initially population is generated by stochastically and referred to as a search space. The characteristics of the algorithm can be represented as,

The IPSO uses a population of N particles, which is the dimension of the search space. The position of the ith particle x_i is represented as,

$$x_i(k) = \left[x_{i1}(k), x_{i2}(k), \ldots \ldots, x_{iN}(k) \right] \qquad (4.1)$$

where, k is the iteration number.

49

By adding velocity the position of the particles is updated by the following equation

$$x_i(k+1)=x_i(k)+v_i(k) \tag{4.2}$$

Each particle has its own search space area and search experience depending on objective function calculation. In IPSO mainly two algorithm work: global best (gbest) and local best (pbest). Their calculation is depending on cognitive and social components.

The ith particle velocity in IPSO is calculated as

$$v_i(k+1)=v_i(k)+c_1 rand_1(p_i(k)-x_i(k))+c_2 rand_2(p_g(k)-x_i(k)) \tag{4.3}$$

The parameters $rand_1$ and $rand_2$ are random values, which are uniformly distributed random numbers in the range [0, 1], c_1 and c_2 are the acceleration constant and $p_g(k)$ is the global best position it has visited.

The local best state of the particles is written as,

$$p_i(k)=\left[p_{i1}(k),p_{i2}(k),........,p_{iN}(k)\right] \tag{4.4}$$

The local best position can be updated as

$$p_i(k+1)=p_i(k) \qquad \text{if } J(x_i(k+1))\geq J(p_i(k)) \tag{4.5}$$

$$p_i(k+1)=x_i(k+1) \qquad \text{if } J(x_i(k+1))< J(p_i(k)) \tag{4.6}$$

50

In this thesis, minimization of the objective function J is used. The objective function can be calculated as

$$J=\sum_{i=1}^{N}(\varsigma(k)-\varsigma_0)^2 \tag{4.7}$$

$$\varsigma=\frac{-\sigma}{\sqrt{\sigma^2+\gamma^2}} \tag{4.8}$$

where, ς_0 is the preselected value of damping ratio, σ and γ are the real and imaginary parts of the eigenvalues of the linearized matrix A.

The movement of the particles is predicted by the global best position, the global position in the entire swarm can be defined as

$$p_{gbest}(k)\in\{p_{i1}(k),p_{i2}(k),........,p_{iN}(k)\}|J(p_{gbest}(k))=\min\{p_{i1}(k),p_{i2}(k),........,p_{iN}(k)\} \tag{4.9}$$

The velocity of the particle in the local best is calculated as

$$v_i(k+1)=v_i(k)+c_1\mathrm{rand}_1(p_i(k)-x_i(k))+c_2\mathrm{rand}_2(p_{ilocalbest}(k)-x_i(k)) \tag{4.10}$$

Where $p_{ilocalbest}$ is the local best position. $p_{ilocalbest}$ can be define as

$$p_{ilocalbest}(k+1)\in\{N_i|J(p_{ilocalbest}(k))=\min\{J(x)\}\}\quad\forall x\in N_i \tag{4.11}$$

Exploration and exploitation of an algorithm need to be under consideration. Exploration is the ability that the algorithm can explore the entire search space. Furthermore, exploitation is the ability that algorithm only focuses on an

optimum area and refines the solution. Inertia Weight plays a key role in the process of providing balance between exploration and exploitation process. The Inertia Weight determines the contribution rate of a particle's previous velocity to its velocity at the current time step. Selection of the suitable inertia weight enhances the performance and provides the excellent result. The inertia weight w is shown in (4.12).

$$w = w_{max} - \left(\frac{w_{max} - w_{min}}{iter_{max}} \right) iter \tag{4.12}$$

where, $iter_{max}$ is the maximum number of iterations and $iter$ is the current iteration number.

Improvement in the inertia weight helps to converge the objective function fast. The velocity equation for the gbest and local best with inertia weight can be written as,

$$v_i(k+1) = w v_i(k) + c_1 rand_1(p_i(k) - x_i(k)) + c_2 rand_2(p_g(k) - x_i(k)) \tag{4.13}$$

$$v_i(k+1) = w v_i(k) + c_1 rand_1(p_i(k) - x_i(k)) + c_2 rand_2(p_{ilocalbest}(k) - x_i(k)) \tag{4.14}$$

The major advantages of IPSO are: its simplicity, lower computational complexity, and lower computational effort due to its fast convergence. Because of the fast convergence, IPSO can be used for generating training data for neural network, optimization of cost function, pattern recognition, scheduling assignment and combination optimization.

A flowchart of IPSO algorithm, for generating the optimized parameters of SMES

controller is shown in figure 4.1.

Start

Generate the array of particles with random position and corresponding velocities.

Check the boundaries satisfication — No → Redefine the search area

Yes

Generate the population of Kpg,Kvg,Tpg and Tvg by using rand function.

Load System Information and calculate eigen values

Calculate the objective function of each set of controller parameters

$J<pbest$ — Yes → Set $pbest=J$

NO

Search gbest from all particles objective function (J')

$J'<gbest$ — Yes → Set $gbest=J'$

NO

Termination criteria satisfied — Yes → Algorithm Terminate

NO

By Updating the inertia weight, velocity and position

k=k+1

Figure 4.1 Flow Chart of the IPSO algorithm

54

4.1.1 Generation of Trainee Data by Using IPSO

The parameters in the (4.2 and 4.3) were initialized, the cognitive and social acceleration constants C_1 and C_2 were set to 2 [110]. The random numbers rand1 and rand2 were initialized by using "rand" function in MATLAB. The 100 sets of SMES controller parameters have been generated and name this set as the population of the parameters. Load the system information and calculate the eigenvalues for each set of the SMES controller parameters (K_{pg}, K_{vg}, T_{pg} and T_{vg}) from the population. From these eigenvalues, calculate the objective function by using (4.7). A loop runs for 50 iterations, during which the optimized controller parameters are generated using new inertia weight, position and velocity values, based on (4.12-14). The updates are made to the gbest and pbest parameters based on the minimized value of objective function of the particles. It was implemented to find the global best within the iterations. The stop condition was user defined on consideration of the applied problem. Generally, it could be in terms of optimized value or fixed iterations. In this scenario, the stop condition was considered to be a specific number of iterations. A set of 50 iterations provided considerably more stable predicted data than others. So in this work, 50 iterations have been fixed. The value that satisfies the objective function from the values extracted during each iteration was selected as an optimized value. A similar procedure followed to calculate the predicted position parameter of all the particles. One such process of optimization for each of the particles is considered as one iteration.

Now the data has been prepared for the training through artificial neural network. Here, Radial basis function neural network (RBFNN) was used to train the network.

4.2 Radial Basis Function Neural Network (RBFNN)

The radial basis function neural network (RBFNN) consists of three layers: input layer, hidden layer and output layer. The input units are directly connected to the hidden layer with hidden nodes. The hidden layer is fully connected to the output layer via output weights [111]. Figure 4.2 shows the RBFNN structure which has a single hidden layer, which is interconnected to the output layer by linear combination. The performance of the RBFNN is controlled by three parameters; center of the hidden units, the number of hidden units and the RBF functions.
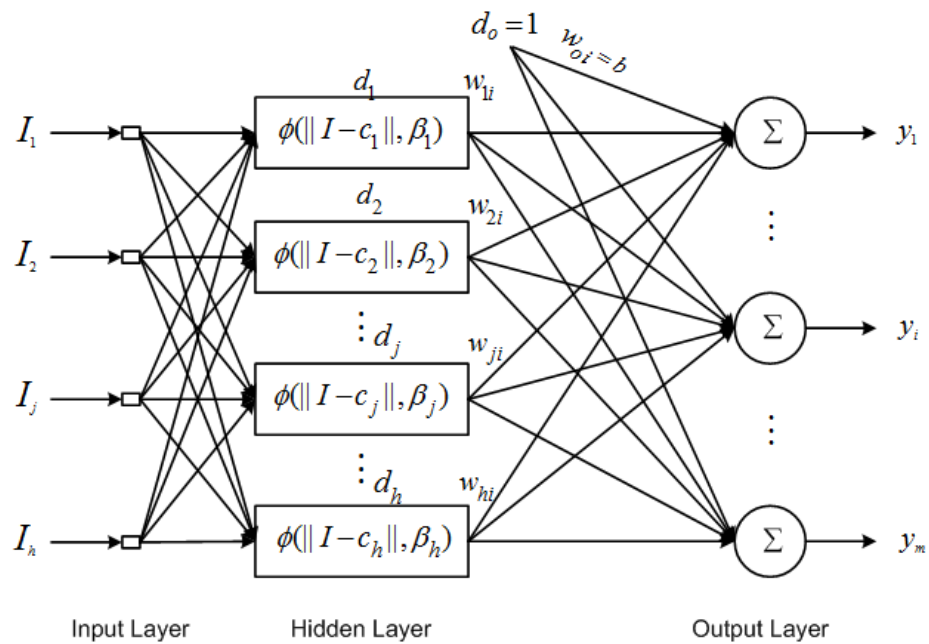
Figure 4.2 RBFNN Structure

For various types of contingencies, a trained network is needed, which identifies the SMES parameters under various contingencies. Here RBFNN is used for training the network. The response of RBFNN is linear with respect to its output-connection weights. This property guarantees fast convergence. Moreover, the local tune ability of the RBFNN reduces the training time and computational overhead and makes the RBFNN a good candidate for tuning. The radial basis function neural network (RBFNN) is a feed forward 3-Layer network that is based on radial basis functions like Gaussians as their activation function [112]. The basic activation function considers Gaussian distribution as shown in Fig. 4.3. This neural network consists of single hidden layer which are interconnected to an output layer by linear units. Every hidden unit calculates a nonlinear function by measuring the distance between the network input and the unit weight vector. This unit vector is usually called the center of the unit and distance is called the Euclidean distance. The Gaussian function is used as a basis function. This function mainly depends on two parameters β and c.

$$\phi(||I\text{-}c_j||,\beta)=\exp(\frac{\text{-}||I\text{-}c_j||}{\beta_j^2}) \tag{4.15}$$

where, I is the input vector, β is the spread factor and c_j is the jth center.

In the Gaussian function, output given by the neuron is maximum at the center and decreases when the neuron moves away from the center. A Gaussian

function is normally used for hidden neurons. The Gaussian function represented by the bell shaped curves as shown in Fig 4.3.
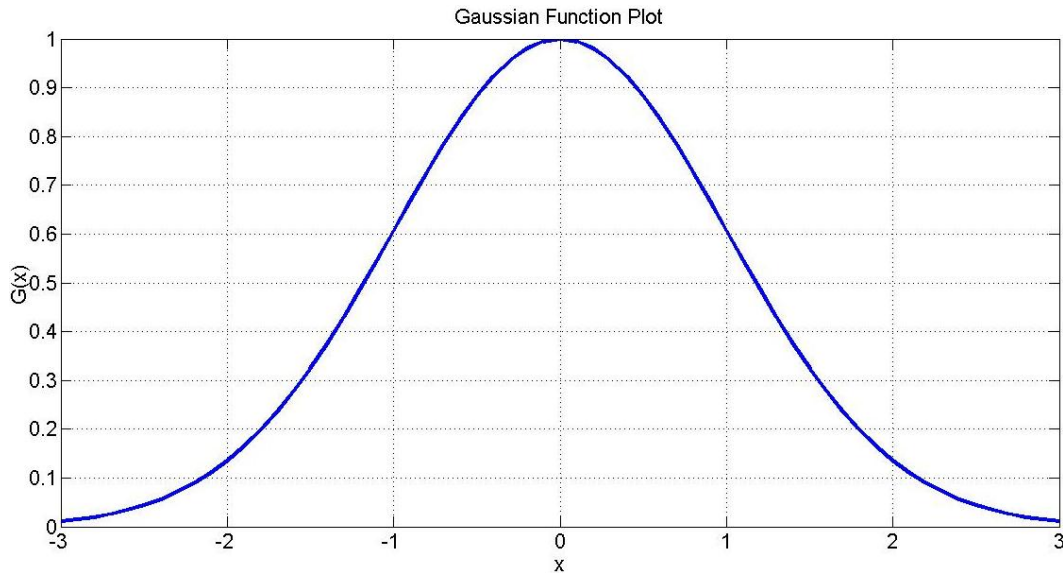
Figure 4.3 Bell shaped curve for Gaussian function

Fig 4.3 shows that the response of a neuron increases or decreases with the distance from the center. This represents that if an input vector which is coincides with the centroid of the cluster then the neuron representing that cluster will give the maximum output. As the distance of the input vector from the centroid of the cluster increases, the response of that cluster decreases. If the receptive fields of the neurons are overlapping, then all the neurons with overlapping fields will give output according to the distance of the vector from the cluster's centroid.

As previously mention that RBFNN is a feed forward 3-layer network. This hidden layer units takes p-dimensional input vector I_p with unit connection weights and calculate the Euclidean distance between input vector and the

center. This result passes to the Gaussian functions. The Hidden layer maps the input space onto a new space by performing the fixed nonlinear transformation. Then output layer performs the linear combination onto this new space by adjusting the weight matrix [113]. In this way RBFNN shows the map of p-dimensional input space to the m-dimensional output space. Equation (4.16) gives the output of the RBFNN is calculated as the weighted sum of the hidden layer outputs.

$$y_i = w_{oi} + \sum_{j=1}^{h} w_{ji} \varphi(||I\text{-}c_j||, \beta_j) \tag{4.16}$$

where, $i=1,2,3\ldots, m$; $j=1,2,3,\ldots, h$; h shows the hidden units; $||I\text{-}c_j||$ shows the Euclidean distance between input and the jth center; $\phi(.)$ is the nonlinear transfer function of the radial basis function; w_{ji} is the weight value between the ith center and j^{th} output node.

4.2.1 Training the Network Using RBFNN

The input vector (I) is directly connected to the single hidden layer with h nodes. It can be observed that h is the key factor not only for the performance but also the computational complexity of the network. For the hth hidden unit, c_h (h=1, 2, 3, ... h) denotes the mean vector of hth cluster. c_h is also known as the center vector or kernel vector. The hth hidden unit Euclidean net function for the pth training pattern can be calculated as

$$ED_p(n) = \sum_{n=1}^{N} (I_p(n) - c_h(n))^2 \qquad\qquad (4.17)$$

where, $c_h(n)$ is the nth element of c_h corresponding to the nth input unit. The mean vector parameter c_h and spread factor parameter β are conventional parameters of RBFNN. The hidden layer is fully connected to the output layer via output weights. So, the output will be calculated through (4.16).

The training mean square error (E_p) for each pattern can be calculated as

$$E_p = \sum_{i=1}^{m} [o_p(i) - y(i)]^2 \qquad\qquad (4.18)$$

where, o_p is the output calculated by IPSO and y is the output calculated by RBFNN and both are the column vectors.

The training data set consists of training patterns $\{I_p, o_p\}$. The input data (I_p) is achieved by taking the values of the generator current, generator angle, generator speed, DC-link capacitor voltage, the inverter current, generator power and terminal voltage at different operating conditions. While the controller parameters (K_{pg}, K_{vg}, T_{pg} and T_{vg}) for a particular operating condition is saved into an output vector. The weights of the hidden layer are trained through RBFNN algorithm. The training data of 800 sets are used in training process.

In RBFNN algorithm spread factor β is an important parameter respect to the input space. Spread factor β determines the width of an area in the input space to

which each neuron responds. If β is 0.1, then each RBF net hidden layer neuron will respond with 0.5 or more to any input vectors within a vector distance of 0.1 from their weight vector. The maximum response output equal to 1. In this work spread factor β is set to be 0.1. The error goal is set to be 0.02. The RBFNN is trained till an error goal 0.02 is reached. The algorithm takes the input vector and calculates the Euclidean distance by using eq (4.17). RBFNN algorithm adds neurons into the hidden layer and maps the input space onto a new space by performing the nonlinear function (Gaussian function). After calculating the nonlinear function, the output layer performs the linear combination by adjusting the weight matrix. Based on weight matrix, mean square error (E_p) of each pattern is calculated through eq (4.18). If E_p is greater than error goal which is defined at the start of the algorithm than add neuron into the hidden layer and repeat the procedure from the Euclidean distance calculation. But on the other hand if the E_p is meeting the error goal than algorithm will be terminated by saving the network to be recalled during simulations. This network is called RBFNN trained network. Fig 4.4 shows the flow chart of RBFNN algorithm.
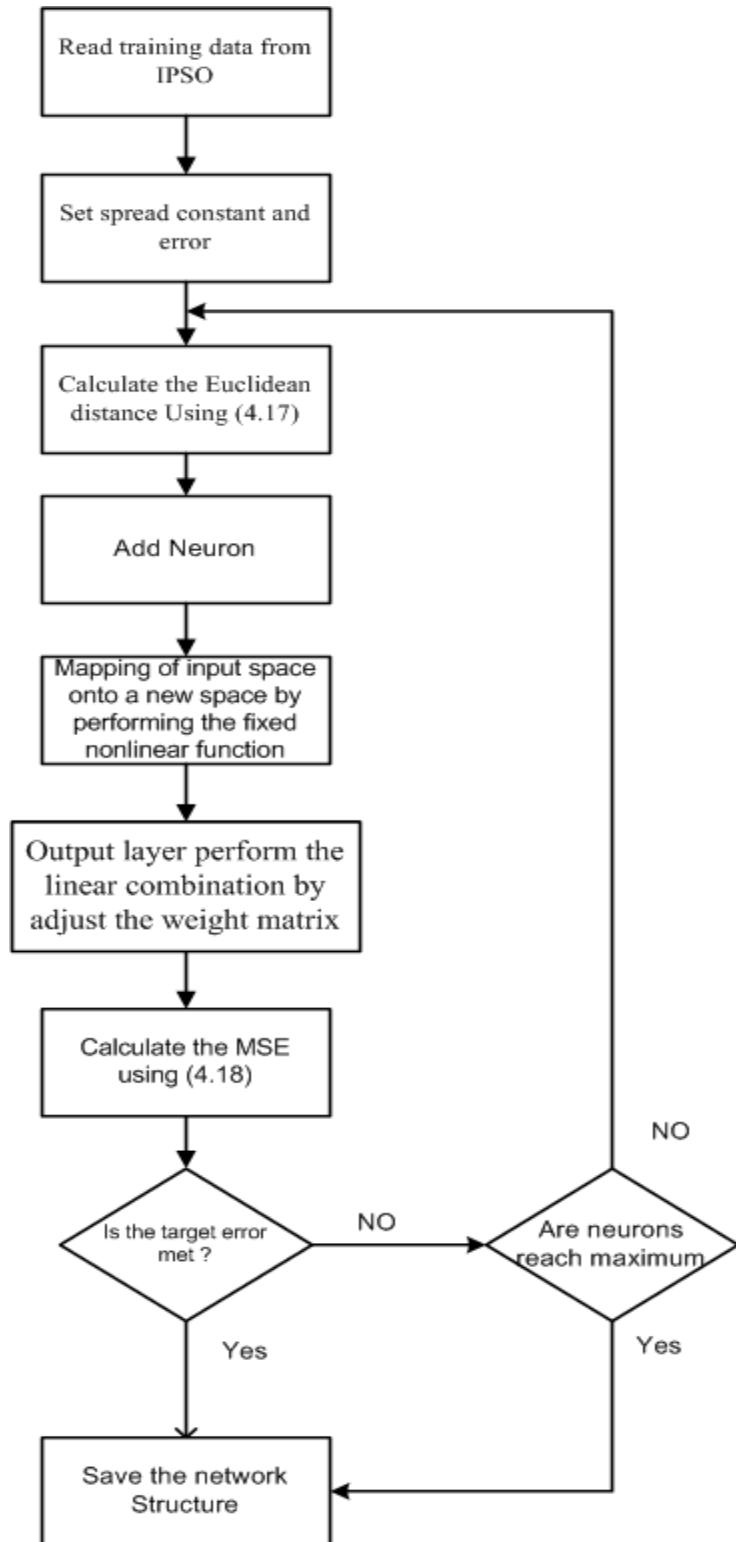
Figure 4.4   RBFNN learning algorithm flow chart

4.3 Adaptive RBFNN Algorithm

4.3.1 Introduction

Combining RBFNN with adaptive algorithm can form a robust control strategy for SMES, and its structure is shown in Fig. 4.5.
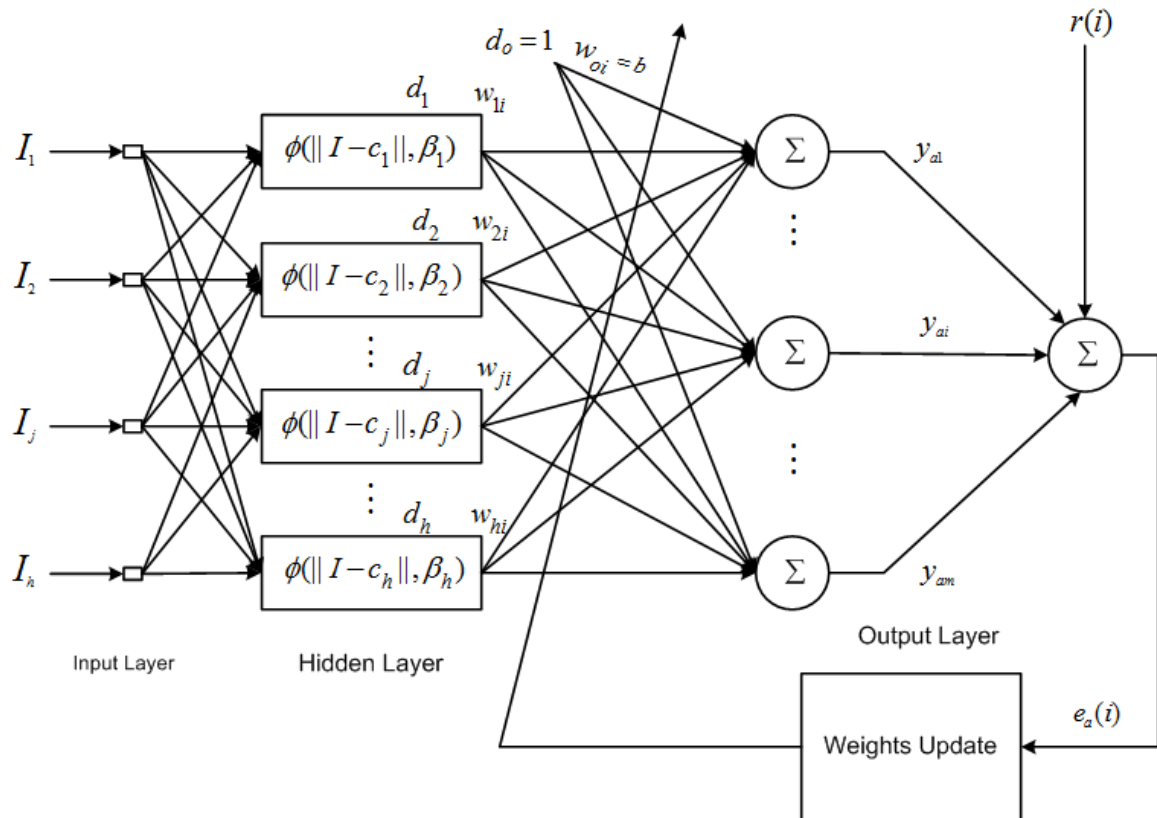
Figure 4.5 Structure of the adaptive RBFNN algorithm

RBFNN is used to tune parameters of the SMES controller to keep system stable in case of any disturbance, and it is adjusted according to the error between the input and output in its loop. The aim of the adaptive strategy is to make the SMES controller more powerful reference to different contingencies or different loading conditions. In case of

disturbance, the adaptive SMES controller based on RBFNN, will take effect more successfully. This approach not only ensures the PSMG performance and robustness of the system but also improves the online tuning for the SMES controller parameters at different contingencies.

Recently, the RBFNN has been widely used to model and approximate non-linear functions. Here a RBFNN is employed to model the relationship between the input variable I_p, and the system control, u. The weightings between hidden layer neurons and output layer neurons are adjusted based on an adaptive rule. Here, a RBFNN-based controller is proposed by an adaptive rule. The control input of the RBFNN controller is

$$u = \sum_{j=1}^{N} w_j \exp\left(\frac{-\|I - c_j\|^2}{\beta_j^2}\right) \tag{4.19}$$

The adaptive rule is used to adjust the weightings for searching the optimal weighting values and obtaining the stable convergence property. The adaptive rule is derived from the steepest descent rule to minimize the value of e_a with respect to w_j . Then the updated equation of the weighting parameters is [114],

$$w_{jnew} = w_{jold} + w_j(t+1) \tag{4.20}$$

where, $w_j(t+1)$ is the predicted value of weight vector, w_{jold} is the present value of the weight vector and w_{jnew} is the new value of the weight vector.

$$w_j(t+1) = -\eta \frac{\partial(e_a(t))^2}{\partial w_j(t)} \tag{4.21}$$

$$e_a(t)=r(t)-y(t) \tag{4.22}$$

where, $r(t)$ is the summation of the output of the RBFNN model, $y(t)$ is the output generated by the system, $k=1,2,3\ldots\ldots m$; η is the regulation factor.

The error e_a is a linear difference between r and y, used to update the weights vector.

Based on the chain rule, the equation (4.21) can be rewritten as,

$$w_j(t+1)=-\eta\frac{\partial(e_a(t))^2}{\partial u(t)}\frac{\partial u(t)}{\partial w_j(t)}=\rho e_a(t)\frac{\partial u(t)}{\partial w_j(t)} \tag{4.23}$$

$$w_j(t+1)=\rho e_{a(t)}\exp\left(\frac{-\|x-c_j\|^2}{\beta_j^2}\right)=\rho e_{a(t)}\phi_j \tag{4.24}$$

where, ρ is the learning rate parameter.

The overall weights of the network will be updated by using an adaptive RBFNN algorithm is,

$$w_{1new}=w_{1old}+w_1(t+1) \tag{4.25}$$

$$\vdots$$

$$w_{mnew}=w_{mold}+w_m(t+1) \tag{4.26}$$

4.4.2 The Adaptive RBFNN for SMES Controller

The model of adaptive control scheme is presented in Fig 4.6. The proposed adaptive strategy will be used to extract adaptive SMES controller parameters at different

contingencies. The input vector contains generator current, generator angle, generator speed, DC-link capacitor voltage, the inverter current, generator power and terminal voltage. This data set is used as input to the RBFNN for training. The output data set contains SMES controller parameters (K_{pg}, K_{vg}, T_{pg} and T_{vg}) are obtained by applying IPSO algorithm. When the network was trained, weight vector of the RBFNN was fixed. The proposed algorithm uses the RBFNN trained network as a reference model.

From Fig 4.6, SMES controller provides the appropriate signal of ΔP_{SM} and ΔQ_{SM} to the system to compensate the power. In order calculate the adaptive parameters of SMES controller, the adaptive RBFNN output y_a as close as possible to the desired output r, specified by the reference model. The error $e_a(t)$ between the reference model and outputs is generating by the system to adjust the weights of the RBFNN. The adaptive algorithm will allow the weights update between the hidden layer and the output layer using eq (4.20). When the system face the disturbance in terms of wind speed change or other type of disturbance, system parameters such as generator current, generator angle, generator speed, DC-link capacitor voltage, the inverter current, generator power and terminal voltage vary according to the disturbance. The reference model generates the new optimum values of K_{pg}, K_{vg}, T_{pg} and T_{vg}. By setting the new values of K_{pg}, K_{vg}, T_{pg} and T_{vg} as the targets, the predicted value of weights of the adaptive RBFNN is calculated using eq (4.21)-(4.24). After updating the weights, new values of SMES controller parameters are applied to the system for calculating the real and the reactive powers of SMES according to the demand.
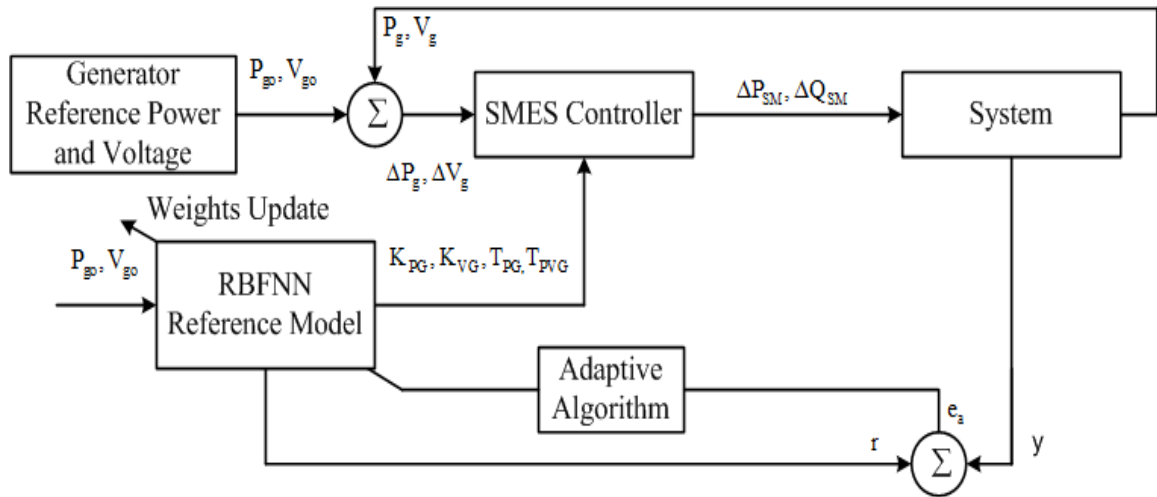
Figure 4.6 Model of adaptive control scheme

CHAPTER 5

SIMULATION RESULTS

The PMSG system given in Fig. 5.1 was simulated to test the adaptive SMES control strategy. Results are presented for different type of contingencies compared without any feedback control operation. Simulation studies involve the following.

1. Generation of optimum output training data for the neural network through IPSO.

2. Training the radial basis function neural network (RBFNN) to generate nominal weighting function for the RBFNN controller.

3. Testing the controller considering different contingencies.

The system data is appearing in appendix A.
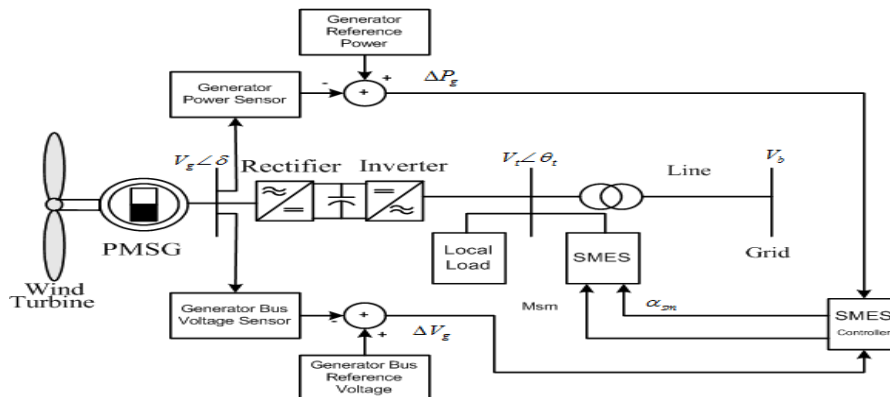
Figure 5.1 Configuration of PMSG system with proposed SMES controller

5.1 Generation of Optimum Training Data through IPSO

The training data for the radial basis function neural network (RBFNN) is generated using the improved particle swarm optimization (IPSO). The IPSO finds the optimum set of SMES controller parameters for given initial condition. The algorithm begins with the generator current, generator angle, generator speed, DC-link capacitor voltage, the inverter current, generator power and terminal voltage as input and generates the population of size 100 by taking the random values of SMES controller parameters (K_{pg}, K_{vg}, T_{pg} and T_{vg}). The IPSO algorithm set the minimum and maximum values of the SMES controller parameters as,

$$
\begin{aligned}
-30 \le K_{PG} \le 30 \\
-30 \le K_{VG} \le 30 \\
0.001 \le T_{PG} \le 1 \\
0.001 \le T_{VG} \le 1
\end{aligned}
\tag{5.1}
$$

The IPSO tries to find the optimum values of SMES controller parameters within the above range.

SMES controller parameters were optimized using IPSO, which made use of an eigenvalue based objective function to obtain the optimized parameters. The objective function to be minimized is written as,

$$
J = \sum_{i=1}^{N} (\varsigma(k) - \varsigma_o)^2
\tag{5.2}
$$

where, ς_o is the preselected value of damping ratio.

For a torque pulse of 20% for 0.3sec, Fig 5.2 shows the convergence characteristic of the IPSO objective function (J) for one step size of simulation time. The IPSO converges the objective function to the optimum value in 22 iterations. The convergence of the SMES controller parameters are shown in Figs. 5.3, 5.4, 5.5 and 5.6 as a function of no. of iterations for a same step size as that of Fig. 5.2. The optimized SMES controller parameters for one step size of simulation time for 20% torque pulse are given in Table 2.

Disturbance	K_{pg}	K_{vg}	T_{pg}	T_{vg}
Torque pulse of 20% for 0.3sec	3.75	9.25	0.2001	0.23

Table 2 Optimum SMES controller parameters for one step size of simulation time for 20% torque pulse for 0.3 sec.
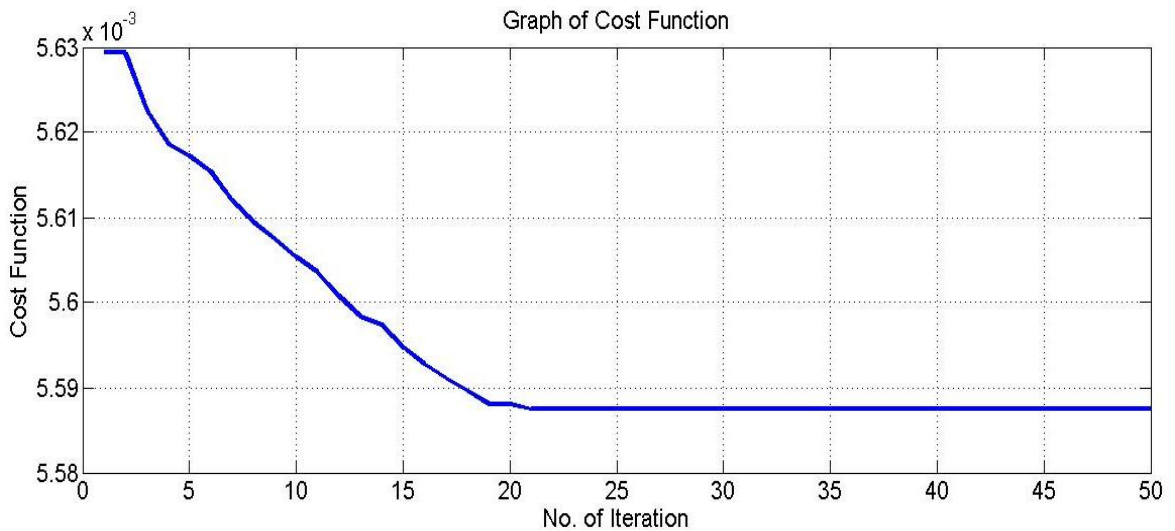
Figure 5.2 Cost functions vs. no of iterations for a disturbance of input torque pulse of 20% for one time step.
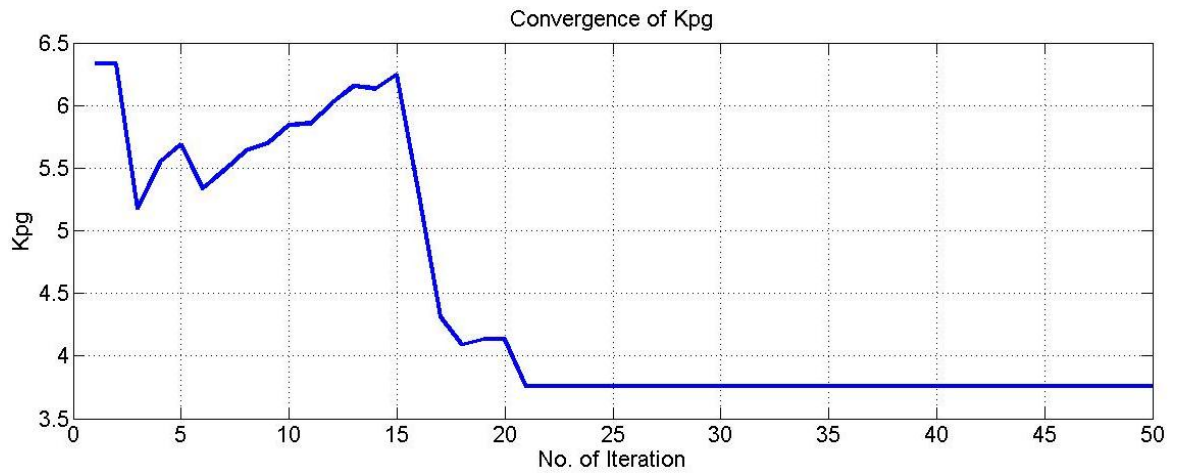
Figure 5.3 Convergence of Kpg vs. no. of iterations for a disturbance of input torque pulse of 20% for one time step.
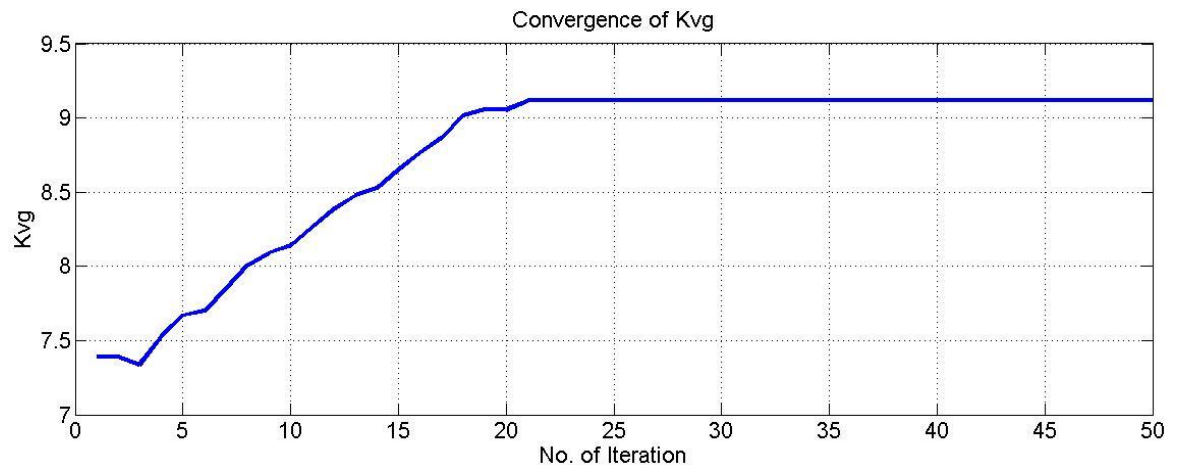
Figure 5.4 Convergence of Kvg vs. no. of iterations for a disturbance of input torque pulse of 20% for one time step.
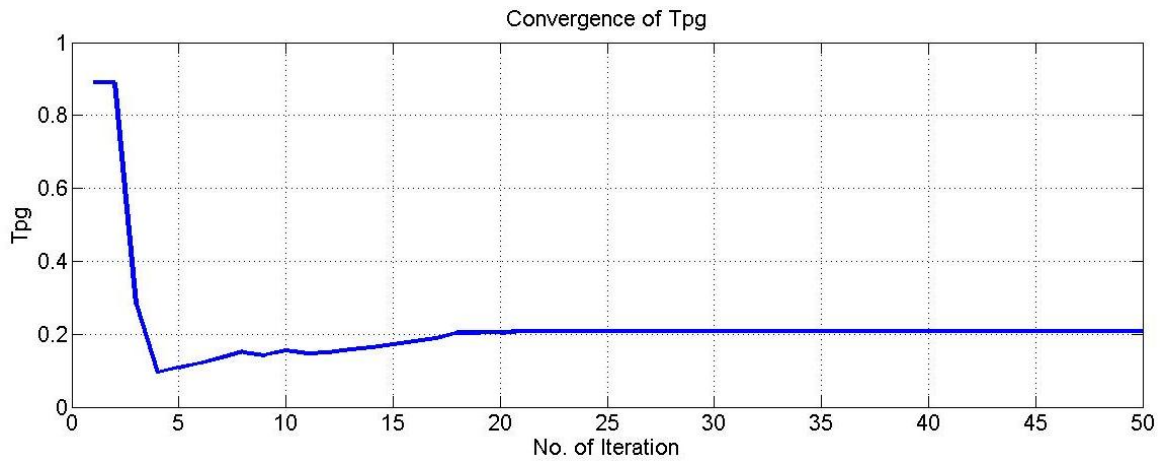
Figure 5.5 Convergence of Tpg vs. no. of iterations for a disturbance of input torque pulse of 20% for one time step.
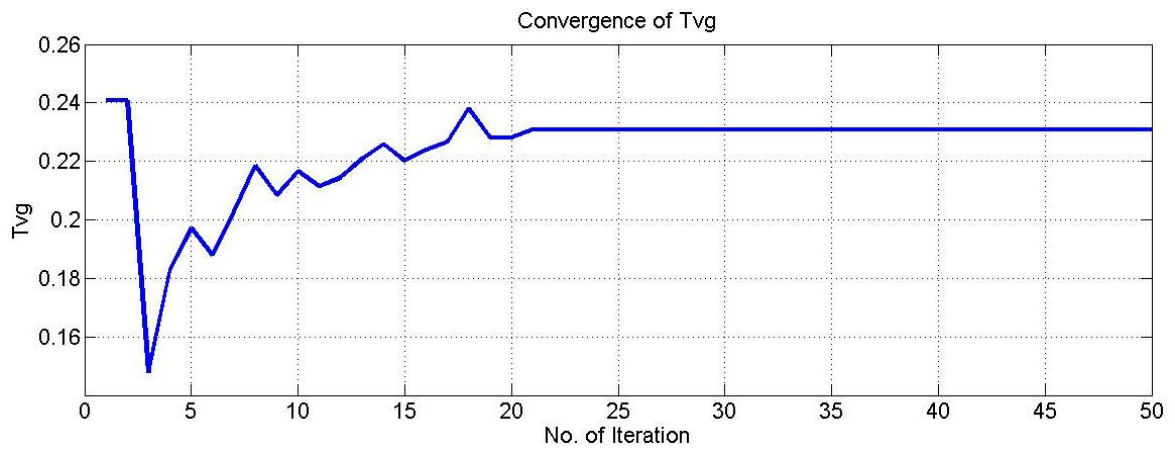
Figure 5.6 Convergence of Tvg vs. no. of iterations for a disturbance of input torque pulse of 20% for one time step.

5.2 Eigen Values of the Closed Loop System

The eigenvalues of the system as shown in Fig 5.1, without any control and with the proposed SMES control under a rated wind speed of V=9 m/s for one step size of simulation time are, respectively, listed in Table 3. The eigenvalues E_1-E_5 listed in Table 3 are related to the PMSG system whereas the eigenvalues E_6– E_8 refer to the proposed SMES unit. An examination of these eigenvalues listed in Table 3 reveals that the eigenvalues E_1 and E_2 are almost fixed on the complex plane. The system without the SMES unit has eigenvalue E_4 that is close to the imaginary axis of the complex plane. The damping of E_3- E_5 is improved when the proposed SMES system is included in the wind system.

With proposed SMES control, all the eigenvalues having damping at least greater than or equal to ς_0 and hence the resultant controller parameters found are optimal parameters that minimizes the objective function defined in (5.2).

Eigen Values	PMSG Without Control	PMSG With SMES
E_1	$-530.8766 \pm j1063.1562$	$-530.8766 \pm j1063.1560$
E_2	$-4.6210 \pm j377.3165$	$-4.6210 \pm j377.2155$
E_3	$-0.5778 \pm j27.6791$	$-4.8112 \pm j25.6013$
E_4	$-0.0998 \pm j4.0035$	$-0.7948 \pm j13.8378$
E_5	-1.0095	-1.0206
E_6	-	-10.1237
E_7	-	-9.9999
E_8	-	-0.5131

Table 3 System eigenvalues at 9 m/sec for the PMSG without control and with SMES control.

5.3 Generation of Nominal Weighting Function through RBFNN

The results of IPSO algorithm has been used to train the radial basis function neural network (RBFNN). The input vector contains generator current, generator angle, generator speed, DC-link capacitor voltage, the inverter current, generator power and terminal voltage, while the SMES controller parameters (K_{pg}, K_{vg}, T_{pg} and T_{vg}) are the outputs. In this learning process, a collection of input desired output pairs that would like the RBFNN to learn. For learning phase 800 input-output data sets were obtained. For online tuning using RBFNN, the centers and network weights are updated at each iteration. Initial centers which have been generated randomly in the input domain are updated based on how far the current input vector is away from the last updated centers (Euclidean distance). After calculating the Euclidean distance, the nonlinear function (Gaussian function) is updated. The outputs of the hidden layer can be calculated by updating the weight matrix.

The mean squared error (MSE) of RBFNN is calculated using eq (4.18). The MSE is set to 0.02 in this work. The training process continues till the targeted error is met as shown in Fig. 5.7. The training error converges in about 1625 epochs.
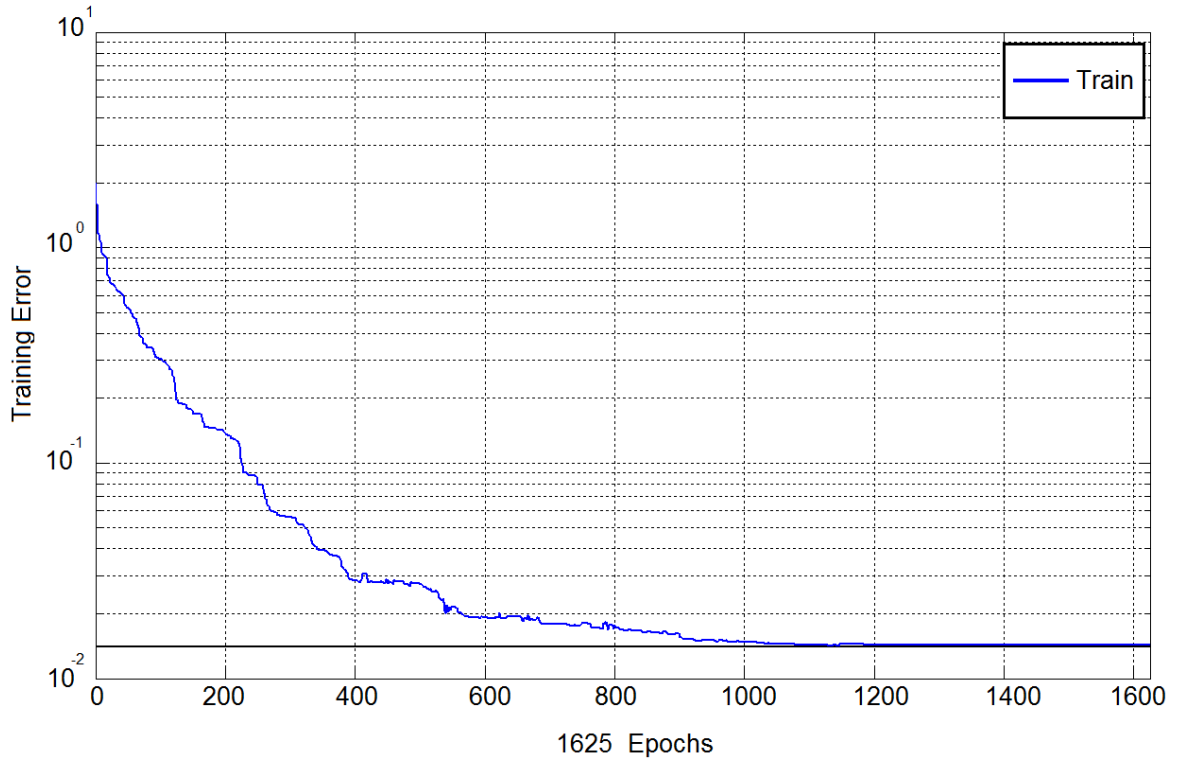
Figure 5.7 Mean squared error convergence of RBFNN

5.3 Testing Adaptive RBFNN SMES Controller

The adaptive RBFNN controller design procedure outlined in section 4.6.2 is tested through simulations of different disturbances on the PMSG system. The disturbances considered are

- Torque pulses of various magnitudes and duration
    1. Input torque pulse of 20% for 0.3sec.
    2. Input torque pulse of 10% for 2sec.
- Low voltage condition on the grid simulated through symmetrical 3-ϕ fault.
- Wind gust.

The responses recorded are the variations of generator stator current, generator speed, DC-link capacitor voltage, generator bus voltage, generated power, SMES real and reactive powers and SMES controller parameters.

5.3.1 Torque Pulse Disturbance

In this case two types of input torque pulses are considered. The application of short 20% input torque pulse is used to verify the robustness of the adaptively tuned SMES controller. Initially the wind generator is operating at 95% loading. This high loading conditions was intentionally used to study the worst case scenario. At this load even a relatively short disturbance throws the system into oscillations without any control.

Figs. 5.8-10 show the generator stator current, generator speed variation and DC-link capacitor voltage. It is evident from the Fig.5.8 that stator current of PMSG is effectively damped in 4 seconds. With the increase in input torque pulse of 20%, generator speed variation also increases but settles in about 4 seconds as is evident shown in Fig. 5.9. Since DC-link capacitor voltage fluctuation may cause grid frequency deviation, it is necessary to limit the DC-link voltage within ±5% range. Fig 5.10 shows that SMES successfully smoothens the DC-link voltage fluctuations in less than 4 seconds.

With a relatively large 10% input torque pulse for 2sec, the SMES adaptive controller takes the longer time to restore the normal operation. It can be observed from Figs. 5.11-12 that without any control the oscillations continue to grow and PMSG has to be disconnected. The variation in electrical power of PMSG is shown in Fig. 5.11. From Fig. 5.11, it can be seen that the SMES adaptive controller provides good damping to the generator so transient oscillations have been effectively suppressed within 5 seconds.

From the generator terminal voltage response as illustrated in Fig 5.12, it can be seen that the voltage remains within 5% of the initial value. This is because the fact that the adaptive tuned SMES controller can quickly control both real and reactive powers of SMES. Fig. 5.13 shows that SMES absorbs 0.12 p.u power during the disturbance. Fig 5.14 shows the reactive power of the SMES helps to restore the terminal voltage. The dotted line shows the behavior of the system without SMES control.

Figs.5.15-18 also show the plots of adaptive tuned SMES controller parameter variations during the transient period following a 10% input torque pulse for 2 sec. The controller gains change rapidly in the initial transient period following the disturbance. It is seen from the Figs. 5.11-14 that system oscillations are damped as the controller parameters adjust themselves. The adaptive change in the controller parameters helps to improve the performance of PMSG wind generation system.

Figure 5.8 Response of the stator current with the disturbance of 20% torque pulse at t=0.5sec (a) With adaptive tuned SMES controller (b) Without SMES controller

77

Figure 5.9 Variation of generator speed with the disturbance of 20% torque pulse at t=0.5sec (a) With adaptive tuned SMES controller (b) Without SMES controller.

Figure 5.10 Response of the DC-link capacitor voltage with the disturbance of 20% torque pulse at t=0.5sec (a) With adaptive tuned SMES controller (b) Without SMES controller.

78
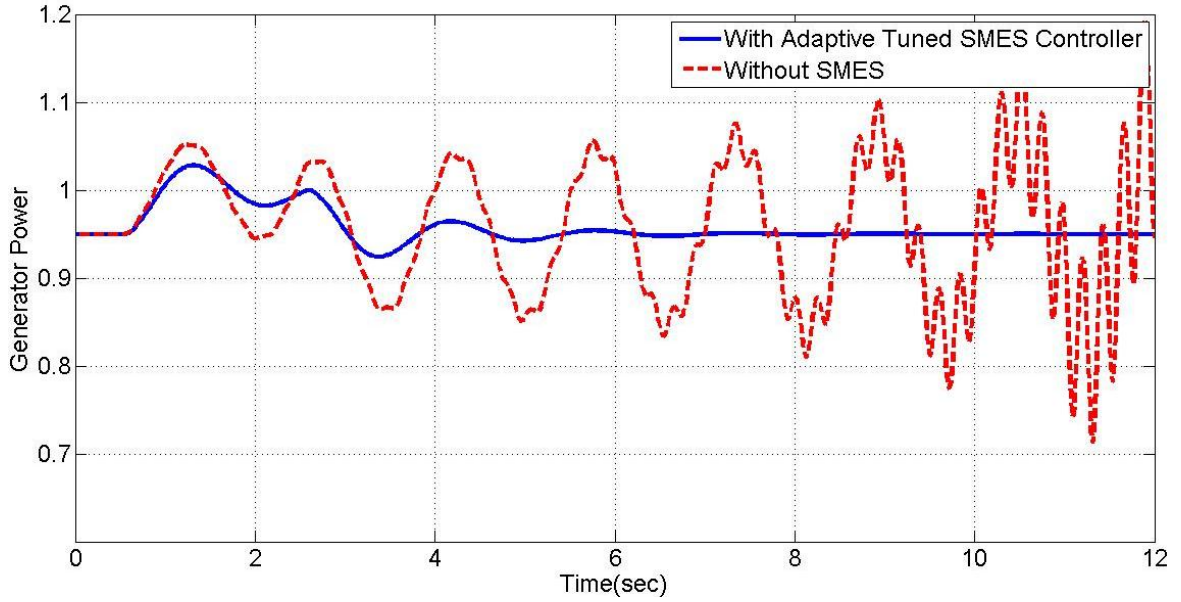
Figure 5.11 Variation of PMSG generated power with the disturbance of 10% torque pulse for 2sec (a) with adaptive tuned SMES controller (b) without SMES controller.
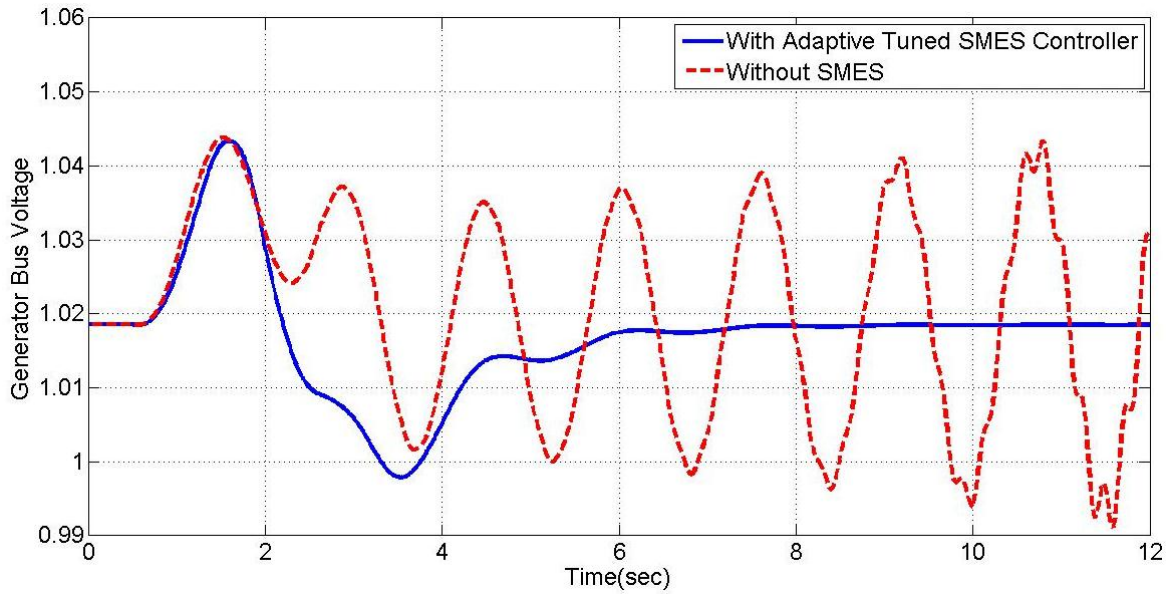
Figure 5.12 PMSG bus voltage with the disturbance of 10% torque pulse for 2sec (a) with adaptive tuned SMES controller (b) without SMES controller
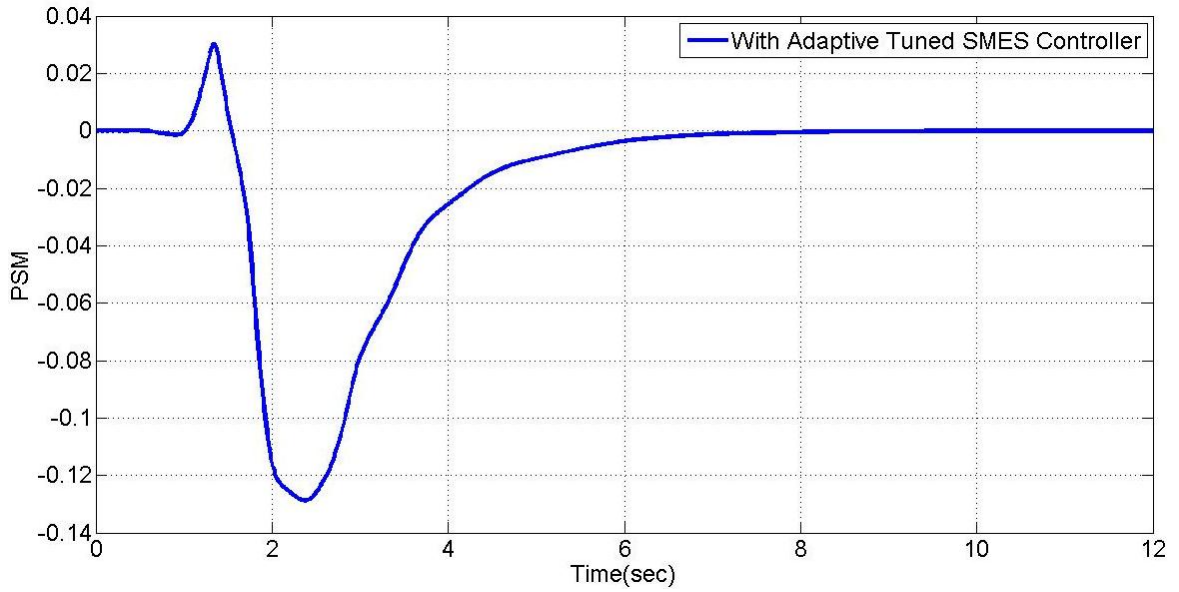
Figure 5.13 Compensated SMES active power with the disturbance of 10% torque pulse for 2sec with adaptive tuned SMES controller.
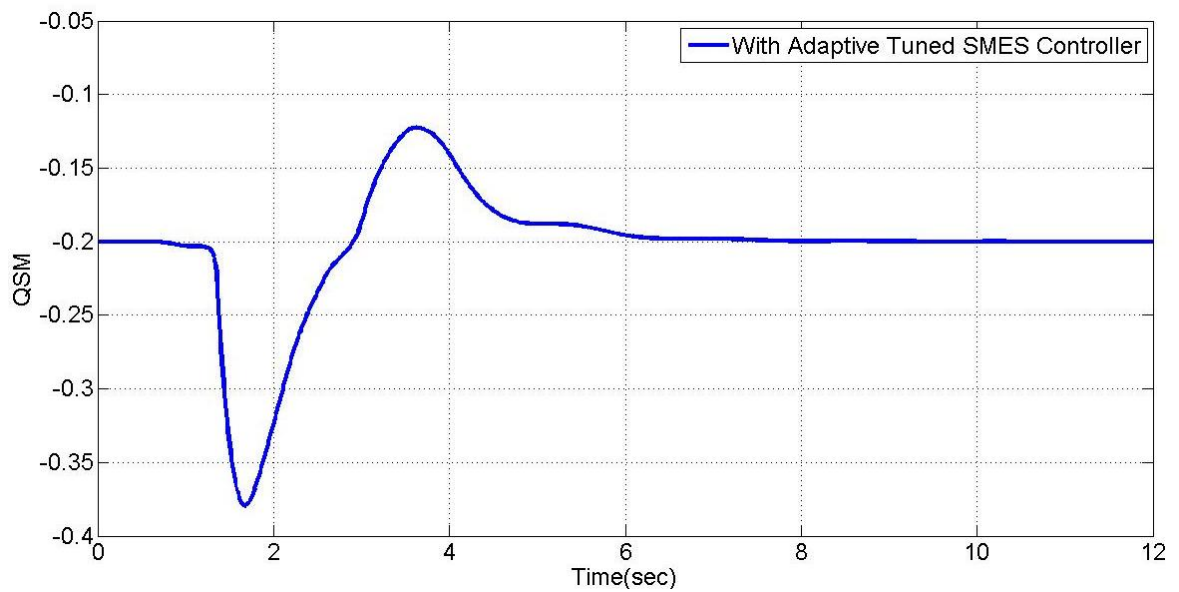
Figure 5.14 Compensated SMES reactive power with the disturbance of 10% torque pulse for 2sec with adaptive tuned SMES controller.

80
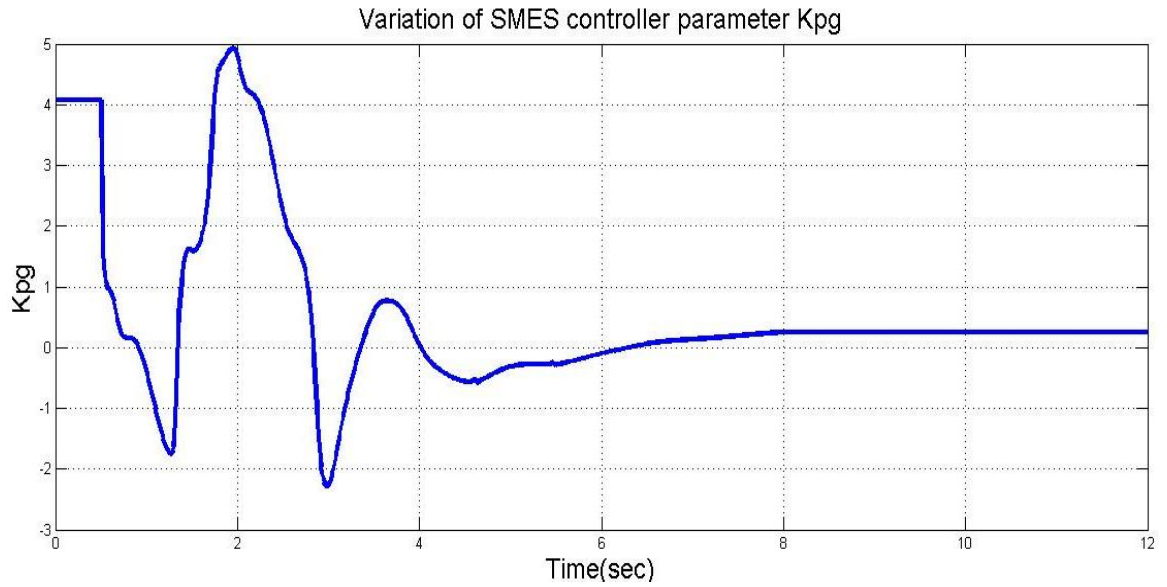
Figure 5.15 Variation of the SMES controller parameter Kpg with the disturbance of 10% torque pulse for 2sec with adaptive tuned SMES controller.
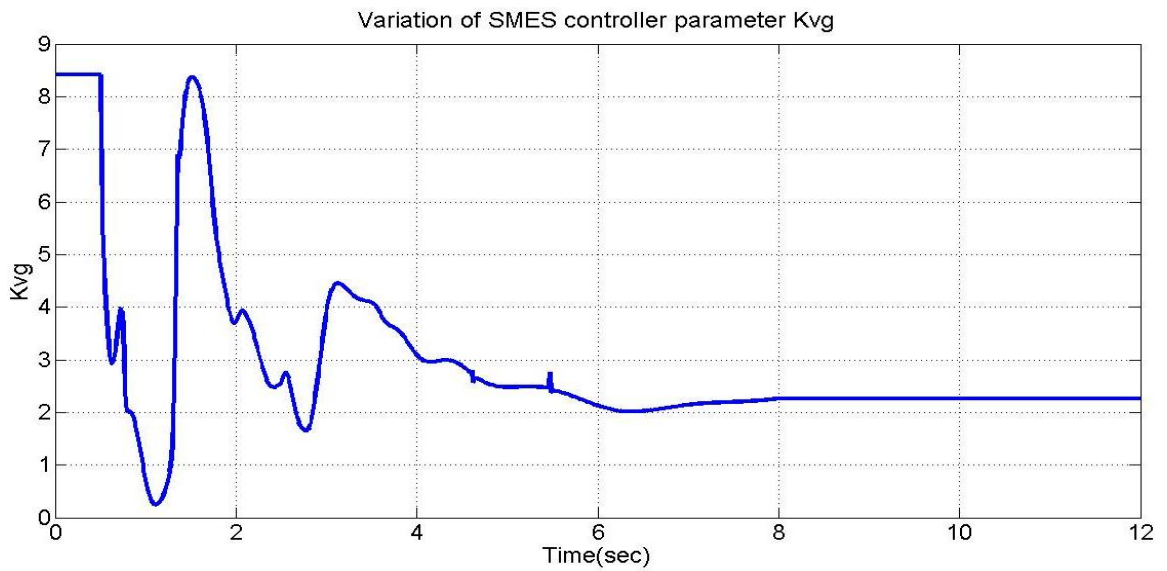
Figure 5.16 Variation of the SMES controller parameter Kvg with the disturbance of 10% torque pulse for 2sec with adaptive tuned SMES controller.

81
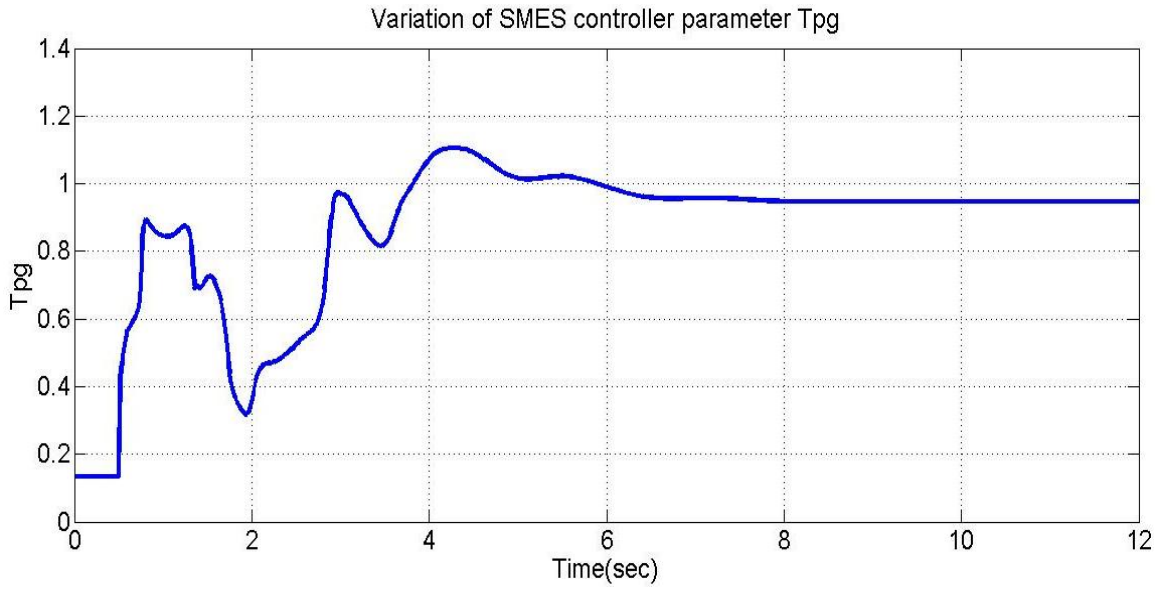
Figure 5.17 Variation of the SMES controller parameter Tpg with the disturbance of 10% torque pulse for 2sec with adaptive tuned SMES controller.
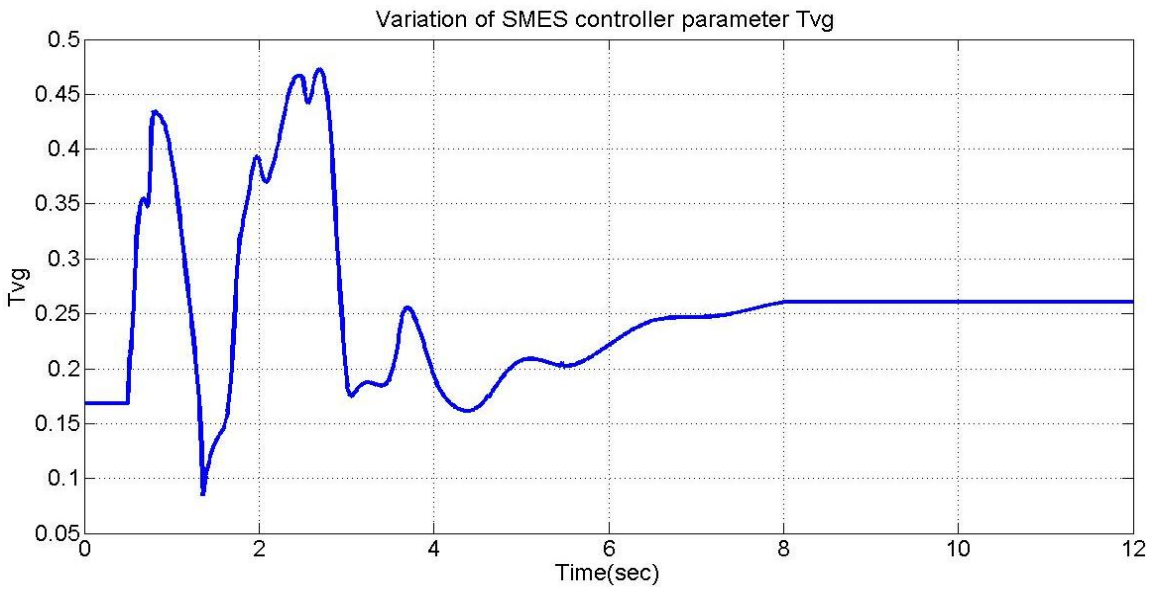
Figure 5.18 Variation of the SMES controller parameter Tvg with the disturbance of step change in mechanical power by 10% for 2 sec.

5.3.2 Low Voltage Condition at the Grid Bus

The transient response of the PMSG wind generation system under a severe three-phase short circuit fault at the utility grid is presented in this section. The stator current, generator speed variation, generator power, generator bus voltage responses of the PMSG system with and without adaptive SMES control for a 0.3sec duration of three phase fault are given in Figs. 5.19-22. From the above system variables responses, it can be observed that system cannot survive this severe low voltage condition without SMES control. Fig 5.19 shows that stator current takes short time with less overshoot to reach the steady state value with SMES control but on the other hand stator current oscillations grown up with time elapses. From Fig 5.20, it can be seen that the generator speed variations are the lowest and steady state value is reached quickly within 1.5 seconds during a 3 phase fault on the grid bus. Fig. 5.21 shows that the active power delivered to the grid with the adaptive tuned SMES controller can be quickly suppressed to the operating point in 4 seconds. Fig. 5.22 shows that the oscillations of the PMSG generator bus voltage have been effectively suppressed by the adaptive tuned SMES controller. The generator bus voltage reaches to 0.83 p.u from 1.02 p.u but because of the reactive power support from the SMES, the generator bus voltage returns to initial value within 3.5seconds. It is seen from Fig. 5.23 that the variation of the reactive power of SMES helps in generator voltage restoration.

SMES controller parameters variations for the three phase fault condition are shown in Figs 5.24-27. The online tuning of the SMES controller parameters provides a good damping to the system with minimum transients. It can be concluded that performance of

the system with designed adaptive tuned SMES controller is very satisfactory in terms of transient and steady state responses.
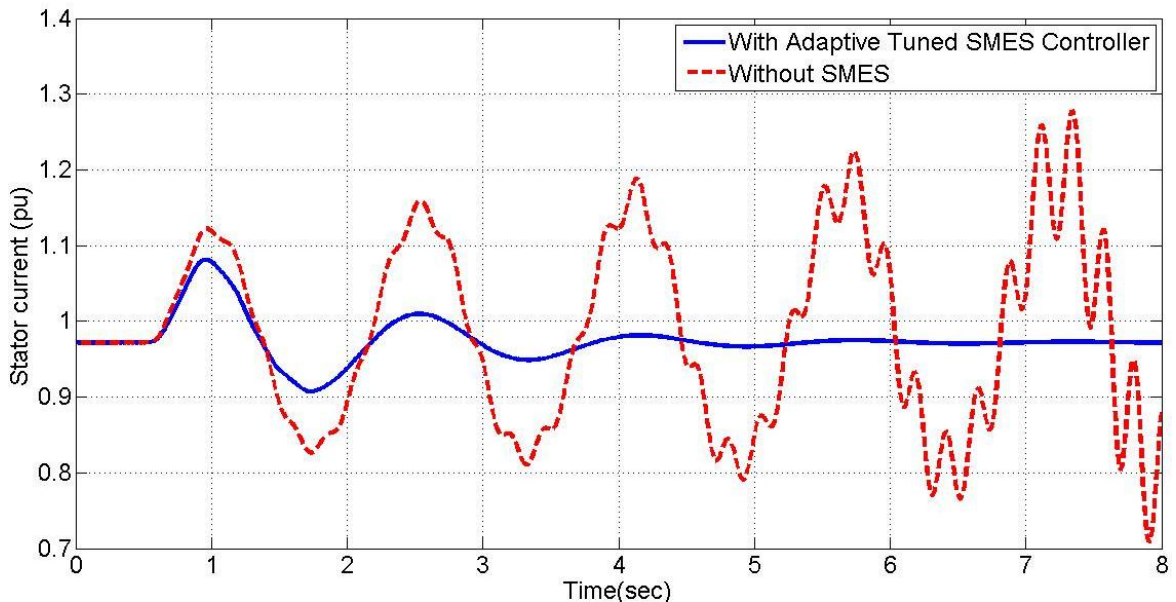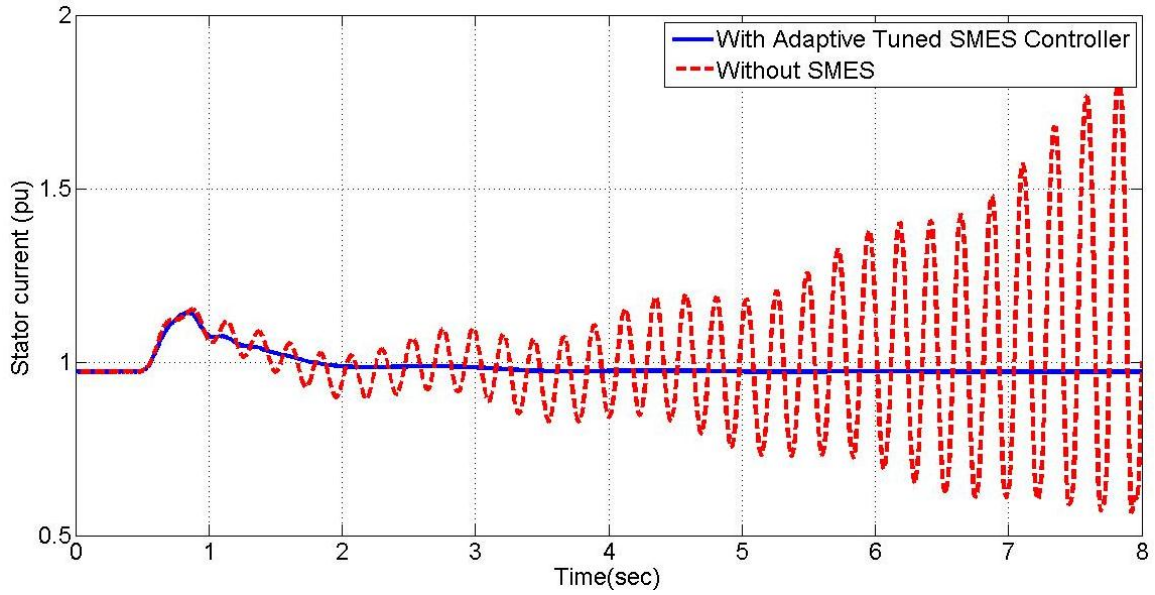

Figure 5.19 Response of the stator current with the disturbance of three phase fault at grid at t=0.5sec (a) With adaptive tuned SMES controller (b) Without SMES controller
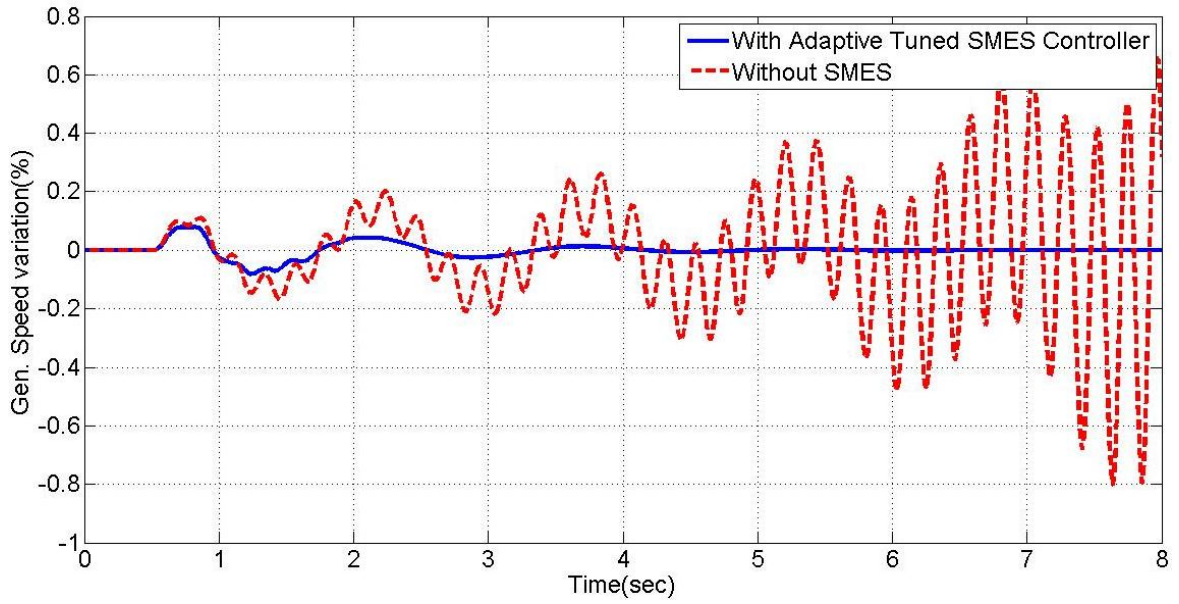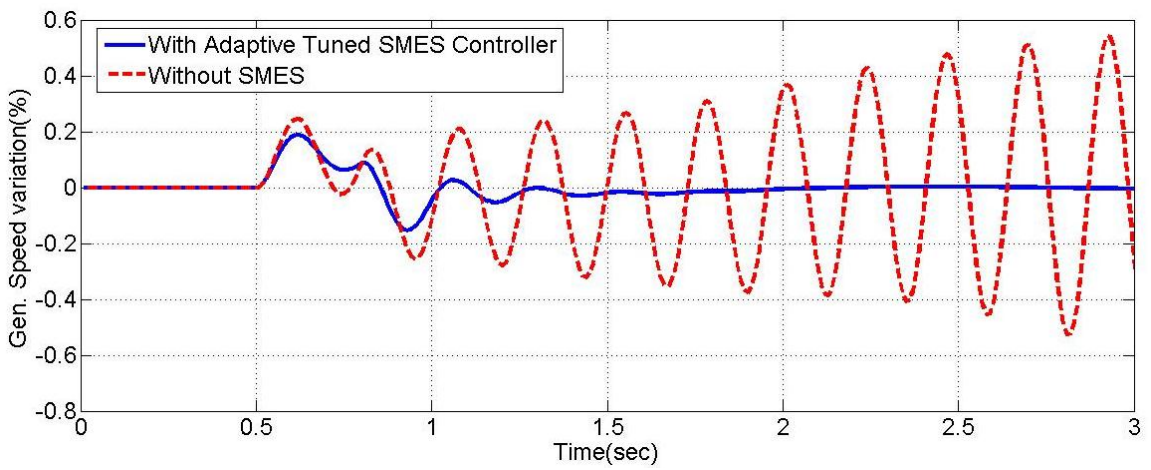
Figure 5.20 Variation of generator speed with the disturbance of three phase fault at grid at t=0.5sec (a) With adaptive tuned SMES controller (b) Without SMES controller
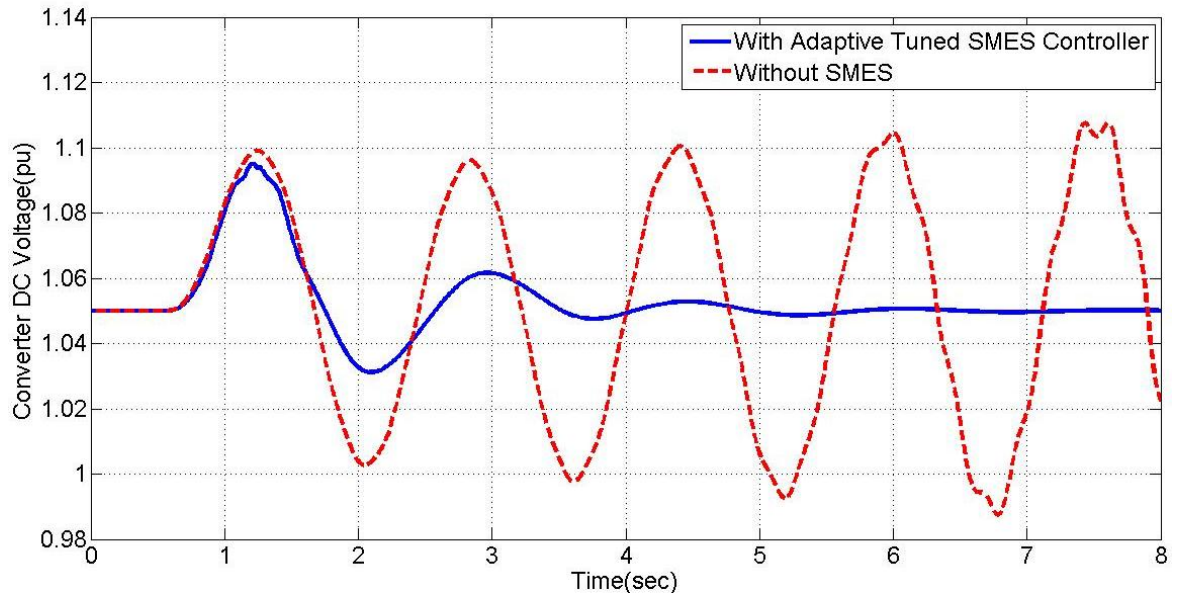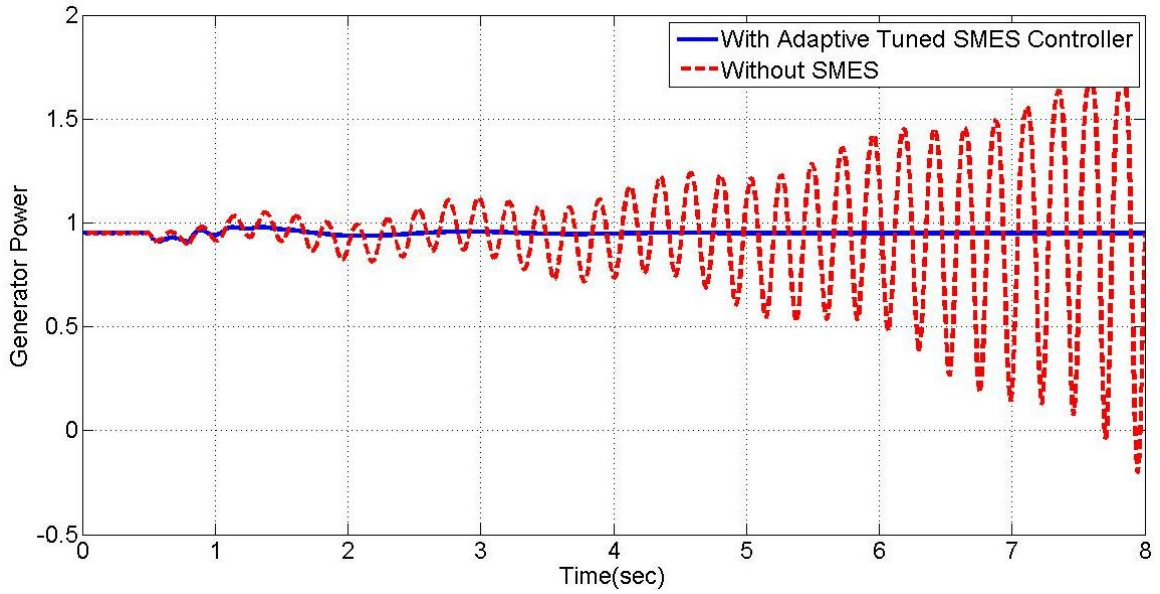

Figure 5.21 Variation of PMSG generated power with the disturbance of three phase fault at grid at t=0.5sec (a) With adaptive tuned SMES controller (b) Without SMES controller
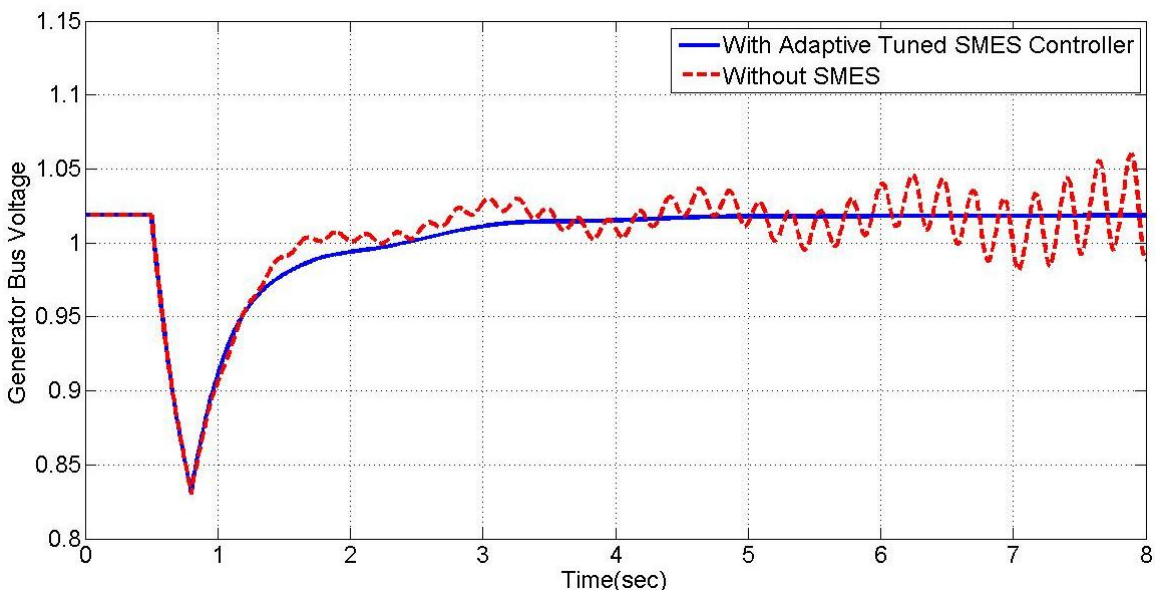
Figure 5.22 PMSG bus voltage with the disturbance of three phase fault at grid at t=0.5sec (a) With adaptive tuned SMES controller (b) Without SMES controller
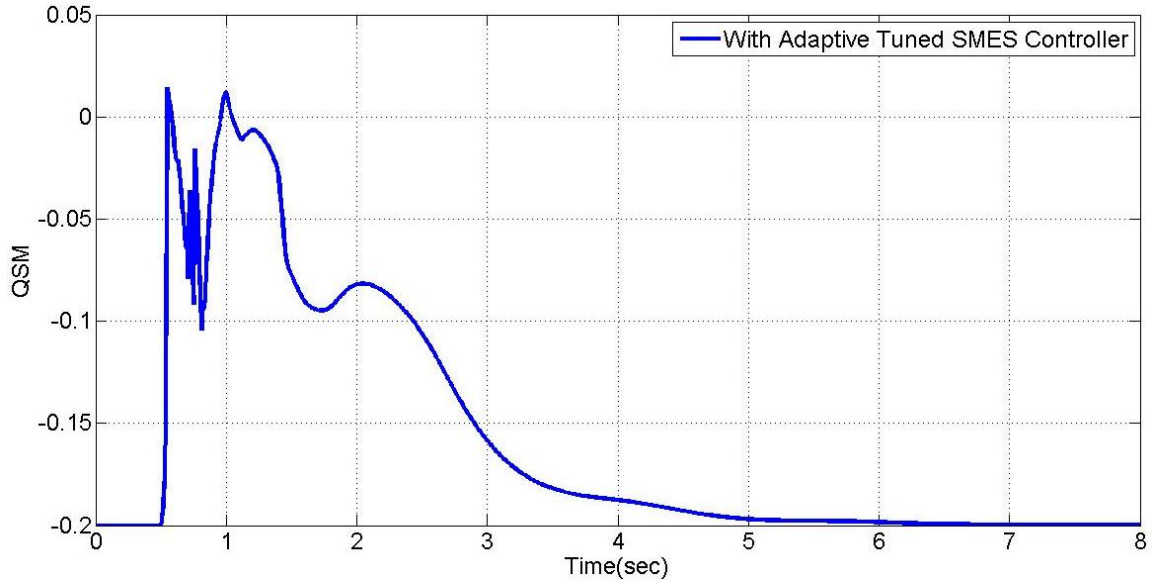
Figure 5.23 Compensated SMES reactive power with the disturbance of three phase fault at grid at t=0.5sec with adaptive tuned SMES controller.
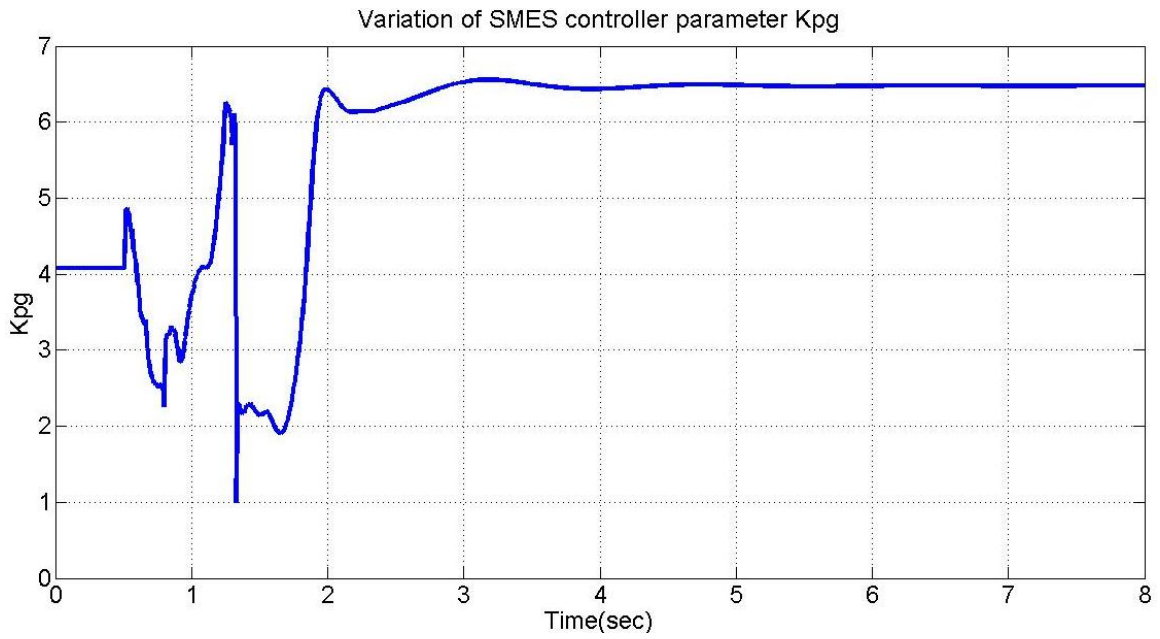
Figure 5.24 Variation of the SMES controller parameter Kpg with the disturbance of three phase fault at grid at t=0.5sec.
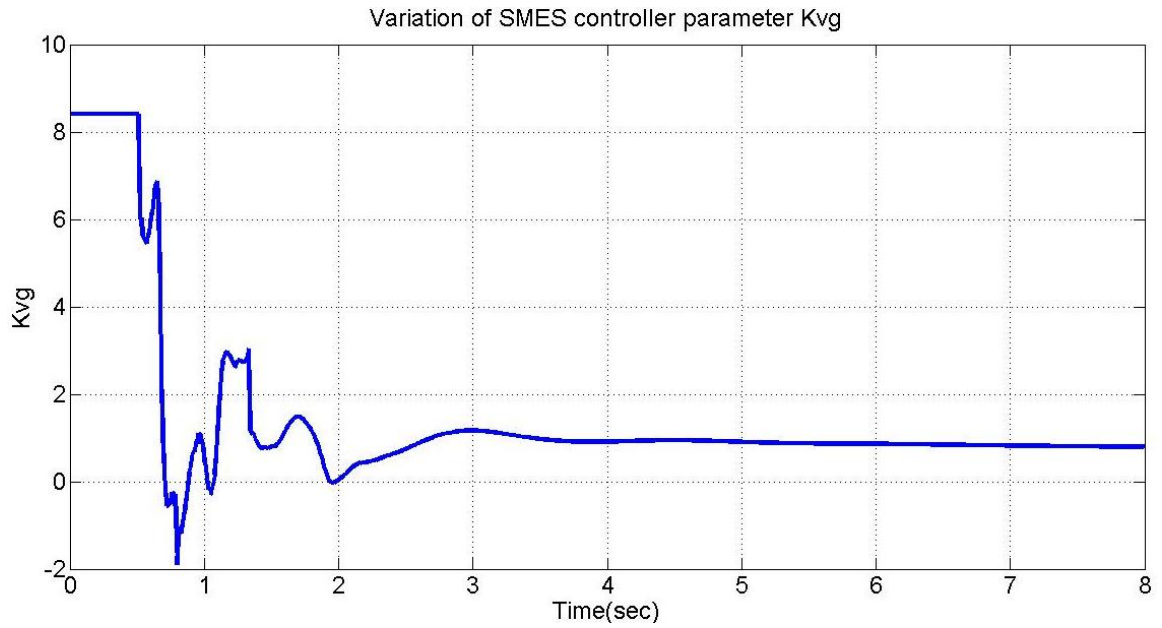
Figure 5.25Variation of the SMES controller parameter Kvg with the disturbance of three phase fault at grid at t=0.5sec.
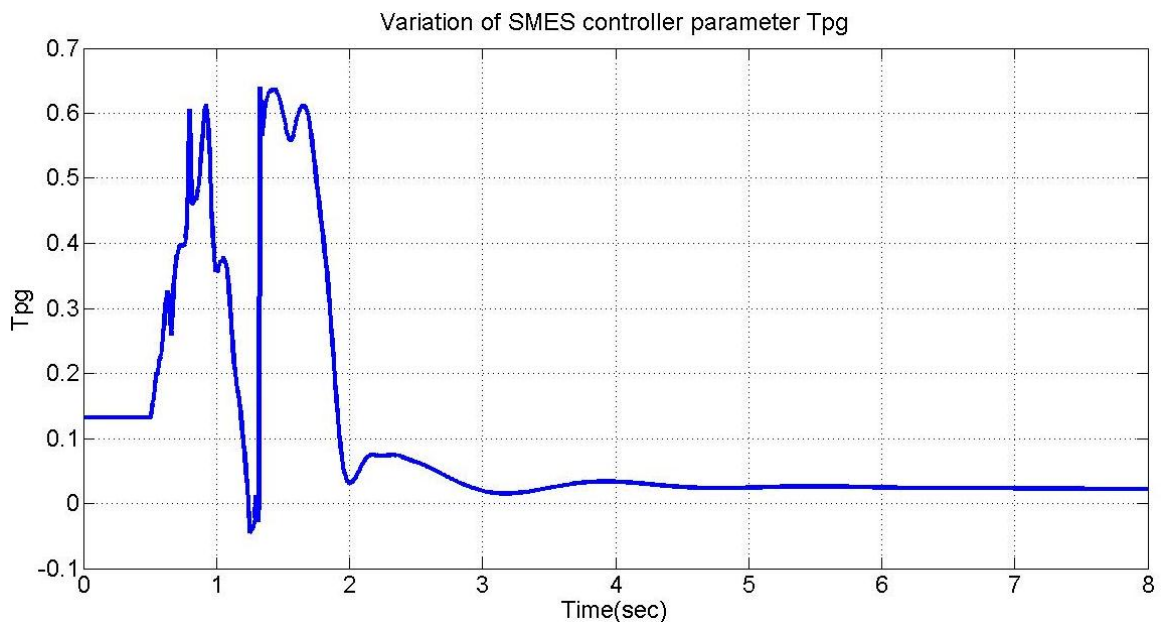
Figure 5.26Variation of the SMES controller parameter Tpg with the disturbance of three phase fault at grid at t=0.5sec.
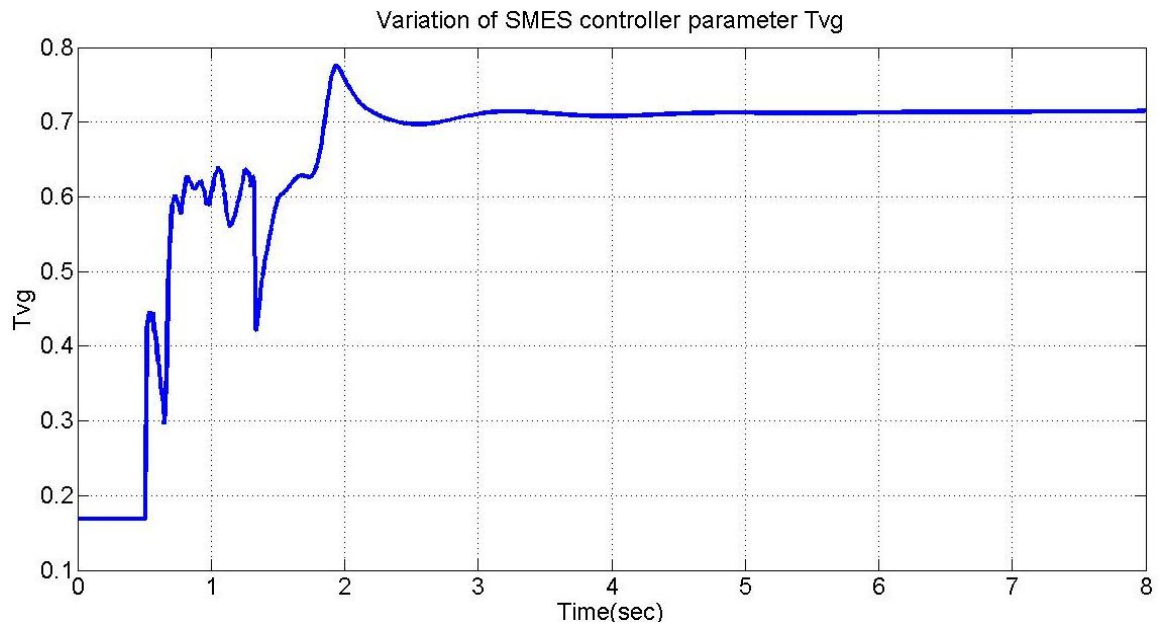
Figure 5.27Variation of the SMES controller parameter Tvg with the disturbance of three phase fault at grid at t=0.5sec.

5.3.3 Wind Gust

In this case, wind gust is applied to the system as disturbance. The wind data collected from actual measurement, scaled and normalized was used to test the adaptive SMES controller [115]. The random wind speed data collected for testing the system is shown in Fig. 5.28. The gust data was used for 2 seconds in simulation study. The variation of mechanical power respond to the wind speed change is illustrated in Fig 5.29. The responses of the system are illustrated in Figs 5.30-37.

The power angle variation of the PMSG is presented in Fig 5.30. Even after the fault cleared, the power angle does not come back to steady state without SMES control and oscillations growing up with time. On the other hand with SMES control, power angle variations are very small and steady state value is reached quickly within 2.5 seconds. It can be observe from Fig. 5.31 that during wind gust period, the generator speed oscillations are not settling due to the penetration level of mechanical power, but with SMES control, there is a small variation during the wind disturbance but as time elapses generator speed variations are reduced within 2.5 seconds. Fig 5.32 illustrated the response of grid side inverter current with and without SMES control. Without control, the grid side converter current is distorted because of the sensitivity of the converter due to wind disturbance and goes away after 6 seconds because of no power compensation in the absence of SMES. However, proposed SMES controller restores the grid side inverter current to its nominal condition in less than 4 seconds. The terminal voltage of PMSG, shown in Fig 5.33, demonstrates that the voltage remains within 5% of the initial value and damped quickly within 3 sec. However, without SMES control, generator bus voltage

is not damped even in the 8 sec period. This sharp voltage drop fails to recover even when the disturbance is removed. Fig 5.34 and 5.35 show the real and reactive power variations of the SMES system which change polarity depending on the system need. In Fig 5.35 SMES reactive power variate between 0.1 pu to -0.4 pu for voltage support of the generator bus.

Figs. 5.36-37 show the adaptive SMES controller parameters variations during the transient period. This continuous update of parameters allows good damping to the system transients. It can be seen that the generator is sensitive to sudden wind change shown with dotted curves. From the results, it can conclude that system is unable to sustain the random change in wind speed and hence transients are not damped properly and provide a poor response as compared to the adaptive SMES controller.
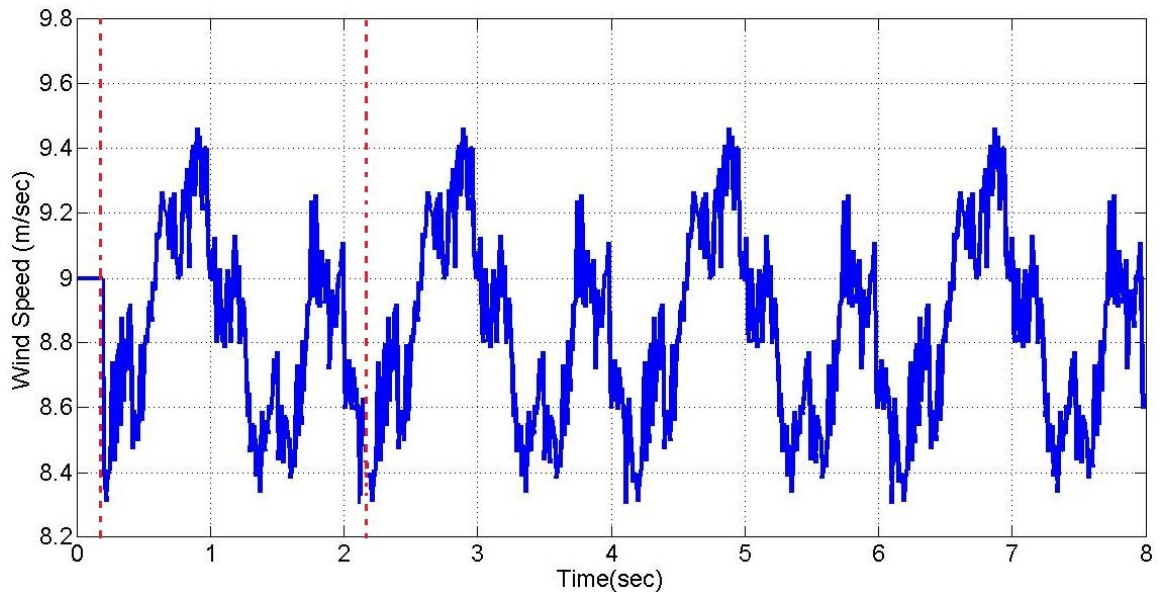
Figure 5.28 Wind speed gust as a function of time
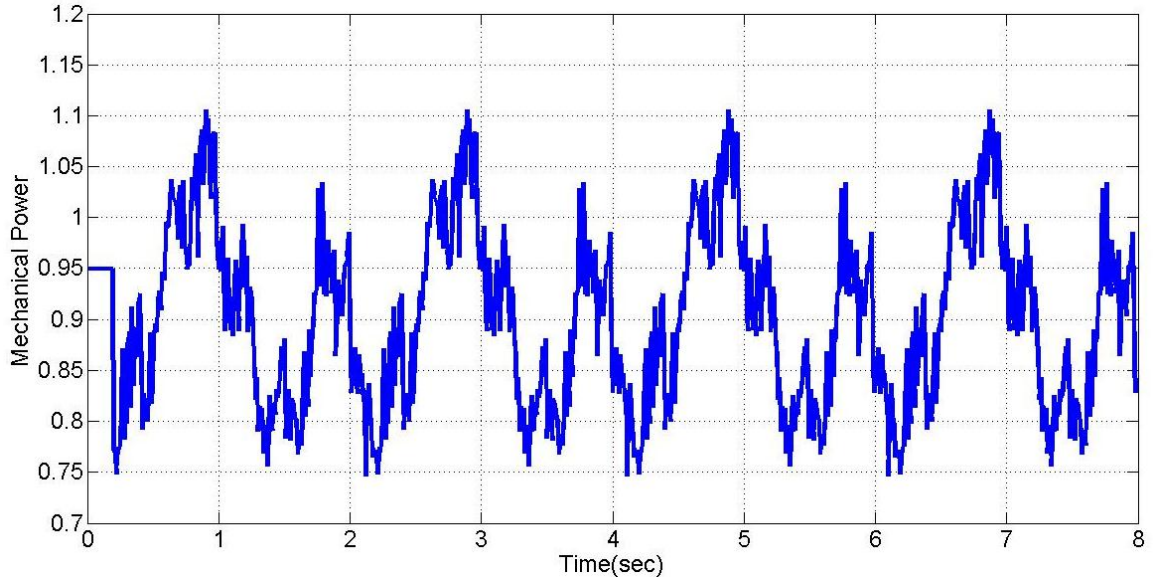
Figure 5.29 Variation of mechanical power due to wind gust
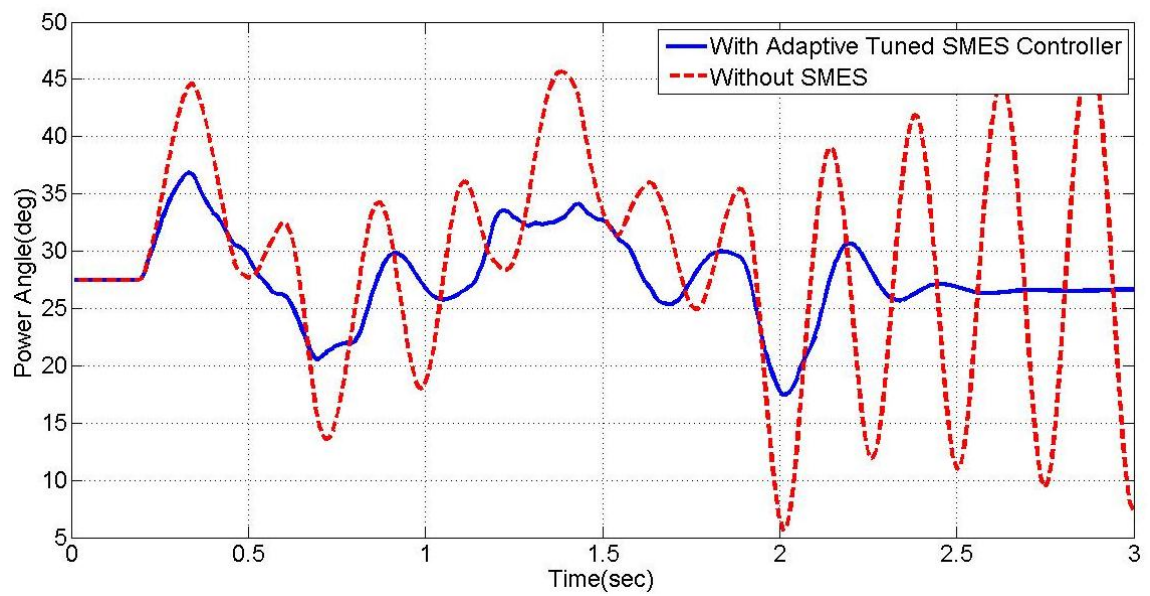
Figure 5.30 Response of the power angle with wind gust applied at t=0.2sec (a) With adaptive tuned SMES controller (b) Without SMES controller
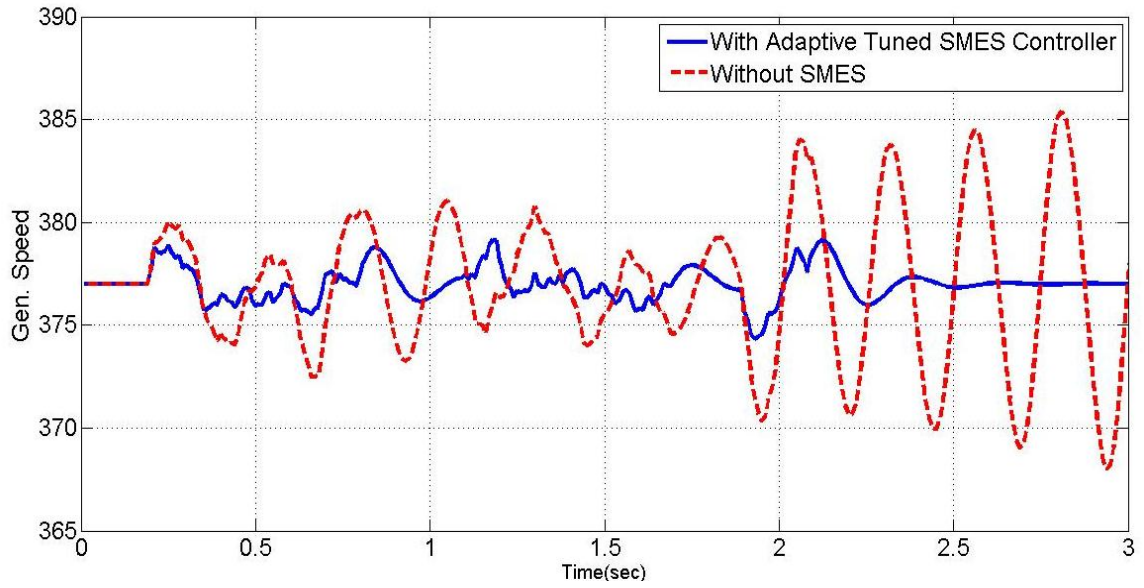
Figure 5.31 Generator speed with wind gust applied at t=0.2sec (a) With adaptive tuned SMES controller (b) Without SMES controller
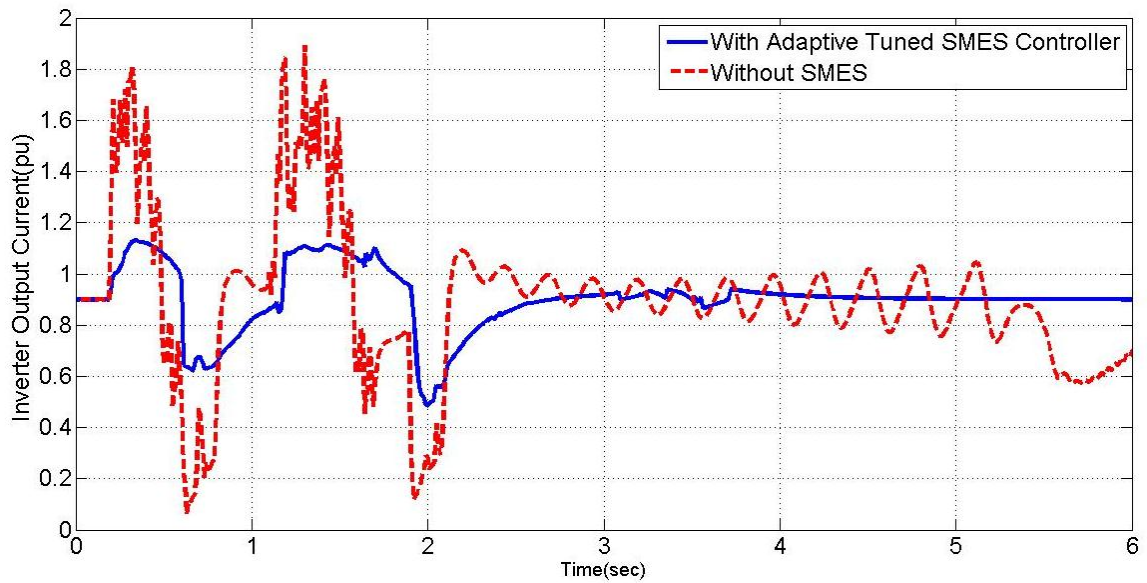
Figure 5.32 Variation of inverter output current with wind gust applied at t=0.2sec (a) With adaptive tuned SMES controller (b) Without SMES controller
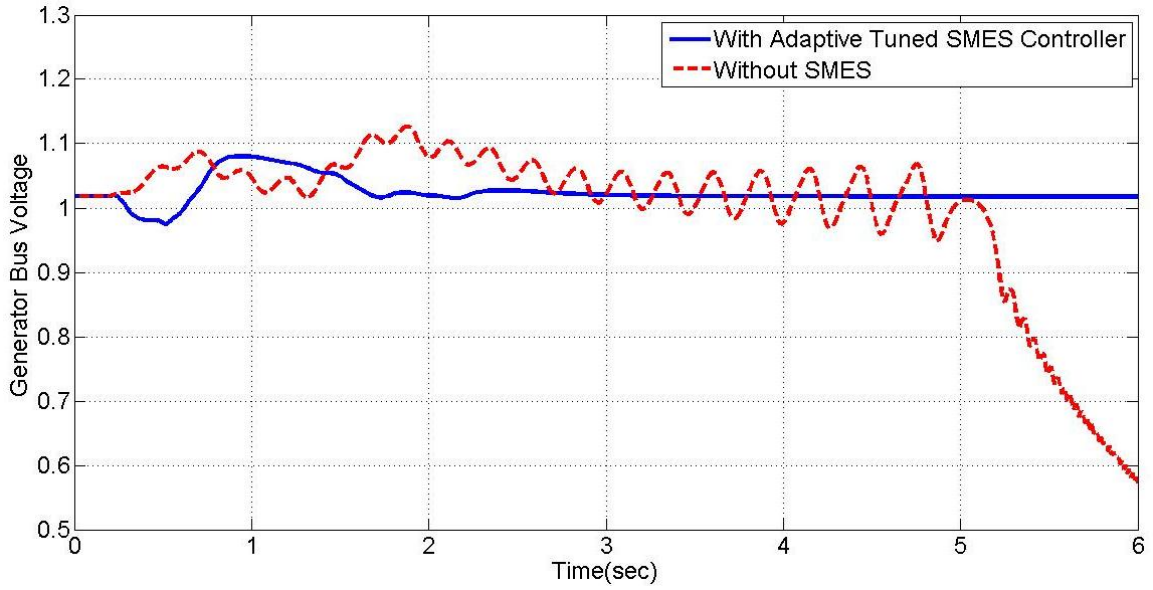
Figure 5.33 PMSG bus voltage with wind gust applied at t=0.2sec (a) With adaptive tuned SMES controller (b) Without SMES controller
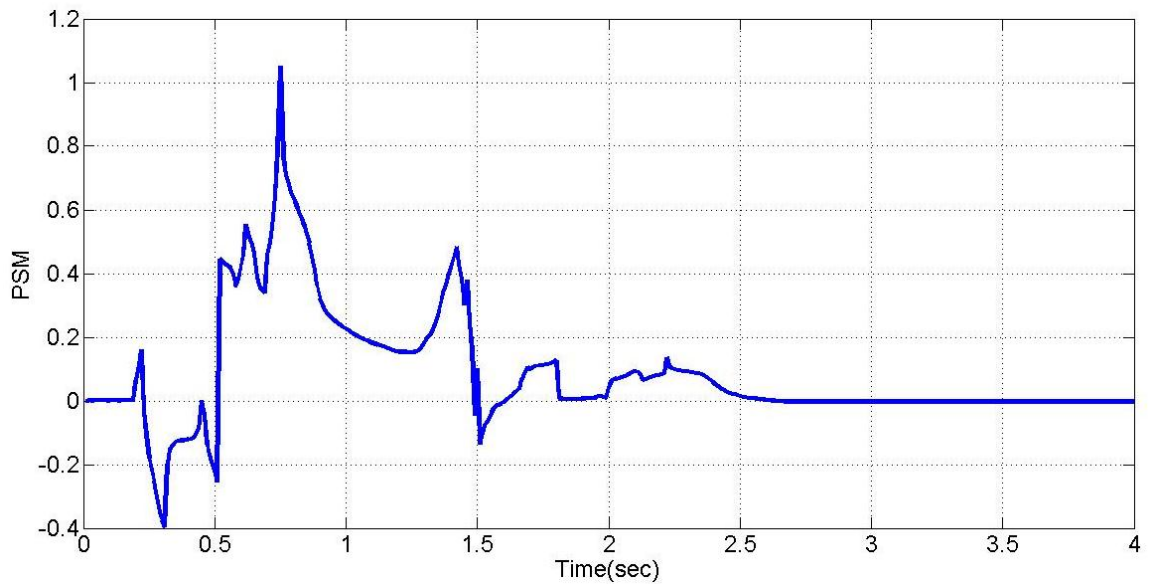
Figure 5.34 Compensated SMES active power with wind gust applied at t=0.2sec with adaptive tuned SMES controller.
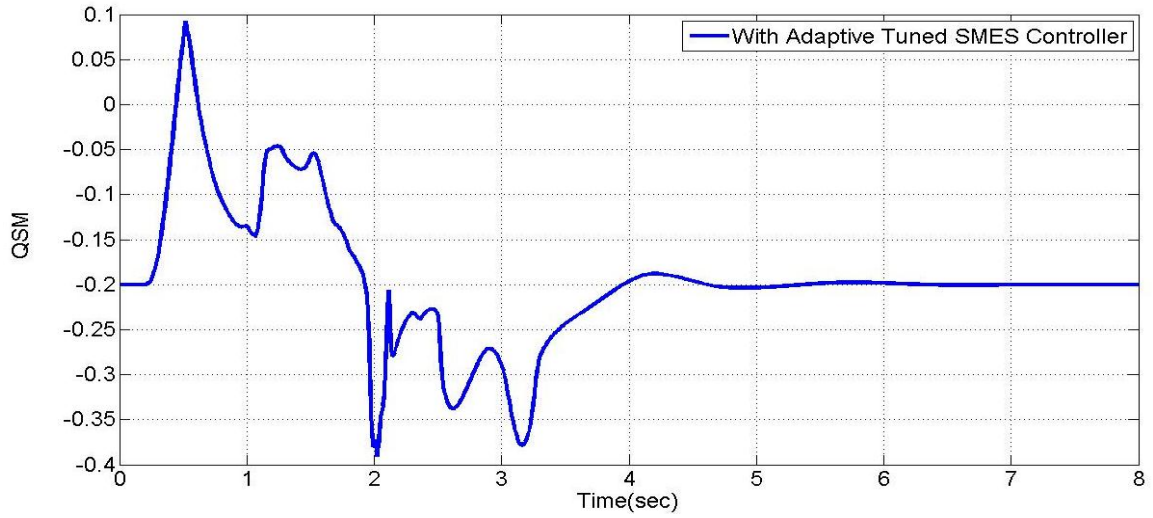
Figure 5.35 Compensated SMES reactive power with wind gust applied at t=0.2sec with adaptive tuned SMES controller.
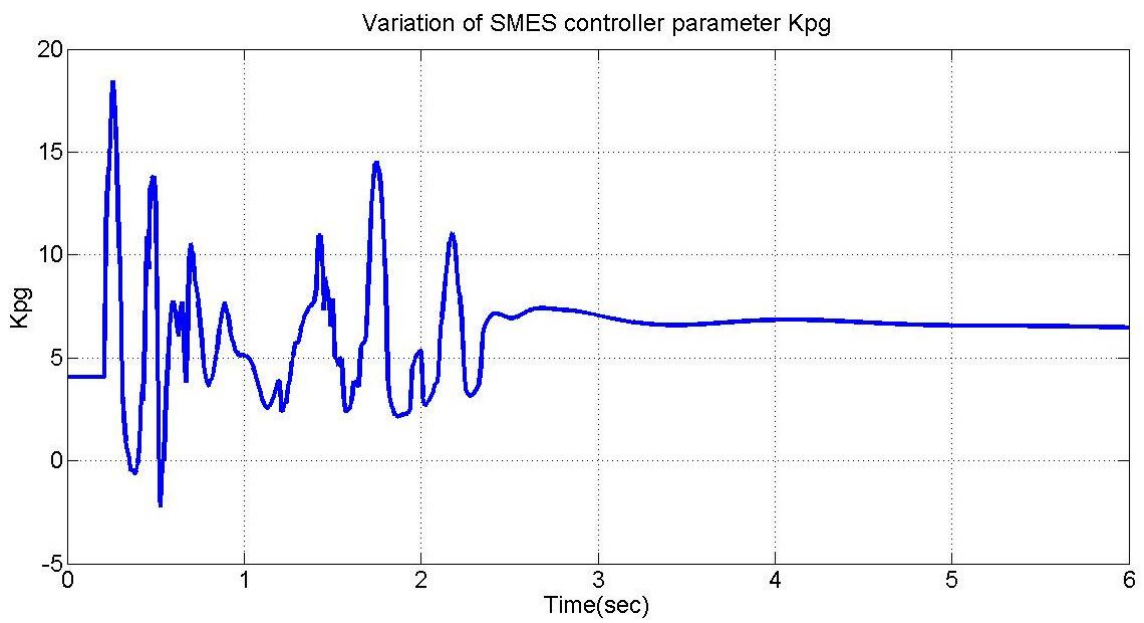
Figure 5.36 Variation of the SMES controller parameter Kpg with wind gust applied at t=0.2sec.
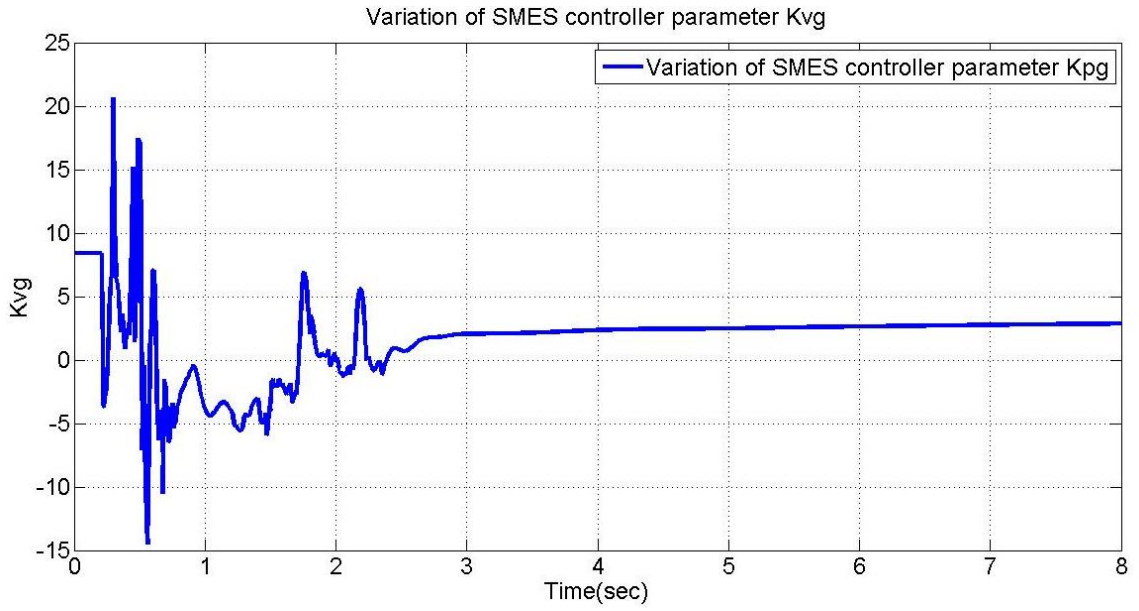
Figure 5.37 Variation of the SMES controller parameter Kvg with wind gust applied at t=0.2sec.

CHAPTER 6

CONCLUSIONS AND FUTURE WORK

6.1 Conclusions

A dynamic model of the PMSG system with an SMES controller connected at the inverter terminal is developed. A strategy for tuning the SMES controller parameters strategy using an adaptive RBFNN is presented. The control strategy involves generation of optimized parameters of SMES controller through IPSO, training the controller parameters using RBFNN and adaptively tuning the network weights according to changes in the system variables.

The nominal weights of the adaptive RBFNN were found from training data which, in turn, were generated through a modified particle swarm optimization technique. The convergence in traditional particle swarm optimization (PSO) is made faster by updating the inertia weight of the IPSO. The RBFNN is simple, easy to generalize and also it provides better approximation. It also performs the fast training because only a few hidden units updates for a given input, thus the network modifies the weights only in the vicinity of the sample point and retains constant weights in the other regions, so they have only the local effect.

Adaptive algorithm adjusts only the weights of the RBFNN between the hidden layer and output layer, which have a linear relationship. Therefore, fast convergence can be achieved. Also, the update process could be initiated based on threshold value of e_a (error between reference RBFNN and adaptive neural network), giving flexibility to the algorithm and saving excessive computations.

The effectiveness of the proposed adaptive control scheme in improving the PMSG wind system dynamics has been verified through the nonlinear time domain simulations. The system is tested under several types of disturbances like torque pulses, three phase fault at grid, and wind gust scenarios. Simulation results show that adaptively tuned SMES controller is able to keep the transients to a minimum and is able to restore normal operating conditions fairly quickly. The performance improvement is because of the capability of the SMES to inject/absorb both real and reactive power as required by the system. PMSG equipped with adaptive tuned SMES improves the overall system performance over a wide range of operating conditions and for different contingencies.

Although SMES control is a well-known technology, its application to improve PMSG wind generator system is considered to be novel.

6.2 Future Work

This work can be extended to include the following.

- The impact of selecting other output variables in tuning the parameters can be examined.

- The study can be extended to include a multi machine system.

- Different controllers like PI or PID controllers, fuzzy logic controllers etc. could be studied to improve the performance of PMSG system with SMES.

- The pitch angle control is one of the ways for adjusting the aerodynamic torque of the wind turbine when the wind speed is above rated speed. Controlling the power of PMSG with SMES through turbine blade pitch control can be considered.

- Time-domain based objective function or multi-objective functions may be considered in design phase of intelligent technique.

- Comparison of the performance can be made by using other types of neural networks like back propagation neural network.

- The proposed design scheme can be further explored in large scale wind farm.

APPENDIX A

System Data

Parameters	Values in p.u
Turbine inertia constant (H_t)	3
Generator inertia constant (H_g)	0.5
Shaft stiffness constant (K_s)	0.3
Stator resistance (R_a)	0.01
Stator reactance (X_d)	1
DC-link capacitor (C)	1
Grid side inverter resistance (R_i)	0.05
Grid side inverter reactance (X_i)	0.1
Load admittance (Y_L)	0.2-j0.4
SMES inductance (L_{SC})	2
SMES commutation reactance (X_{CM})	0.5
SMES resistance (R_{SC})	0.0
Transmission line resistance (R_L)	0.1
Transmission line reactance (X_L)	0.2
SMES real power (P_{smo})	0.0
SMES reactive power (Q_{smo})	-0.2

IPSO and RBFNN Data:

Parameters	Values
Special constant (c_1, c_2)	2,2
Spread factor (β)	0.1

APPENDIX B

Linearized Model

The PMSG wind turbine system is linearized around operating conditions

Stator d-axis current (i_{gd})

The state equation of the d-axis current of PMSG can be written as

$$\dot{i}_{gd} = -\left(\frac{\omega_o R_a}{x_d}\right)i_{gd} + \left(\frac{\omega_o x_q}{x_d}\right)i_{gq}\omega - \left(\frac{v_{gd}\omega_o}{x_d}\right) \tag{B.1}$$

Linearize the Eq (B.1)

$$\Delta \dot{i}_{gd} = -(\frac{\omega_o R_a}{x_d})\Delta i_{gd} + (\frac{\omega_o x_q}{x_d})(\omega \Delta i_{gq} + \Delta \omega i_{gqo})$$

$$-(\frac{\omega_o}{x_d})(m_{gco} V_{co} \cos\delta_o \Delta\delta + m_{gco} \sin\delta_o \Delta V_c + V_{co} \sin\delta_o \Delta m_{gc})$$

(B.2)

$$\Delta \dot{i}_{gd} = -(\frac{\omega_o R_a}{x_d})\Delta i_{gd} + (\frac{\omega_o x_q}{x_d})\Delta i_{gq} + (\frac{\omega_o x_q}{x_d})i_{gqo}\Delta\omega$$

$$-(\frac{\omega_o}{x_d} m_{gco} V_{co} \cos\delta_o)\Delta\delta - (\frac{\omega_o}{x_d} m_{gco} \sin\delta_o)\Delta V_c - (\frac{\omega_o}{x_d} V_{co} \sin\delta_o)\Delta m_{gc})$$

(B.3)

Stator q-axis current (i_{gq})

The state equation of the q-axis current of PMSG can be written as

$$\dot{i}_{gq} = -(\frac{\omega_o x_d}{x_q})i_{gd}\omega - (\frac{\omega_o R_a}{x_q})i_{gq} - (\frac{E_{res}\omega_o}{x_q})\omega - (\frac{v_{gq}\omega_o}{x_q})$$

(B.4)

Linearize the Eq (B.4)

$$\Delta \dot{i}_{gq} = -(\frac{\omega_o x_d}{x_q})\Delta i_{gd} - (\frac{\omega_o R_a}{x_q})\Delta i_{gq} + \frac{\omega_o(E_{reso} - x_d i_{gdo})}{x_q}\Delta\omega$$

$$-(\frac{\omega_o}{x_q})(-m_{gco} V_{co} \sin\delta_o \Delta\delta + m_{gco} \cos\delta_o \Delta V_c + V_{co} \cos\delta_o \Delta m_{gc})$$

(B.5)

$$\Delta \dot{i}_{gq} = -(\frac{\omega_o x_d}{x_q})\Delta i_{gd} - (\frac{\omega_o R_a}{x_q})\Delta i_{gq} + (\frac{\omega_o m_{gco} V_{co} \sin\delta_o}{x_q})\Delta\delta +$$

$$+\frac{\omega_o(E_{reso} - x_d i_{gdo})}{x_q}\Delta\omega - (\frac{\omega_o m_{gco} \cos\delta_o}{x_q})\Delta V_c - (\frac{\omega_o V_{co} \cos\delta_o}{x_q})\Delta m_{gc}$$

(B.6)

Generator Angle (δ)

The power angle of the generator is

$$\dot{\delta}=\omega_o(\omega-1) \tag{B.7}$$

Linearize (B.7)

$$\dot{\Delta\delta}=\omega_o\Delta\omega \tag{B.8}$$

Generator d-q axis voltages (v_{gd},v_{gq})

Generator bus d-axis voltages can be written as

$$v_{gd}=m_{gc}V_c\sin\delta \tag{B.9}$$

The linearize form of (B.9),

$$\Delta v_{gd}=(m_{gco}V_{co}\cos\delta_o)\Delta\delta+(m_{gco}\sin\delta_o)\Delta V_c+(V_{co}\sin\delta_o)\Delta m_{gc} \tag{B.10}$$

Generator bus q-axis voltages can be written as

$$v_{gq}=m_{gco}V_c\cos\delta \tag{B.11}$$

The linearize form of (B.11)

$$\Delta v_{gq}=-(m_{gco}V_{co}\sin\delta_o)\Delta\delta+(m_{gco}\cos\delta_o)\Delta V_c+(V_{co}\cos\delta_o)\Delta m_{gco} \tag{B.12}$$

Electrical Power Generated by PMSG (P_e)

The electrical power generated by PMSG is

$$P_e = v_{gd}i_{gd} + v_{gq}i_{gq} + (i_{gd}^2 + i_{gq}^2)R_a \tag{B.13}$$

The linearize form of (B.13) can be written as

$$\Delta P_e = v_{gdo}\Delta i_{gd} + i_{gdo}\Delta v_{gd} + v_{gqo}\Delta i_{gq} + i_{gqo}\Delta v_{gq} + (2i_{gdo}\Delta i_{gd} + 2i_{gqo}\Delta i_{gq})R_a \tag{B.14}$$

$$\begin{aligned}\Delta P_e = {} & v_{gdo}\Delta i_{gd} + i_{gdo}(m_{gco}V_{co}\cos\delta_o\Delta\delta + m_{gco}\sin\delta_o\Delta V_c + V_{co}\sin\delta_o\Delta mgc) \\ & + V_{gqo}\Delta i_{gq} + i_{gqo}(-m_{gco}V_{co}\sin\delta_o\Delta\delta + m_{gco}\cos\delta_o\Delta V_c + V_{co}\cos\delta_o\Delta m_{gc}) \\ & + (2i_{gdo}\Delta i_{gd} + 2i_{gqo}\Delta i_{gq})R_a \end{aligned} \tag{B.15}$$

$$\begin{aligned}\Delta P_e = {} & (m_{gco}V_{co}\sin\delta_o + 2i_{gdo}R_a)\Delta i_{gd} + (m_{gco}V_{co}\cos\delta_o + 2i_{gqo}R_a)\Delta i_{gq} \\ & + (m_{gco}V_{co}i_{gdo}\cos\delta_o - m_{gco}V_{co}i_{gqo}\sin\delta_o)\Delta\delta \\ & + (m_{gco}i_{gdo}\sin\delta_o + m_{gco}i_{gqo}\cos\delta_o)\Delta V_c \\ & + (V_{co}i_{gdo}\sin\delta_o + V_{co}i_{gqo}\cos\delta_o)\Delta m_{gc} \end{aligned} \tag{B.16}$$

Generator Speed (ω)

The generator speed is given by (B.17)

$$\dot{\omega} = \frac{1}{2H_g}(K_s\theta_s - P_e) \tag{B.17}$$

The linearize form of (B.17) is

$$\Delta\dot{\omega} = \frac{1}{2H_g}(K_s\Delta\theta_s - \Delta P_e) \tag{B.18}$$

$$\dot{\Delta\omega}=\frac{1}{2H_g}(K_s\Delta\theta_s\text{-}(m_{gco}V_{co}\sin\delta_o+2i_{gdo}R_a)\Delta i_{gd}\text{-}(m_{gco}V_{co}\cos\delta_o+2i_{gqo}R_a)\Delta i_{gq}$$

$$\text{-}(m_{gco}V_{co}i_{gdo}\cos\delta_o\text{-}m_{gco}V_{co}i_{gqo}\sin\delta_o)\Delta\delta\text{-}\frac{D_g}{2H_g}\Delta\omega\text{-}\frac{K_s}{2H_g}\Delta\theta_s \qquad \text{(B.19)}$$

$$\text{-}(m_{gco}i_{gdo}\sin\delta_o+m_{gco}i_{gqo}\cos\delta_o)\Delta V_c$$

$$\text{-}(V_{co}i_{gdo}\sin\delta_o+V_{co}i_{gqo}\cos\delta_o)\Delta m_{gc}))$$

Torsional Twist Angle (θ_s)

The shaft torsional angle is given by

$$\dot{\theta}_s=\omega_o(\omega_t\text{-}\omega) \qquad \text{(B.20)}$$

Linearize form of (B.20)

$$\dot{\Delta\theta}_s=\omega_o(\Delta\omega_t\text{-}\Delta\omega) \qquad \text{(B.21)}$$

$$\dot{\Delta\theta}_s=\omega_o\Delta\omega_t\text{-}\omega_o\Delta\omega \qquad \text{(B.22)}$$

Turbine Speed (ω_t)

$$\dot{\omega}_t=\frac{1}{2H_t}(P_m\text{-}K_s\theta_s\text{-}D_t(\omega_t\text{-}1)) \qquad \text{(B.23)}$$

The linearize form of (B.23) is

$$\dot{\Delta\omega}_t=\frac{1}{2H_t}(\text{-}K_s\Delta\theta_s\text{-}D_t\Delta\omega_t) \qquad \text{(B.24)}$$

$$\dot{\Delta\omega}_t=\text{-}(\frac{K_s}{2H_t})\Delta\theta_s\text{-}(\frac{D_t}{2H_t})\Delta\omega_t \qquad \text{(B.25)}$$

Incoming and Outgoing powers of the Converters (P_{in}, P_o)

Power coming towards the DC-Link capacitor is

$$P_{in} = v_{gd} i_{gd} + v_{gq} i_{gq} \tag{B.26}$$

The linearized version of incoming power is shown in (B.28)

$$\Delta P_{in} = (v_{gdo} \Delta i_{gd} + i_{gdo} \Delta v_{gd}) + (v_{gqo} \Delta i_{gq} + i_{gqo} \Delta v_{gq}) \tag{B.27}$$

$$\begin{aligned}
\Delta P_{in} &= (m_{gco} V_{co} \sin\delta_o) \Delta i_{gd} + (m_{gco} V_{co} \cos\delta_o) \Delta i_{gq} \\
&\quad + (m_{gco} V_{co} i_{gdo} \cos\delta_o - m_{gco} V_{co} i_{gqo} \sin\delta_o) \Delta\delta \\
&\quad + (m_{gco} i_{gdo} \sin\delta_o + m_{gco} i_{gqo} \cos\delta_o) \Delta V_c \\
&\quad + (V_{co} i_{gdo} \sin\delta_o + V_{co} i_{gqo} \cos\delta_o) \Delta m_{gc}
\end{aligned} \tag{B.28}$$

The Power comes out from the DC-link capacitor is

$$P_o = v_{id} i_{id} + v_{iq} i_{iq} \tag{B.28}$$

$$\Delta P_o = (v_{ido} \Delta i_{id} + i_{ido} \Delta v_{id}) + (v_{iqo} \Delta i_{iq} + i_{iqo} \Delta v_{iq}) \tag{B.29}$$

d-q axis voltages of the inverter (v_{id}, v_{iq})

The d-axis voltages of inverter is

$$v_{id} = m_{ic} V_c \cos\alpha_{ic} \tag{B.30}$$

Linearize form of (B.30) is

$$\Delta v_{id} = (m_{ico} \cos\alpha_{ico}) \Delta V_c - (m_{ico} V_{co} \sin\alpha_{ico}) \Delta\alpha_{ic} + (V_{co} \cos\alpha_{ico}) \Delta m_{ic} \tag{B.31}$$

The q-axis voltages of inverter is

$$v_{iq} = m_{ic} V_c \sin\alpha_{ic} \qquad (B.32)$$

Linearize form of (B.32) is

$$\Delta v_{iq} = (m_{ico} \sin\alpha_{ico})\Delta V_c + (m_{ico} V_{co} \cos\alpha_{ico})\Delta\alpha_{ic} + (V_{co} \sin\alpha_{ico})\Delta m_{ic} \qquad (B.33)$$

Using equation (B.29), linearize form of output power from the inverter is

$$\begin{aligned}
\Delta P_o = &(-m_{ico} V_{co} \cos\alpha_{ico})\Delta i_{id} + (m_{ico} V_{co} \sin\alpha_{ico})\Delta i_{iq} \\
&+ (-m_{ico} i_{ido} \cos\alpha_{ico} + m_{ico} i_{iqo} \sin\alpha_{ico})\Delta V_c \\
&+ (-V_{co} i_{ido} \cos\alpha_{ico} + V_{co} i_{iqo} \sin\alpha_{ico})\Delta m_{ic} \\
&+ (-m_{ico} V_{co} i_{ido} \sin\alpha_{ico} + m_{ico} V_{co} i_{iqo} \cos\alpha_{ico})\Delta\alpha_{ic}
\end{aligned} \qquad (B.34)$$

DC-Link Capacitor Voltage (V_C)

The DC-link capacitor voltage is given by (B.35)

$$CV_c \dot{V_c} = P_{in} - P_{out} \qquad (B.35)$$

Linearization of (B.35) is

$$\Delta\dot{V_c} = \frac{\Delta P_{in} - \Delta P_o}{CV_{co}} \qquad (B.36)$$

$$\Delta \dot{V}_c = \frac{1}{C}((m_{gco}\sin\delta_o)\Delta i_{gd} + (m_{gco}\cos\delta_o)\Delta i_{gq} + (m_{gco}i_{gdo}\cos\delta_o - m_{gco}i_{gqo}\sin\delta_o)\Delta\delta$$
$$+ (m_{gco}i_{gdo}\sin\delta_o + m_{gco}i_{gqo}\cos\delta_o + m_{ico}i_{ido}\cos\alpha_{ico} - m_{ico}i_{iqo}\sin\alpha_{ico})\Delta V_c$$
$$+ (m_{ico}\cos\alpha_{ico})\Delta i_{id} - (m_{ico}\sin\alpha_{ico})\Delta i_{iq} + (i_{gdo}\sin\delta_o + i_{gqo}\cos\delta_o)\Delta m_{gc}$$
$$+ (i_{ido}\cos\alpha_{ico} - i_{iqo}\sin\alpha_{ico})\Delta m_{ic} - (-m_{ico}i_{ido}\sin\alpha_{ico} + m_{ico}i_{iqo}\cos\alpha_{ico})\Delta\alpha_{ic})$$

(B.37)

SMES d-q axis currents (i_{smd}, i_{smq})

The d-axis component of SMES current is written as

$$i_{smd} = M_{SM}I_{dc}\cos(\theta_t - \alpha_{SM})$$

(B.38)

Linearized form of (B.38) is

$$\Delta i_{smd} = \Delta M_{SM}I_{dco}\cos(\theta_{to} - \alpha_{SMo}) + M_{SMo}\cos(\theta_{to} - \alpha_{SMo})\Delta I_{dco}$$
$$- M_{SMo}I_{dco}\sin(\theta_{to} - \alpha_{SMo})(\Delta\theta_{to} - \Delta\alpha_{SMo})$$

(B.39)

$$\Delta i_{smd} = I_{dco}\cos(\theta_{to} - \alpha_{SMo})\Delta M_{SM} + M_{SMo}\cos(\theta_{to} - \alpha_{SMo})\Delta I_{dco}$$
$$- M_{SMo}I_{dco}\sin(\theta_{to} - \alpha_{SMo})\Delta\theta_{to} + M_{SMo}I_{dco}\sin(\theta_{to} - \alpha_{SMo})\Delta\alpha_{SMo}$$

(B.40)

The q-axis component of SMES current is written as

$$i_{smq} = M_{SM}I_{dc}\sin(\theta_t - \alpha_{SM})$$

(B.41)

Linearized form of (B.41) is

$$\Delta i_{smq} = I_{dco}\sin(\theta_{to} - \alpha_{SMo})\Delta M_{SM} + M_{SMo}\sin(\theta_{to} - \alpha_{SMo})\Delta I_{dco}$$
$$- M_{SMo}I_{dco}\cos(\theta_{to} - \alpha_{SMo})(\Delta\theta_{to} - \Delta\alpha_{SMo})$$

(B.42)

$$\Delta i_{smq} = I_{dco}\sin(\theta_{to} - \alpha_{SMo})\Delta M_{SM} + M_{SMo}\sin(\theta_{to} - \alpha_{SMo})\Delta I_{dco}$$
$$+ M_{SMo}I_{dco}\cos(\theta_{to} - \alpha_{SMo})\Delta\theta_{to} - M_{SMo}I_{dco}\cos(\theta_{to} - \alpha_{SMo})\Delta\alpha_{SMo}$$

(B.43)

d-q axis voltages of AC Bus (t)

The d-axis component of AC bus voltage at which SMES and local load connected is

$$v_{td} = k_1(i_{id} + i_{smd}) + k_2(i_{iq} + i_{smq}) + (k_1 g_{Line} + k_2 b_{Line})V_b \tag{B.44}$$

Linearized form of (B.44) is

$$\Delta v_{td} = k_1\Delta i_{id} + k_1\Delta i_{smd} + k_2\Delta i_{iq} + k_2\Delta i_{smq} \tag{B.45}$$

$$\Delta v_{td} = k_1\Delta i_{id} + k_2\Delta i_{iq} + C_M\Delta M_1 + C_{IDC}\Delta I_{DC} + C_{THETAV}\Delta\theta_V + C_{ALPHASM}\Delta\alpha_{SM} \tag{B.46}$$

where

$$C_M = k_1 I_{dco}\cos(\theta_{Vo} - \alpha_{SMo}) + k_2 I_{dco}\sin(\theta_{Vo} - \alpha_{SMo})$$
$$C_{IDC} = k_1 M_{SMo}\cos(\theta_{Vo} - \alpha_{SMo}) + k_2 M_{SMo}\sin(\theta_{Vo} - \alpha_{SMo})$$
$$C_{THETAV} = k_2 M_{SMo}I_{dco}\cos(\theta_{Vo} - \alpha_{SMo}) - k_1 M_{SMo}I_{dco}\sin(\theta_{Vo} - \alpha_{SMo})$$
$$C_{ALPHASM} = k_1 M_{SMo}I_{dco}\sin(\theta_{Vo} - \alpha_{SMo}) - k_2 M_{SMo}I_{dco}\cos(\theta_{Vo} - \alpha_{SMo})$$

(B.47)

The q-axis component of AC bus voltage

$$v_{tq} = k_3(i_{id} + i_{smd}) + k_4(i_{iq} + i_{smq}) + (k_3 g_{Line} + k_4 b_{Line})V_b \tag{B.48}$$

Linearized form of (B.48) is

$$\Delta v_{tq} = k_3\Delta i_{id} + k_3\Delta i_{smd} + k_4\Delta i_{iq} + k_4\Delta i_{smq} \tag{B.49}$$

$$\Delta v_{tq} = k_3 \Delta i_{id} + k_4 \Delta i_{iq} + C_{M_i} \Delta M_1 + C_{IDC_i} \Delta I_{DC} + C_{THETAV_i} \Delta \theta_t + C_{ALPHASM_i} \Delta \alpha_{SM} \qquad \text{(B.50)}$$

Where

$$
\begin{aligned}
C_{M_i} &= k_3 I_{dco} \cos(\theta_{Vo} - \alpha_{SMo}) + k_4 I_{dco} \sin(\theta_{Vo} - \alpha_{SMo}) \\
C_{IDC_i} &= k_3 M_{SMo} \cos(\theta_{Vo} - \alpha_{SMo}) + k_4 M_{SMo} \sin(\theta_{Vo} - \alpha_{SMo}) \\
C_{THETAV_i} &= k_4 M_{SMo} I_{dco} \cos(\theta_{Vo} - \alpha_{SMo}) - k_3 M_{SMo} I_{dco} \sin(\theta_{Vo} - \alpha_{SMo}) \\
C_{ALPHASM_i} &= k_3 M_{SMo} I_{dco} \sin(\theta_{Vo} - \alpha_{SMo}) - k_4 M_{SMo} I_{dco} \cos(\theta_{Vo} - \alpha_{SMo})
\end{aligned}
\qquad \text{(B.51)}
$$

Inverter side d-q axis currents (i_{id}, i_{iq})

The d-axis inverter current is given by (B.52)

$$\dot{i}_{id} = \left(\frac{\omega_o}{x_i}\right)(v_{id} - v_{td} - R_i i_{id} + \omega X_i i_{iq}) \qquad \text{(B.52)}$$

Linearizing (B.52)

$$\Delta \dot{i}_{id} = \frac{\omega_o}{x_i}(\Delta v_{id} - \Delta v_{td} - R_i \Delta i_{id} + \omega_o X_i \Delta i_{iq} + i_{iqo} X_i \Delta \omega) \qquad \text{(B.53)}$$

$$
\begin{aligned}
\Delta \dot{i}_{id} = {}& T_{38} \Delta \omega + T_{39} \Delta V_c + T_{53} \Delta i_{id} + T_{54} \Delta i_{iq} + T_{55} \Delta I_{SMDC} + T_{56} \Delta delP_{SM} \\
& + T_{57} \Delta delQ_{SM} + T_{48} \Delta m_{ic} - T_{49} \Delta \alpha_{ic}
\end{aligned}
\qquad \text{(B.54)}
$$

The q-axis inverter current is given by (B.55)

$$\dot{i}_{iq} = \left(\frac{\omega_o}{X_i}\right)(v_{iq} - v_{tq} - R_i i_{iq} - \omega x_i i_{id}) \qquad \text{(B.55)}$$

Linearized form of (B.55) is

$$\Delta \dot{i}_{iq} = \frac{\omega_o}{x_i}(\Delta v_{iq} - \Delta v_{tq} - R_i \Delta i_{iq} + \omega_o X_i \Delta i_{iq} + i_{ido} X_i \Delta \omega) \qquad \text{(B.56)}$$

$$\Delta \dot{i}_{iq} = T_{40}\Delta\omega + T_{41}\Delta V_c + T_{58}\Delta i_{id} + T_{59}\Delta i_{iq} + T_{60}\Delta I_{SMDC} + T_{61}\Delta delP_{SM}$$
$$+ T_{62}\Delta delQ_{SM} + T_{48}\Delta m_{ic} + T_{49}\Delta\alpha_{ic} \qquad \text{(B.57)}$$

SMES DC current (I_{smdc})

The SMES DC coil current is given by (B.58)

$$L_{sc}\dot{I}_{smdc} = -I_{smdc}R_{sc} + \sqrt{v_{td}{}^2 + v_{tq}{}^2}\cos\alpha_{sm} - (\pi/12)I_{smdc}x_{cm} \qquad \text{(B.58)}$$

Linearized form of (B.58) is

$$\Delta \dot{I}_{smdc} = \frac{-V_{to}\sin\alpha_{SMo}\Delta\alpha_{SM}}{L_{SC}} - \frac{\Delta V_t \cos\alpha_{SMo}}{L_{SC}} - \frac{(\pi/12)x_{cm}}{L_{SC}}\Delta I_{smdc} \qquad \text{(B.59)}$$

$$\Delta \dot{I}_{smdc} = \frac{-V_{to}\sin\alpha_{SMo}\Delta\alpha_{SM}}{L_{SC}} + \frac{v_{tdo}\cos\alpha_{SMo}}{V_{to}L_{SC}}\Delta v_{td}$$
$$+ \frac{v_{tqo}\cos\alpha_{SMo}}{V_{to}L_{SC}}\Delta v_{tq} - \frac{(\pi/12)X_{cm}}{L_{SC}}\Delta I_{smdc} \qquad \text{(B.60)}$$

$$\Delta \dot{I}_{SMDC} = T_{63}\Delta i_{id} + T_{64}\Delta i_{iq} + T_{65}\Delta I_{SMDC} + T_{66}\Delta delP_{SM} + T_{67}\Delta delQ_{SM} \qquad \text{(B.61)}$$

Modulation Index of SMES (M_{SM}) and Firing Angle (α_{SM})

The Modulation index of SMES is written as

$$M_{SM} = \frac{\sqrt{P_{SM}{}^2 + Q_{SM}{}^2}}{V_t I_{dc}} \qquad \text{(B.62)}$$

Linearized form of (B.62) is

$$\Delta M_{SM} = T_{30}\Delta i_{id} + T_{31}\Delta i_{iq} + T_{32}\Delta I_{DC} + T_{33}\Delta delP_{SM} + T_{34}\Delta delQ_{SM} \qquad (B.63)$$

The SMES converter firing angle is given by (B.64)

$$\alpha_{SM} = \tan^{-1}(\frac{Q_{SM}}{P_{SM}}) \qquad (B.64)$$

Linearizing (B.64)

$$\Delta\alpha_{SM} = T_{22}\Delta delP_{SM} - \cot(\alpha_{SMo})T_{22}\Delta delQ_{SM} \qquad (B.65)$$

SMES real (P_{SM}) and reactive powers (Q_{SM})

The SMES compensated real power is given by (B.66)

$$del\dot{P}_{SM} = \frac{1}{T_{PG}}(K_{PG}\Delta P_g - delP_{SM}) \qquad (B.66)$$

Linearizing (B.66)

$$\Delta del\dot{P}_{SM} = \frac{1}{T_{PG}}(K_{PG}del\Delta P_g - \Delta delP_{SM}) \qquad (B.67)$$

$$
\begin{aligned}
\Delta del\dot{P}_{SM} = &-\frac{K_{PG}}{T_{PG}}(m_{gco}V_{co}\sin\delta_o + 2i_{gdo}R_a)\Delta i_{gd} - \frac{K_{PG}}{T_{PG}}(m_{gco}V_{co}\cos\delta_o + 2i_{gqo}R_a)\Delta i_{gq} - \\
&\frac{K_{PG}}{T_{PG}}(m_{gco}V_{co}i_{gdo}\cos\delta_o - m_{gco}V_{co}i_{gqo}\sin\delta_o)\Delta\delta - \\
&\frac{K_{PG}}{T_{PG}}(m_{gco}i_{gdo}\sin\delta_o + m_{gco}i_{gqo}\cos\delta_o)\Delta V_c - \frac{1}{T_{PG}}\Delta delP_{SM} - \\
&\frac{K_{PG}}{T_{PG}}(V_{co}i_{gdo}\sin\delta_o + V_{co}i_{gqo}\cos\delta_o)\Delta m_{gc}
\end{aligned}
\qquad (B.68)
$$

The SMES compensated reactive power is given by (B.69)

$$\dot{delQ}_{SM} = \frac{1}{T_{VG}}(K_{VG}\Delta V_g - delQ_{SM})$$ (B.69)

Linearized form of (B.69) is

$$\Delta \dot{delQ}_{SM} = \frac{1}{T_{VG}}(K_{VG}del\Delta V_g - \Delta delQ_{SM})$$ (B.69)

$$\Delta \dot{delQ}_{SM} = -\frac{K_{VG}}{T_{VG}V_{go}}(m_{gco}V_{gdo}V_{co}\cos\delta_o + m_{gco}V_{gqo}V_{co}\sin\delta_o)\Delta\delta -$$

$$\frac{K_{VG}}{T_{VG}V_{go}}(m_{gco}V_{gdo}\sin\delta_o + m_{gco}V_{gqo}\cos\delta_o)\Delta V_c$$ (B.70)

$$-\frac{1}{T_{VG}}\Delta delQ_{SM} - \frac{K_{VG}}{T_{VG}V_{go}}(V_{gdo}V_{co}\sin\delta_o + V_{gqo}V_{co}\cos\delta_o)\Delta m_{gc}$$

APPENDIX C

The components of linearized matrix A is mention below,

$a(1,1)= -(\frac{\omega_o x_d}{x_q})$, $a(1,2)= -(\frac{\omega_o R_a}{x_q})$, $a(1,3)=$

$-(\frac{\omega_o}{x_d} m_{gco} V_{co} \cos\delta_o)$,

$a(1,4)= (\frac{\omega_o x_q}{x_d}) i_{gqo}$, $a(1,7)= -(\frac{\omega_o}{x_d} m_{gco} \sin\delta_o)$

$a(2,1)= -(\frac{\omega_o x_d}{x_q})$, $a(2,2)= -(\frac{\omega_o R_a}{x_q})$, $a(2,3)=$

$(\frac{\omega_o m_{gco} V_{co} \sin\delta_o}{x_q})$,

$a(2,4)= \frac{\omega_o(E_{reso}-x_d i_{gdo})}{x_q}$, $a(2,7)= -(\frac{\omega_o m_{gco} \cos\delta_o}{x_q})$

$a(3,4)= \omega_o$

$a(4,1)= \frac{-(m_{gco} V_{co} \sin\delta_o + 2 i_{gdo} R_a)}{2H_g}$, $a(4,2)= \frac{-(m_{gco} V_{co} \cos\delta_o + 2 i_{gqo} R_a)}{2H_g}$

$a(4,3)= \frac{-(v_{gdo} i_{gdo} - v_{gqo} i_{gqo})}{2H_g}$, $a(4,4)= \frac{-D_g}{2H_g}$, $a(4,5)= \frac{-K_s}{2H_g}$

$$a(4,7)= \frac{-(m_{gco}i_{gdo}\sin\delta_o + m_{gco}i_{gqo}\cos\delta_o)}{2H_g},$$

$$a(5,4)= -\omega_o \qquad\qquad a(5,6)= \omega_o$$

$$a(6,5)= \frac{-K_s}{2H_t}, \qquad\qquad a(6,6)= -(\frac{D_t}{2H_t})$$

$$a(7,1)= \frac{m_{gco}\sin\delta_o}{C}, \qquad a(7,2)= \frac{m_{gco}\cos\delta_o}{C}, \quad a(7,3)=$$

$$\frac{(m_{gco}i_{gdo}\cos\delta_o - m_{gco}i_{gqo}\sin\delta_o)}{C},$$

$$a(7,7)= \frac{(m_{gco}i_{gdo}\sin\delta_o + m_{gco}i_{gqo}\cos\delta_o + m_{ico}i_{ido}\cos\alpha_{ico} - m_{ico}i_{iqo}\sin\alpha_{ico})}{C},$$

$$a(7,8)= \frac{(m_{ico}\cos\alpha_{ico})}{C}, \qquad\qquad a(7,9)= \frac{(m_{ico}\sin\alpha_{ico})}{C}$$

$$a(8,4)= T_{38}, \qquad a(8,7)= T_{39}, \qquad a(8,8)= T_{53}, \qquad a(8,9)= T_{54},$$

$$a(8,10)= T_{55}, \qquad a(8,11)= T_{56}, \qquad a(8,12)= T_{57}$$

$$a(9,4)= T_{40}, \qquad a(9,7)= T_{41}, \qquad a(9,8)= T_{58}, \qquad a(9,9)= T_{59},$$

$$a(9,10)= T_{60}, \qquad a(9,11)= T_{61}, \qquad a(9,12)= T_{62}$$

$$a(10,8)= T_{63}, \qquad a(10,9)= T_{64} \qquad a(10,10)= T_{65} \qquad a(10,11)= T_{66}$$

$$a(10,12)= T_{67}$$

$$a(11,1)= -\frac{K_{PG}(m_{gco}V_{co}\sin\delta_o+2i_{gdo}R_a)}{T_{PG}}, \qquad a(11,2)=$$

$$-\frac{K_{PG}(m_{gco}V_{co}\cos\delta_o+2i_{gqo}R_a)}{T_{PG}},$$

$$a(11,3)= \frac{K_{PG}(m_{gco}V_{co}i_{gdo}\cos\delta_o-m_{gco}V_{co}i_{gqo}\sin\delta_o)}{T_{PG}},$$

$$a(11,7)= \frac{K_{PG}(m_{gco}i_{gdo}\sin\delta_o+m_{gco}i_{gqo}\cos\delta_o)}{T_{PG}}, \qquad a(11,11)= -\frac{1}{T_{PG}}$$

$$a(12,3)= -\frac{K_{VG}(m_{gco}V_{gdo}V_{co}\cos\delta_o+m_{gco}V_{gqo}V_{co}\sin\delta_o)}{T_{VG}V_{go}},$$

$$a(12,7)= \frac{K_{VG}(m_{gco}V_{gdo}\sin\delta_o+m_{gco}V_{gqo}\cos\delta_o)}{T_{VG}V_{go}}, \qquad a(12,12)= -\frac{1}{T_{VG}}$$

APPENDIX D

The linearized constants are mention below,

$$c = \frac{v_{tdo}\cos(\alpha_{SM})}{V_t L_{sc}}$$

$$d = \frac{v_{tqo}\cos(\alpha_{SM})}{V_t L_{sc}}$$

$$S_s = P_{smo} + jQ_{smo}$$

$$S_{so} = \sqrt{(P_{smo}+delP_{smo})^2+(Q_{smo}+delQ_{smo})^2}$$

$$C_{VT} = \frac{(I_{smdco}S_{so})}{(V_t I_{smdco})^2}$$

$$C_{delP_{sm}} = \frac{(P_{smo}+delP_{smo})}{(V_t I_{smdco}S_{so})}$$

$$C_{delQ_{sm}} = \frac{(Q_{smo}+delQ_{smo})}{(V_t I_{smdco}S_{so})}$$

$$C_{IDCM_{SM}} = \frac{(V_t S_{so})}{(V_t I_{smdco})^2}$$

$$C_{VT_1} = \frac{(C_{VT} v_{tdo})}{V_t}$$

$$C_{VT_2} = \frac{(C_{VT} v_{tqo})}{V_t}$$

$$M_{CC} = (C_T \ C_M \ M_C - C_T \ C_{M_1} \ M_C \cot(\theta_{to}))$$

$$C_{AC} = (C_T - C_{ALPHAC1} - C_T \cot(\theta_{to}) C_{ALPHASM_1})$$

$$T_1 = (T_{CC} \ C_{ID})$$

$$T_2 = (T_{CC} \ C_{IQ})$$

$$T_3 = (T_{CC} \ C_{SM})$$

$$T_4 = (T_{CC} \ M_{CC})$$

$$C_T = \frac{-1}{(V_{tqo}(cosec(\theta_{to}))^2)}$$

$$T_{CC} = \frac{1}{(1 - C_{THETAV} + \cot(\theta_{to}) \ C_{THETAV1})}$$

$$M_C = \frac{1}{(1 + C_{VT_1} C_M + C_{VT_2} C_{M_1})}$$

$$C_{ID} = (CTk_1 - CT\cot(\theta_{to})k_3)$$

$$C_{IQ} = (CTk_2 - CT\cot(\theta_{to})k_4)$$

$$C_{SM} = (C_T C_{IDC} - C_T C_{IDC_1} \cot(\theta_{to}))$$

$$T_5 = (T_{CC} \, C_{AC})$$

$$T_6 = -\frac{T_5}{((Q_{smo} + delQ_{smo}) \, (cosec(\alpha_{SMo}))^2))}$$

$$T_7 = \frac{1}{(1 + C_{VT1} \, C_{THETAV} + C_{VT2} \, C_{THETAV1})}$$

$$T_8 = T_4 (C_{VT1} \, k_1 + C_{VT_2} \, k_3)$$

$$T_9 = T_4 (C_{VT1} \, k_2 + C_{VT_2} \, k_4)$$

$$T_{10} = T_4 (C_{IDCM_1} + C_{VT1} \, C_{IDC} + C_{VT_2} \, C_{IDC_1})$$

$$T_{11} = T_4 \, T_5 (C_{VT_1} \, C_{ALPHASM} + C_{VT_2} \, C_{ALPHASM_1})$$

$$T_{12} = (C_{IDCM_1} + C_{VT_1} \, C_{IDC} + C_{VT_2} \, C_{IDC_1})$$

$$T_{13} = (C_{VT_1} \, k_1 + C_{VT_2} \, k_3)$$

$$T_{14} = (C_{VT_1} \, k_2 + C_{VT_2} \, k_4)$$

$$T_{15} = \frac{((C_{VT_1} \, C_{ALPHASM} + C_{VT_2} \, C_{ALPHASM_1}) M_c)}{((Q_{smo} + delQ_{smo})(cosec(\alpha_{SM}))^2)}$$

$$T_{16} = (C_{VT_1} \, C_{THETAV} + C_{VT_2} \, C_{THETAV_1})$$

$$T_{17} = (T_{16} \ T_1 \ T_7 - T_7 \ T_8 \ T_{16})$$

$$T_{18} = (T_2 \ T_7 \ T_{16} - T_9 \ T_7 \ T_{16})$$

$$T_{19} = (T_3 \ T_7 \ T_{16} - T_7 \ T_{10} \ T_{16})$$

$$T_{20} = (T_4 \ T_7 \ T_{16} \ C_{delP_{sm}} - T_7 \ T_{11} \ T_6 + T_6 \ T_7 \ T_{16})$$

$$T_{21} = (T_4 \ T_7 \ T_{16} \ C_{delQ_{sm}} + T_{11} \ T_7 \ T_{16} \cot(\alpha_{SM}) - T_6 \ T_7 \ T_{16} \cot(\alpha_{SM}))$$

$$T_{22} = \frac{-1}{((Q_{smo} + delQ_{smo})(\csc(\alpha_{SM}))^2)}$$

$$T_{23} = \frac{-(\omega_O \ C_{THETAV})}{X_i}$$

$$T_{24} = (T_1 \ T_7 - T_7 \ T_8)$$

$$T_{25} = (T_2 \ T_7 - T_7 \ T_9)$$

$$T_{26} = (T_3 \ T_7 - T_7 \ T_{10})$$

$$T_{27} = (T_4 \ T_7 \ C_{delP_{sm}} - T_7 \ T_{11} + T_6 \ T_7)$$

$$T_{28} = (T_4 \ T_7 \ C_{delQ_{sm}} + T_{11} \ T_7 \cot(\alpha_{SM}) - T_6 \ T_7 \cot(\alpha_{SM}))$$

$$T_{29} = -\frac{(\omega_O \ C_M)}{X_i}$$

$$T_{30} = -(M_C\ T_{13} + T_{17})$$

$$T_{31} = -(T_{14}\ M_C + T_{18})$$

$$T_{32} = -(T_{12}\ M_C + T_{19})$$

$$T_{33} = (M_C\ C_{delP_{sm}} + T_{15} - T_{20})$$

$$T_{34} = (M_C\ C_{delQ_{sm}} + T_{15} - T_{21})$$

$$T_{35} = \frac{-(\omega_o\ C_{ALPHASM})}{x_i}$$

$$T_{36} = \frac{-(\omega_o\ (R_i + k_1))}{x_i}$$

$$T_{37} = \frac{(\omega_o\ (Xi - k2))}{x_i}$$

$$T_{38} = \omega_o\ i_{iqo}$$

$$T_{39} = \frac{-(\omega_o\ m_{2o}\ \cos(\alpha_{2o}))}{x_i}$$

$$T_{40} = -\omega_o\ i_{ido}$$

$$T_{41} = \frac{(\omega_o\ m_{2o}\ \sin(\alpha_{2o}))}{x_i}$$

$$T_{42} = \frac{-(\omega_o\ (Xi + k3))}{x_i}$$

$$T_{43} = \frac{-(\omega_o\ (Ri+k4))}{x_i}$$

$$T_{44} = \frac{-(\omega_o\ C_{IDC1})}{x_i}$$

$$T_{45} = \frac{-(\omega_o\ C_{M1})}{x_i}$$

$$T_{46} = \frac{-(\omega_o\ C_{ALPHASM_1})}{x_i}$$

$$T_{47} = \frac{-(\omega_o\ C_{THETAV1})}{x_i}$$

$$T_{48} = \frac{(\omega_o\ Vco\ \sin(alpha2o)}{x_i}$$

$$T_{49} = \frac{(\omega_o\ m2o\ Vco\ \cos(\alpha_{2o})}{x_i}$$

$$T_{50} = (c\ C_{IDC} + d\ C_{IDC1} - (\frac{pi\ Xi}{12\ Lsc}))$$

$$T_{51} = (c\ C_M + d\ C_{M1})$$

$$T_{52} = \frac{(-V_t\ \sin(\alpha_{SM}))}{Lsc} + c\ C_{ALPHASM} + d\ C_{ALPHASM_1}$$

$$T_{53} = T_{36} + T_{23} \; T_{24} + T_{29} \; T_{30}$$

$$T_{54} = T_{37} + T_{23} \; T_{25} + T_{29} \; T_{31}$$

$$T_{55} = -C_{IDC} \frac{\omega_o}{X_i} + T_{23} \; T_{26} + T_{29} \; T_{32}$$

$$T_{56} = T_{23} \; T_{27} + T_{29} \; T_{33} + T_{22} \; T_{35}$$

$$T_{57} = T_{23} \; T_{28} + T_{29} \; T_{34} - T_{22} \; T_{35} \cot(\alpha_{SMo})$$

$$T_{58} = T_{42} + T_{30} \; T_{45} + T_{24} \; T_{47}$$

$$T_{59} = T_{43} + T_{31} \; T_{45} + T_{25} \; T_{47}$$

$$T_{60} = T_{44} + T_{32} \; T_{45} + T_{26} \; T_{47}$$

$$T_{61} = T_{33} \; T_{45} + T_{46} \; T_{22} + T_{27} \; T_{47}$$

$$T_{62} = T_{34} \; T_{45} + T_{28} \; T_{47} - T_{22} \; T_{46} \cot(\alpha_{SMo})$$

$$T_{63} = (Ck_1 + dk_3) + T_{51} \; T_{30} + T_{53} \; T_{24}$$

$$T_{64} = (Ck_2 + dk_4) + T_{51} \; T_{31} + T_{53} \; T_{25}$$

$$T_{65} = T_{51} \; T_{32} + T_{50} + T_{53} \; T_{26}$$

$$T_{66} = T_{51} \; T_{33} + T_{52} \; T_{33} + T_{53} \; T_{27}$$

$$T_{67} = T_{51} \; T_{34} + T_{52} \; T_{22} \cot(\alpha_{SMo}) + T_{53} \; T_{28}$$

NOMENCLATURE

Abbreviations

AC	Alternating Current
DC	Direct Current
DFIG	Doubly Fed Induction Generator
BESS	Battery Energy Storage System
FACT	Flexible AC Transmission System
LVRT	Low Voltage Ride Through
IGBT	Insulated Gate Bipolar Transistor
IPSO	Improved Particle Swarm Optimization
PI	Proportional plus Integral
PMSG	Permanent Magnet Synchronous Generator
RBFNN	Radial Basis Function Neural Network
STATCOM	Static Synchronous Compensator
SVC	Static Var Compensator
SMES	Superconducting Magnetic Energy Storage System
WECS	Wind Energy Conversion System
WRIG	Wound Rotor Induction Generator

<u>Symbols</u>

i_{gd}	d-axis stator current
i_{gq}	q-axis stator current
v_{gd}	d-axis generator bus voltage
v_{gq}	q-axis generator bus voltage
δ	PMSG power angle
ω	PMSG synchronous speed
θ_s	Shaft torsional twist angle
ω_t	Turbine speed
V_c	DC-link capacitor voltage
i_{id}	d-axis inverter current
i_{iq}	q-axis inverter current
I_{dc}	SMES DC Current
P_{SM}	Compensated SMES real power
Q_{SM}	Compensated SMES reactive power
P_{gref}	PMSG reference power
V_{gref}	PMSG bus reference voltage
R_a	PMSG stator resistance
x_d	Synchronous reactance
H_g	Generator inertia constant

H_t	Turbine inertia constant
K_S	Shaft stiffness constant
P_m	Mechanical power
P_e	PMSG generated electrical power
C	Capacitance of DC-link capacitor
P_{in}	Input power to the generator side inverter
P_o	Output power of the grid side inverter
v_{id}	d-axis grid side inverter voltage
v_{iq}	q-axis grid side inverter voltage
v_{td}	d-axis voltage of the AC bus
v_{tq}	q-axis voltage of the AC bus
R_i	Resistance of the line between the AC bus and grid side inverter
x_i	Reactance of the line between the AC bus and grid side inverter
m_{gc}	Modulation index of generator side inverter
m_{ic}	Modulation index of grid side inverter
α_{gc}	Firing angle of generator side inverter
α_{ic}	Firing angle of grid side inverter
V_b	Infinite bus voltage
i_{smd}	d-axis SMES current
i_{smq}	q-axis SMES current

M_{SM}	Modulation index of SMES
α_{SM}	Firing angle of SMES
K_{PG}	SMES controller gain (generator real power)
K_{PV}	SMES controller gain (generator bus voltage)
T_{PG}	SMES Controller time response (generator real power)
T_{PV}	SMES Controller time response (generator bus voltage)
R_{SC}	Resistance of superconducting coil of SMES
L_{SC}	Inductance of superconducting coil of SMES
x_{CM}	Commutation reactance of the power controller of SMES
c_1, c_2	Acceleration constants of IPSO
w	Inertia weight of IPSO
ς	Damping coefficient of the system
σ	Real part of eigenvalue
γ	Imaginary part of eigenvalue
β	Spread factor of RBFNN
y_i	Output of RBFNN
E_p	Mean square error of RBFNN
η	Regulation factor of Adaptive RBFNN
ρ	Learning parameter of Adaptive RBFNN

BIBLIOGRAPHY

[1]   M.-S. Lu, C.-L. Chang, and W.-J. Lee, "Impact of Wind Generation on a Transmission System," *2007 39th North American Power Symposium*, IEEE, 2007, pp. 348–352.

[2]   T.N.Z. Haiqing, "Operation of quoting and bidding system in Shanghai power generation market," *2003 IEEE PES Transmission and Distribution Conference and Exposition (IEEE Cat. No.03CH37495)*, IEEE, , pp. 689–697.

[3]   A. Dhanju, J. Firestone, and W. Kempton, "Potential role of power authorities in offshore wind power development in the US," *Energy Policy*, vol. 39, Nov. 2011, pp. 7025–7035.

[4]   P. Perez, D. Hertem, J. Driesen, and R. Belmans, "Wind power in the European Union: grid connection and regulatory issues," *2006 IEEE PES Power Systems Conference and Exposition*, IEEE, 2006, pp. 776–783.

[5]   "Wind Farm" Available: http://en.wikipedia.org/wiki/Wind_farm.

[6]   H. Ahuja, G. Bhuvaneswari, and R. Balasubramanian, "Performance comparison of DFIG and PMSG based WECS," *IET Conference on Renewable Power Generation (RPG 2011)*, IET, 2011, pp. 1–6.

[7]   Y. Ditkovich, A. Kuperman, A. Yahalom, and M. Byalsky, "A Generalized Approach to Estimating Capacity Factor of Fixed Speed Wind Turbines," *IEEE Transactions on Sustainable Energy*, vol. 3, Jul. 2012, pp. 607–608.

[8]   P.W. Carlin, A.S. Laxson, and E.B. Muljadi, "The History and State of the Art of Variable-Speed Wind Turbine Technology," *Wind Energy*, vol. 6, Apr. 2003, pp. 129–159.

[9]   R. Mittal, K.S. Sandhu, and D.K. Jain, "Fault ride- through capability of grid connected variable speed permanent magnet synchronous generator for wind energy conversion system," *2009 IEEE Electrical Power & Energy Conference (EPEC)*, IEEE, 2009, pp. 1–6.

[10] M. Chinchilla, S. Arnaltes, and J.C. Burgos, "Control of Permanent-Magnet Generators Applied to Variable-Speed Wind-Energy Systems Connected to the Grid," *IEEE Transactions on Energy Conversion*, vol. 21, Mar. 2006, pp. 130–135.

[11] W. Li and G. Joos, "Comparison of Energy Storage System Technologies and Configurations in a Wind Farm," *2007 IEEE Power Electronics Specialists Conference*, IEEE, 2007, pp. 1280–1285.

[12] A. Mohd, E. Ortjohann, A. Schmelter, N. Hamsic, and D. Morton, "Challenges in integrating distributed Energy storage systems into future smart grid," *2008 IEEE International Symposium on Industrial Electronics*, IEEE, 2008, pp. 1627–1632.

[13] H. Geng, D. Xu, B. Wu, and G. Yang, "Active Damping for PMSG-Based WECS With DC-Link Current Estimation," *IEEE Transactions on Industrial Electronics*, vol. 58, Apr. 2011, pp. 1110–1119.

[14] V. Sheeja, B. Singh, and R. Uma, "BESS Based Voltage and Frequency Controller for Stand Alone Wind Energy Conversion System Employing PMSG," *2009 IEEE Industry Applications Society Annual Meeting*, IEEE, 2009, pp. 1–6.

[15] K.-H. Kim, Y.-C. Jeung, D.-C. Lee, and H.-G. Kim, "Robust control of PMSG wind turbine systems with back-to-back PWM converters," *The 2nd International Symposium on Power Electronics for Distributed Generation Systems*, IEEE, 2010, pp. 433–437.

[16] A.D. Hansen and G. Michalke, "Modelling and control of variable-speed multi-pole permanent magnet synchronous generator wind turbine," *Wind Energy*, vol. 11, Sep. 2008, pp. 537–554.

[17] A.D. Hansen and G. Michalke, "Multi-pole permanent magnet synchronous generator wind turbines' grid support capability in uninterrupted operation during grid faults," *IET Renewable Power Generation*, vol. 3, 2009, pp. 333–348.

[18] C.-L. Dang, L. Zhang, and M.-X. Zhou, "Optimal Power Control Model of Direct Driven PMSG," *Energy Procedia*, vol. 12, Jan. 2011, pp. 844–848.

[19] W.-M. Lin, C.-M. Hong, M.-R. Lee, C.-H. Huang, C.-C. Huang, and B.-L. Wu, "Fuzzy sliding mode-based control for PMSG maximum wind energy capture with

compensated pitch angle," *2010 International Symposium on Computer, Communication, Control and Automation (3CA)*, IEEE, 2010, pp. 397–400.

[20] H. Geng, G. Yang, D. (David) Xu, and B. Wu, "Unified Power Control for PMSG-Based WECS Operating Under Different Grid Conditions," *IEEE Transactions on Energy Conversion*, vol. 26, Sep. 2011, pp. 822–830.

[21] X. Shen, Y. Wang, and Y. Li, "A Novel UPF Control Strategy of PMSG Based on Stator Flux Orientation," *2011 Asia-Pacific Power and Energy Engineering Conference*, IEEE, 2011, pp. 1–4.

[22] L. Wang and D.-N. Truong, "Dynamic Stability Improvement of Four Parallel-Operated PMSG-Based Offshore Wind Turbine Generators Fed to a Power System Using a STATCOM," *IEEE Transactions on Power Delivery*, 2012, pp. 111–119.

[23] W. Li and D. Truong, "Stability Enhancement of a Power System with a PMSG-based and a DFIG-based Offshore Wind Farms Using a SVC with an Adaptive-Network-based Fuzzy Inference System," *IEEE Transactions on Industrial Electronics*, 2012, p. 1.

[24] J.F. Conroy and R. Watson, "Low-voltage ride-through of a full converter wind turbine with permanent magnet generator," *IET Renewable Power Generation*, vol. 1, 2007, pp. 182–189.

[25] A. Abedini and A. Nasiri, "Applications of super capacitors for PMSG wind turbine power smoothing," *2008 34th Annual Conference of IEEE Industrial Electronics*, IEEE, 2008, pp. 3347–3351.

[26] T.H. Nguyen, D.-C. Lee, S.-H. Song, and E.-H. Kim, "Improvement of power quality for PMSG wind turbine systems," *2010 IEEE Energy Conversion Congress and Exposition*, IEEE, 2010, pp. 2763–2770.

[27] S.-S. Chen, L. Wang, W.-J. Lee, and Z. Chen, "Power flow control and damping enhancement of a large wind farm using a superconducting magnetic energy storage unit," *IET Renewable Power Generation*, vol. 3, 2009, pp. 23–28.

[28] M.H. Ali and J. Tamura, "SMES strategy to minimize frequency fluctuations of wind generator system," *2008 34th Annual Conference of IEEE Industrial Electronics*, IEEE, 2008, pp. 3382–3387.

[29] F. Zhou, G. Joos, C. Abbey, L. Jiao, and B.T. Ooi, "Use of large capacity SMES to improve the power quality and stability of wind farms," *IEEE Power Engineering Society General Meeting, 2004.*, IEEE, , pp. 2025–2030.

[30] S.M. Muyeen, M.H. Ali, R. Takahashi, T. Murata, and J. Tamura, "Wind Generator Output Power Smoothing and Terminal Voltage Regulation by Using STATCOM/ESS," *2007 IEEE Lausanne Power Tech*, IEEE, 2007, pp. 1232–1237.

[31] J. Shi, Y.J. Tang, L. Ren, J.D. Li, and S.J. Chen, "Application of SMES in wind farm to improve voltage stability," *Physica C: Superconductivity*, vol. 468, Sep. 2008, pp. 2100–2103.

[32] A.D. Hansen and L.H. Hansen, "Wind turbine concept market penetration over 10 years (1995–2004)," *Wind Energy*, vol. 10, Jan. 2007, pp. 81–97.

[33] I. Erlich, W. Winter, and A. Dittrich, "Advanced grid requirements for the integration of wind turbines into the German transmission system," *2006 IEEE Power Engineering Society General Meeting*, IEEE, 2006, p. 1.

[34] F. Blaabjerg, Z. Chen, and S.B. Kjaer, "Power Electronics as Efficient Interface in Dispersed Power Generation Systems," *IEEE Transactions on Power Electronics*, vol. 19, Sep. 2004, pp. 1184–1194.

[35] E. Hau., *Wind turbines: fundamentals, technologies, application, economics.*, Springer Verlag Berlin Heidelberg, 2000.

[36] J.F. Brudny, R. Pusca, and H. Roisse, "Wind turbines using self-excited three-phase induction generators: an innovative solution for voltage-frequency control," *The European Physical Journal Applied Physics*, vol. 43, Jul. 2008, pp. 173–187.

[37] E. Jafari and A. Marjanian, "Theoretical implementation of a novel isolated three-phase induction generator with controllable output voltage using a three-phase four-switch STATCOM," *2011 2nd International Conference on Electric Power and Energy Conversion Systems (EPECS)*, IEEE, 2011, pp. 1–6.

[38] J.C. Ferreira, I.R. Machado, E.H. Watanabe, and L.G.B. Rolim, "Wind power system based on Squirrel Cage Induction Generator," *XI Brazilian Power Electronics Conference*, IEEE, 2011, pp. 943–948.

[39] A.D. Hansen, P. Sorensen, L. Janosi, and J. Bech, "Wind farm modelling for power quality," *IECON'01. 27th Annual Conference of the IEEE Industrial Electronics Society (Cat. No.37243)*, IEEE, 2001, pp. 1959–1964.

[40] W. Qiao, G. Venayagamoorthy, and R. Harley, "Real-Time Implementation of a STATCOM on a Wind Farm Equipped with Doubly Fed Induction Generators," *Conference Record of the 2006 IEEE Industry Applications Conference Forty-First IAS Annual Meeting*, IEEE, 2006, pp. 1073–1080.

[41] Z.M.Y.C.L.L.Y. Yu, "Dynamic performance improvement of wind farm with doubly fed induction generators using STATCOM," *2010 International Conference on Power System Technology*, IEEE, 2010, pp. 1–6.

[42] W.Q.X.G.L. Qu, "Output maximization control for DFIG wind turbines without using wind and shaft speed measurements," *2009 IEEE Energy Conversion Congress and Exposition*, IEEE, 2009, pp. 404–410.

[43] L. chun, K. Yong, C. Jian, K. Lee, L. Xinchun, L. Xiaohu, and X. Feidong, "Simplified Active and Reactive Power Control of Doubly Fed Induction Generator and the Simulation with STATCOM," *2009 Twenty-Fourth Annual IEEE Applied Power Electronics Conference and Exposition*, IEEE, 2009, pp. 1927–1931.

[44] J.G. Slootweg and W.L. Kling, "The impact of large scale wind power generation on power system oscillations," *Electric Power Systems Research*, vol. 67, Oct. 2003, pp. 9–20.

[45] K. Ibrahima and C. Zhao, "Modeling of wind energy conversion system using doubly fed induction generator equipped batteries energy storage system," *2011 4th International Conference on Electric Utility Deregulation and Restructuring and Power Technologies (DRPT)*, IEEE, 2011, pp. 1780–1787.

[46] L. Holdsworth, X.G. Wu, J.B. Ekanayake, and N. Jenkins, "Comparison of fixed speed and doubly-fed induction wind turbines during power system disturbances," *IEE Proceedings - Generation, Transmission and Distribution*, vol. 150, 2003, pp. 343–352.

[47] H. Xu, J. Hu, and Y. He, "Integrated Modeling and Enhanced Control of DFIG Under Unbalanced and Distorted Grid Voltage Conditions," *IEEE Transactions on Energy Conversion*, vol. 27, Sep. 2012, pp. 725–736.

[48] R. Pena, J.C. Clare, and G.M. Asher, "Doubly fed induction generator using back-to-back PWM converters and its application to variable-speed wind-energy generation," *IEE Proceedings - Electric Power Applications*, vol. 143, 1996, pp. 231–241.

[49] L. Xu and Y. Wang, "Dynamic modeling and control of DFIG-based wind turbines under unbalanced network conditions," *Power Systems, IEEE Transactions on*, vol. 22, 2007, pp. 314–323.

[50] G.D. Marques and D.M. Sousa, "Understanding the Doubly Fed Induction Generator During Voltage Dips," *IEEE Transactions on Energy Conversion*, vol. 27, Jun. 2012, pp. 421–431.

[51] S. Fukui, J. Ogawa, T. Sato, O. Tsukamoto, N. Kashima, and S. Nagaya, "Study of 10 MW-Class Wind Turbine Synchronous Generators With HTS Field Windings," *IEEE Transactions on Applied Superconductivity*, vol. 21, Jun. 2011, pp. 1151–1154.

[52] Cé.C. Scharlau, L.F.A. Pereira, L.A. Pereira, and Sé. Haffner, "Performance of a Five-Phase Induction Machine With Optimized Air Gap Field Under Open Loop V/f Control," *IEEE Transactions on Energy Conversion*, vol. 23, Dec. 2008, pp. 1046–1056.

[53] M. Stiebler, "PM synchronous generator with diode rectifier for wind systems using FACTS compensators," *International Symposium on Power Electronics Power Electronics, Electrical Drives, Automation and Motion*, IEEE, 2012, pp. 1295–1300.

[54] R. Mittal, K.S. Sandhu, and D.K. Jain, "Battery energy storage system for variable speed driven PMSG for wind energy conversion system," *2010 Joint International Conference on Power Electronics, Drives and Energy Systems & 2010 Power India*, IEEE, 2010, pp. 1–5.

[55] G.H. Kim, A.R. Kim, S. Kim, M. Park, I.K. Yu, K.C. Seong, and Y.J. Won, "A novel HTS SMES application in combination with a permanent magnet synchronous generator type wind power generation system," *Physica C: Superconductivity*, vol. 471, Nov. 2011, pp. 1413–1418.

[56] C. Xia, "Input–Output Feedback Linearization and Speed Control of a Surface Permanent-Magnet Synchronous Wind Generator With the Boost-Chopper

Converter," *IEEE Transactions on Industrial Electronics*, vol. 59, Sep. 2012, pp. 3489–3500.

[57]   L.N. Modran, "Power flow control on wind power plant with permanent magnet synchronous generator," *2008 11th International Conference on Optimization of Electrical and Electronic Equipment*, IEEE, 2008, pp. 419–426.

[58]   J.-C. Dai, Y.-P. Hu, D.-S. Liu, and J. Wei, "Modelling and analysis of direct-driven permanent magnet synchronous generator wind turbine based on wind-rotor neural network model," *Proceedings of the Institution of Mechanical Engineers, Part A: Journal of Power and Energy*, vol. 226, Oct. 2011, pp. 62–72.

[59]   M. Mansour, M.N. Mansouri, and M.F. Mimouni, "Study of performance of a variable-speed wind turbine with pitch control based on a Permanent Magnet Synchronous Generator," *Eighth International Multi-Conference on Systems, Signals & Devices*, IEEE, 2011, pp. 1–6.

[60]   S. Li and T.A. Haskew, "Characteristic study of vector-controlled direct driven permanent magnet synchronous generator in wind power generation," *Power and Energy Society General Meeting-Conversion and Delivery of Electrical Energy in the 21st Century, 2008 IEEE*, IEEE, 2009, pp. 1–9.

[61]   J.M. Carrasco, L.G. Franquelo, J.T. Bialasiewicz, E. Galván, R.C.P. Guisado, M.A.M. Prats, J.I. León, and N. Moreno-Alfonso, "Power-electronic systems for the grid integration of renewable energy sources: A survey," *Industrial Electronics, IEEE Transactions on*, vol. 53, 2006, pp. 1002–1016.

[62]   A.J. Mitcham and N. Grum, "An integrated LP shaft generator for the More Electric aircraft," *IEE Colloquium on All Electric Aircraft*, IEE, 1998, pp. 8/1 – 8/9.

[63]   A.M. Garcia, D. Holmes, and T. Lipo, "Reduction of Bearing Currents in Doubly Fed Induction Generators," *Industry Applications Conference, 2006. 41st IAS Annual Meeting. Conference Record of the 2006 IEEE*, IEEE, 2006, pp. 84–89.

[64]   D.M. Vilathgamuwa, S.D.G. Jayasinghe, and U.K. Madawala, "Space vector modulated cascade multi-level inverter for PMSG wind generation systems," *2009 35th Annual Conference of IEEE Industrial Electronics*, IEEE, 2009, pp. 4600–4605.

[65] M. Bash, S. Pekarek, S. Sudhoff, J. Whitmore, and M. Frantzen, "A comparison of permanent magnet and wound rotor synchronous machines for portable power generation," *2010 Power and Energy Conference At Illinois (PECI)*, IEEE, 2010, pp. 1–6.

[66] J.S. Thongam, P. Bouchard, V. Giurgiu, H.T. Bui, and M. Ouhrouche, "Sensorless vector control of PMSG for variable speed wind energy applications," *CCECE 2010*, IEEE, 2010, pp. 1–5.

[67] M. Molina and P. Mercado, "A new control strategy of variable speed wind turbine generator for three-phase grid-connected applications," *Transmission and Distribution Conference and Exposition: Latin America, 2008 IEEE/PES*, IEEE, 2008, pp. 1–8.

[68] M.G. Molina and P.E. Mercado, *Wind Power in Power Systems*, Chichester, UK: John Wiley & Sons, Ltd, 2005.

[69] G. l. Hunt, "The great battery search," *IEEE Spectrum*, vol. 35, 1998, pp. 21–28.

[70] E. Lerch, "Storage of fluctuating wind energy," *2007 European Conference on Power Electronics and Applications*, IEEE, 2007, pp. 1–8.

[71] R.S. Fritz Crotogino, K. Mohmeyer, *"Huntorf CAES: More than 20 Years of Successful Operation,"* 2001.

[72] N. Zhai, Y. Yao, D. Zhang, and D. Xu, "Design and Optimization for a Supercapacitor Application System," *2006 International Conference on Power System Technology*, IEEE, 2006, pp. 1–4.

[73] D.S. Padimiti and B.H. Chowdhury, "Superconducting Magnetic Energy Storage System (SMES) for Improved Dynamic System Performance," *2007 IEEE Power Engineering Society General Meeting*, IEEE, 2007, pp. 1–6.

[74] R. Boom and H. Peterson, "Superconductive energy storage for power systems," *IEEE Transactions on Magnetics*, vol. 8, Sep. 1972, pp. 701–703.

[75] M.H. Ali and R. a Dougal, "An Overview of SMES Applications in Power and Energy Systems," *IEEE Transactions on Sustainable Energy*, vol. 1, Apr. 2010, pp. 38–47.

[76]   M. Parizh, A.K. Kalafala, and R. Wilcox, "Superconducting magnetic energy storage for substation applications," *IEEE Transactions on Appiled Superconductivity*, vol. 7, Jun. 1997, pp. 849–852.

[77]   C.A. Luongo, "Superconducting storage systems: an overview," *IEEE Transactions on Magnetics*, vol. 32, Jul. 1996, pp. 2214–2223.

[78]   P.G. Therond, I. Joly, and M. Volker, "Superconducting magnetic energy storage (SMES) for industrial applications-comparison with battery systems," *IEEE Transactions on Appiled Superconductivity*, vol. 3, Mar. 1993, pp. 250–253.

[79]   K. Hayakawa, M. Masuda, T. Shintomi, and J. Hasegawa, "Test plant as the first step towards commercialization of SMES for utilities," *IEEE Transactions on Magnetics*, vol. 24, Mar. 1988, pp. 887–890.

[80]   A. Kalafala, J. Bascunan, D. Bell, L. Blecher, F. Murray, M. Parizh, M. Sampson, and R. Wilcox, "Micro superconducting magnetic energy storage (SMES) system for protection of critical industrial and military loads," *Magnetics, IEEE Transactions on*, vol. 32, 1996, pp. 2276–2279.

[81]   L. Chen, Y. Liu, A. Arsoy, P. Ribeiro, M. Steurer, and M. Iravani, "Detailed modeling of superconducting magnetic energy storage (SMES) system," *Power Delivery, IEEE Transactions on*, vol. 21, 2006, pp. 699–710.

[82]   C.-S. Hsu and W.-J. Lee, "Superconducting magnetic energy storage for power system applications," *IEEE Transactions on Industry Applications*, vol. 29, 1993, pp. 990–996.

[83]   W.E. Buckles, M.A. Daugherty, B.R. Weber, and E.L. Kostecki, "THE SSD : A COMMERCIAL APPLICATION OF MAGNETIC ENERGY STORAGE," *IEEE Transactions on Applied Superconductivity*, vol. 3, 1993, pp. 328–331.

[84]   X.D. Xue, K.W.E. Cheng, and D. Sutanto, "Power system applications of superconducting magnetic energy storage systems," *Fourtieth IAS Annual Meeting. Conference Record of the 2005 Industry Applications Conference, 2005.*, IEEE, 2005, pp. 1524–1529.

[85]   W.V. Torre and S. Eckroad, "Improving power delivery through the application of superconducting magnetic energy storage (SMES)," *2001 IEEE Power*

Engineering Society Winter Meeting. Conference Proceedings (Cat. No.01CH37194), IEEE, , pp. 81–87.

[86] X.D. Xue, K.W.E. Cheng, and D. Sutanto, "A study of the status and future of superconducting magnetic energy storage in power systems," *Superconductor Science and Technology*, vol. 19, Jun. 2006, pp. R31–R39.

[87] S. Suzuki, J. Baba, K. Shutoh, and E. Masada, "Effective Application of Superconducting Magnetic Energy Storage (SMES) to Load Leveling for High Speed Transportation System," *IEEE Transactions on Appiled Superconductivity*, vol. 14, Jun. 2004, pp. 713–716.

[88] X.D. Xue, K.W.E. Cheng, and D. Sutanto, "Power system applications of superconducting magnetic energy storage systems," *Fourtieth IAS Annual Meeting. Conference Record of the 2005 Industry Applications Conference, 2005.*, IEEE, , pp. 1524–1529.

[89] P.D. Baumann, "Energy conservation and environmental benefits that may be realized from superconducting magnetic energy storage," *IEEE Transactions on Energy Conversion*, vol. 7, Jun. 1992, pp. 253–259.

[90] T. Kinjo, T. Senjyu, N. Urasaki, and H. Fujita, "Terminal-voltage and output-power regulation of wind-turbine generator by series and parallel compensation using SMES," *IEE Proceedings - Generation, Transmission and Distribution*, vol. 153, 2006, pp. 276–282.

[91] Liyong Yang, "A novel fuzzy logic and anti-windup PI controller for a rectifier with direct driven permanent magnet synchronous generator," *2009 2nd International Conference on Power Electronics and Intelligent Transportation System (PEITS)*, IEEE, 2009, pp. 422–426.

[92] A.G. Aissaoui, A. Tahour, N. Essounbouli, F. Nollet, M. Abid, and M.I. Chergui, "A Fuzzy-PI control to extract an optimal power from wind turbine," *Energy Conversion and Management*, Apr. 2012.

[93] Z.L. Dou, M.Z. Cheng, Z.B. Ling, and X. Cai, "An adjustable pitch control system in a large wind turbine based on a fuzzy-PID controller," *SPEEDAM 2010*, IEEE, 2010, pp. 391–395.

[94] H. Li, K.L. Shi, and P.G. McLaren, "Neural-Network-Based Sensorless Maximum Wind Energy Capture With Compensated Power Coefficient," *IEEE Transactions on Industry Applications*, vol. 41, Nov. 2005, pp. 1548–1556.

[95] R. Khanna, G. Singh, and T.K. Nagsarkar, "Artificial neural network based SMES unit for transient stability improvement," *2010 Joint International Conference on Power Electronics, Drives and Energy Systems & 2010 Power India*, IEEE, 2010, pp. 1–7.

[96] A.M. Hemeida, "Artificial neural network PI controlled superconducting magnetic energy storage, SMES for augmentation of power systems stability," *2008 12th International Middle-East Power System Conference*, IEEE, 2008, pp. 187–191.

[97] A.H.M.A. Rahim and E.P. Nowicki, "A robust damping controller for SMES using loop-shaping technique," *International Journal of Electrical Power & Energy Systems*, vol. 27, Jun. 2005, pp. 465–471.

[98] T. Matsuo, Y. Shirakawa, H. Tsuruda, H. Okada, and T. Ezaki, "Robust transient stabilizer for power systems with superconducting magnetic energy storage unit," *Proceedings of the 1996 IEEE IECON. 22nd International Conference on Industrial Electronics, Control, and Instrumentation*, IEEE, , pp. 1687–1692.

[99] M.H. Ali, T. Murata, and J. Tamura, "Transient Stability Enhancement by Fuzzy Logic-Controlled SMES Considering Coordination With Optimal Reclosing of Circuit Breakers," *IEEE Transactions on Power Systems*, vol. 23, May. 2008, pp. 631–640.

[100] M.H. Ali, M. Park, I.-K. Yu, T. Murata, and J. Tamura, "Improvement of Wind-Generator Stability by Fuzzy-Logic-Controlled SMES," *IEEE Transactions on Industry Applications*, vol. 45, 2009, pp. 1045–1051.

[101] M.G. Rabbani, J.B.X. Devotta, and S. Elangovan, "Fuzzy controlled SMES unit for power system application," *Proceedings of EMPD '98. 1998 International Conference on Energy Management and Power Delivery (Cat. No.98EX137)*, IEEE, , pp. 41–46.

[102] T.H. Nguyen and D.-C. Lee, "A novel current control scheme of grid converters for small PMSG wind turbines under grid voltage distortion," *2012 IEEE Power Electronics and Machines in Wind Applications*, IEEE, 2012, pp. 1–6.

[103] G.W. Chang, "Radial-Basis-Function-Based Neural Network for Harmonic Detection," *IEEE Transactions on Industrial Electronics*, vol. 57, Jun. 2010, pp. 2171–2179.

[104] T. Poggio and F. Girosi, "Regularization algorithms for learning that are equivalent to multilayer networks.," *Science (New York, N.Y.)*, vol. 247, Feb. 1990, pp. 978–82.

[105] W.-M. Lin, C.-M. Hong, T.-C. Ou, and T.-M. Chiu, "Hybrid intelligent control of PMSG wind generation system using pitch angle control with RBFN," *Energy Conversion and Management*, vol. 52, Feb. 2011, pp. 1244–1251.

[106] F.-S. Cheng, "MPPT control strategy for wind energy conversion system based on RBF network," *IEEE 2011 EnergyTech*, IEEE, 2011, pp. 1–6.

[107] A.H.M.A. Rahim, I.O. Habiballah, and E.P. Nowicki, "Dynamic performance enhancement of a DFIG system through converter controls," *2009 IEEE Power & Energy Society General Meeting*, IEEE, 2009, pp. 1–8.

[108] Li Wang; Shiang-Shong Chen; Wei-Jen Lee; Zhe Chen, "Dynamic Stability Enhancement and Power Flow Control of a Hybrid Wind and Marine-Current Farm Using SMES," *IEEE Transactions on Energy Conversion*, vol. 24, Sep. 2009, pp. 626–639.

[109] M.H. Ali, T. Murata, and J. Tamura, "A Fuzzy Logic-Controlled Superconducting Magnetic Energy Storage for Transient Stability Augmentation," *IEEE Transactions on Control Systems Technology*, vol. 15, Jan. 2007, pp. 144–150.

[110] Y. Shi and R. Eberhart, "A modified particle swarm optimizer," *1998 IEEE International Conference on Evolutionary Computation Proceedings. IEEE World Congress on Computational Intelligence (Cat. No.98TH8360)*, IEEE, , pp. 69–73.

[111] S. Chen, X. Hong, B.L. Luk, and C.J. Harris, "Non-linear system identification using particle swarm optimisation tuned radial basis function models," *International Journal of Bio-Inspired Computation*, vol. 1, 2009, pp. 246–258.

[112] M.J.D. Powell, "Radial basis function methods for interpolation to functions of many variables," *HERCMA*, LEA Press, Athens, Hellas, 2001, pp. 2–24.

[113] Y. Feng, H. Lin, J. Yan, Y. Guo, and M. Huang, "A novel energy feedback control method of flywheel energy storage system based on radial basis function neural

network," *2011 International Conference on Electrical Machines and Systems*, IEEE, 2011, pp. 1–4.

[114] S.-J. Huang, K.-S. Huang, and K.-C. Chiou, "Development and application of a novel radial basis function sliding mode controller," *Mechatronics*, vol. 13, May. 2003, pp. 313–329.

[115] S.A. Raza, "Smart Pitch Control Strategy for Wind Generation System Using Doubly Fed Induction Generator," MSc. Thesis, King Fahd University of Petroleum and Minerals (KFUPM), 2012.

VITA

Name	Muhammad Haris Khan
Nationality	Pakistani
Date of Birth	01-Oct-1986
Email	muhammadharisk@gmail.com
Address	Flat # S-1/3, 2nd Floor, Block #3, Al-Karam Square, F.C, Area, Karachi, 75900, Pakistan.
Contact	+966543364631, +923212104031
Education	Received Bachelor of Engineering (B.E) degree in Telecommunication Engineering from Usman Institute of Technology (UIT), Karachi, Pakistan in 2009. Joined King Fahd University of Petroleum and Minerals (KFUPM) in Feb 2010.
Experience	Research Assistant in King Fahd University of Petroleum and Minerals (KFUPM), 2010-2012.
Awards	2nd Position Holder In Bachelor of Engineering (B.E) from Usman Institute of Technology (UIT). Scholarship Holder from Usman Institute of Technology (UIT) from 2005-2009.
Publications	Khan, M.H.; A. H. M. A. Rahim.; , "IPSO Based SMES controller design for a PMSG wind system," Energycon, 2012 Second International Energy Conference and Exhibition on , vol., no., pp.662-667, 9-12 Sep. 2012. A. H. M. A. Rahim., Khan, Muhammad Haris; " An Adaptive Optimum SMES Controller for a PMSG Wind Generation System," Paper sent to Power & Energy Society General Meeting (IEEE), 2013.